

CONTROLLING THE CHARGE DENSITY WAVE IN VSE2
CONTAINING HETEROSTRUCTURES

by

OMAR KYLE HITE

A DISSERTATION

Presented to the Department of Chemistry and Biochemistry
and the Graduate School of the University of Oregon
in partial fulfillment of the requirements
for the degree of
Doctor of Philosophy

December 2017

DISSERTATION APPROVAL PAGE

Student: Omar Kyle Hite

Title: Controlling the Charge Density Wave of VSe₂ Containing Heterostructures

This dissertation has been accepted and approved in partial fulfillment of the requirements for the Doctor of Philosophy degree in the Department of Chemistry and Biochemistry by:

George Nazin	Chairperson
David C. Johnson	Advisor
James Hutchison	Core Member
Richard Taylor	Institutional Representative

and

Sara D. Hodges	Interim Vice Provost and Dean of the Graduate School
----------------	--

Original approval signatures are on file with the University of Oregon Graduate School.

Degree awarded December 2017

© 2017 Omar Kyle Hite

DISSERTATION ABSTRACT

Omar Kyle Hite

Doctor of Philosophy

Department of Chemistry and Biochemistry

December 2017

Title: Controlling the Charge Density Wave in VSe₂ Containing Heterostructures

Exploring the properties of layered materials as a function of thickness has largely been limited to semiconducting materials as thin layers of metallic materials tend to oxidize readily in atmosphere. This makes it challenging to further understand properties such as superconductivity and charge density waves as a function of layer thickness that are unique to metallic compounds. This dissertation discusses a set of materials that use the modulated elemental reactants technique to isolate 1 to 3 layers of VSe₂ in a superlattice in order to understand the role of adjacent layers and VSe₂ thickness on the charge density wave in VSe₂.

The modulated elemental reactants technique was performed on a custom built physical vapor deposition to prepare designed precursors that upon annealing will self-assemble into the desired heterostructure. First, a series of (PbSe)_{1+δ}(VSe₂)_n for $n = 1 - 3$ were synthesized to explore if the charge density wave enhancement in the isovalent (SnSe)_{1.15}VSe₂ was unique to this particular heterostructure. Electrical resistivity measurements show a large change in resistivity compared to room temperature resistivity for the $n = 1$ heterostructure. The overall change in resistivity was larger than what was observed in the analogous SnSe heterostructure.

A second study was conducted on $(\text{BiSe})_{1+\delta}\text{VSe}_2$ to further understand the effect of charge transfer on the charge density wave of VSe_2 . It was reported that BiSe forms a distorted rocksalt layer with antiphase boundaries. The resulting electrical resistivity showed a severely dampened charge density wave when compared to both analogous SnSe and PbSe containing heterostructures but was similar to bulk.

Finally, $(\text{SnSe}_2)_{1+\delta}\text{VSe}_2$ was prepared to further isolate the VSe_2 layers and explore interfacial effects on the charge density wave by switching from a distorted rocksalt structure to 1T- SnSe_2 . SnSe_2 is semiconductor that is used to prevent adjacent VSe_2 layers from coupling and thereby enhancing the quasi two-dimensionality of the VSe_2 layer. Electrical characterization shows behavior similar to that of SnSe and PbSe containing heterostructures. However, structural characterization shows the presence of a SnSe impurity that is likely influencing the overall temperature dependent resistivity.

This dissertation includes previously published and unpublished co-authored materials.

CURRICULUM VITAE

NAME OF AUTHOR: Omar Kyle Hite

GRADUATE AND UNDERGRADUATE SCHOOLS ATTENDED:

University of Oregon, Eugene, Oregon
Pacific University, Forest Grove, Oregon

DEGREES AWARDED:

Doctor of Philosophy, Chemistry, 2017, University of Oregon
Bachelor of Science, Mathematics & Chemistry, 2013, Pacific University

AREAS OF SPECIAL INTEREST:

Structural and Electrical Characterization of Materials
Physical Vapor Deposition

PROFESSIONAL EXPERIENCE

Project Quality Assurance Intern, Thermo Fisher Scientific, 2017-2018
Graduate Research Assistant, University of Oregon, 2013-2017
Intern, Voxtel Inc., 2016
Graduate Teaching Assistant, University of Oregon, 2013-2017

PUBLICATIONS:

Hite, O. K.; Falmbigl, M.; Alemayehu, M. B.; Esters, M.; Wood, S. R.; Johnson, D. C. Charge density wave transition in $(\text{PbSe})_{1+\delta}(\text{VSe}_2)_n$ compounds with $n = 1, 2,$ and 3 . *Chem. Mater.* **2017**, 29, 5646-5653.

Hite, O. K.; Nellist, M.; Ditto, J.; Falmbigl, M.; Johnson, D. C. Transport properties of VSe_2 monolayers separated by bilayers of BiSe . *J. Mater. Res.* **2015**, 31, 886-992.

Westover, R.D.; Mitchson, G.; Hite, O. K.; Hill, K.; Johnson, D.C. Suppression of a charge density wave in $([\text{SnSe}]_{1.15})_1(\text{VSe}_2)_1$ ferecrystals via isoelectronic doping with Ta. *J. Electron. Mater.* **2016**, 45, 4898-4902.

ACKNOWLEDGMENTS

First I would like to thank my advisor, David Johnson, for his guidance throughout my time at the University of Oregon and for the opportunity to work in his lab. I am grateful for many of the people I have had the privilege to work with along the way, Dr. Matti Alemayehu, Dr. Matthias Falmbigl, Dr. Suzannah Wood, Dr. Richard Westover, Dr. Gavin Mitchson, Dr. Sage Bauers, Dr. Devin Merrill, Dr. Daniel Moore, Dr. Noel Gunning, Dr. Jeffrey Ditto, Erik Hadland, Marco Esters, Danielle Hamann, Dmitri Cordova, and Nic Westcott. Thank you to the many undergraduates, Liese Maynard, Kim Ta, Dylan Bardgett, Jake Logan, and Jordan Joke for their willingness to help. A special thanks to my committee members Dr. George Nazin, Dr. James Hutchison, and Dr. Richard Taylor for taking time to meet and giving feedback. I would also like to thank Kris Johnson for taking his time to not only help in troubleshooting but also being willing to teach.

A special thanks to my friends and colleagues, Mike Nellist and James Sadighian, for choosing to work with me during their rotation in the lab and for being a source of support and kindness.

I would like to acknowledge funding from the National Science Foundation under grant DMR-1266217 and OCI-0960354. Use of the Advanced Photon Source, an Office of Science User Facility operated for the U.S. Department of Energy (DOE) Office of Science by Argonne National Laboratory, was supported by the U.S. DOE under contract no. DEAC02-06CH11357. I also acknowledge support through the Collaborative Access Team (CAT): Pooled Resources for Electron Microscopy Informatics, Education and Research (PREMIER) Network Program at Pacific Northwest National Laboratory

(PNNL) and the Environmental Molecular Sciences Laboratory, a national scientific user facility sponsored by DOE's Office of Biological and Environmental Research at PNNL. PNNL is a multi-program national laboratory operated by Battelle for DOE under Contract DE-AC05-76RL01830.

Finally, I would like to thank both of my parents, Rick and Kim Hite, for always believing in me and offering their love and support. I would also like to thank my amazing wife, Elizabeth Hite, for being an inspiration. I will always love all of our adventures. I would also like to thank my Lord and Savior, Jesus Christ, for creating such an interesting place to live and explore.

To my wife,
you're just the best.

TABLE OF CONTENTS

Chapter	Page
I. INTRODUCTION	1
I.1. Authorship Statement	1
I.2. Thin Films and Material Design	1
I.3. Van der Waals Heterostructures	2
I.4. Misfit Layered Compounds and Ferecrystals: Close Cousins to VDWs Heterostructures	3
I.5. Charge Density Waves	5
I.6. VSe ₂ and its Ferecrystals	8
I.7. Dissertation Overview	9
II. EXPERIMENTAL PROCEDURES	11
II.1. Authorship Statement	11
II.2. Modulated Elemental Reactants Technique	11
II.3. Structural Analysis using X-ray Diffraction	14
II.4. Rietveld Refinement	15
II.5. Compositional Analysis	16
II.6. Scanning Transmission Electron Microscopy	17
II.7. Transport Property Measurements	18
III. CHARGE DENSITY WAVE TRANSITION IN (PBSE) _{1+Δ} (VSE ₂) _N WITH N = 1, 2, AND 3	21

Chapter	Page
III.1. Authorship Statement.....	21
III.2. Introduction.....	21
III.3. Experimental Methods.....	24
III.4. Results and Discussion	26
III.5. Conclusions.....	37
III.6. Bridge.....	38
IV. TRANSPORT PROPERTIES OF VSE2 MONOLAYERS SEPARATED BY BILAYERS OF BISe	39
IV.1. Authorship Statement	39
IV.2. Introduction.....	39
IV.3.Experimental.....	41
IV.4. Results and Discussion	43
IV.5. Conclusions.....	51
IV.6. Bridge	52
V. INFLUENCE OF INTERFACIAL STRUCTURE ON THE CHARGE DENSITY WAVE IN VSE2 HETEROSTRUCTURES WITH 1T-SNSe2	53
V.1. Authorship Statement.....	53
V.2. Introduction.....	53
V.3.Experimental	55
V.4. Results and Discussion.....	56
V.5. Conclusion	61

Chapter	Page
VI. CONCLUDING REMARKS.....	63
VI.1. Authorship Statement	63
VI.2. Remarks	63
APPENDIX: SUPPORTING INFORMATION FOR CHARGE DENSITY WAVE TRANSITION IN (PBSE) _{1+Δ} (VSE ₂) _N COMPOUNDS WITH N = 1, 2, AND 3.....	66
REFERENCES CITED.....	69

LIST OF FIGURES

Figure	Page
I.1.	A large variety of heterostructures can be formed by stacking layered materials together similar to a block of Legos 2
I.2.	Misfit layered compounds are formed with two layered materials that alternate in the c-direction. The layers distort to form a commensurate b-lattice and incommensurate a-lattice 3
I.3.	Ferecrystals are formed with stacked blocks of layered materials that have incommensurate a- and b-lattice parameters. The blocks of material are randomly oriented about the c-axis 4
I.4.	(a) In a 1-dimensional chain of hydrogen atoms the half-filled s band can split decreasing the bond distance between atoms to form a unit cell with distance 2a. (b) The hydrogen atoms can oscillate to induce charge movement 6
I.5.	An atomic layer of V atoms sandwiched by atomic layers of Se atoms from a single layer of VSe ₂ . These VSe ₂ layers stack to form bulk VSe ₂ 8
II.1.	An atomic layer of V atoms sandwiched by atomic layers of Se atoms from a single layer of VSe ₂ . These VSe ₂ layers stack to form bulk VSe ₂ 12
II.2.	Two photons that are in phase reflect off different planes separated by a distance d. To remain in phase the angle of incidental light and d must satisfy Bragg's Law 14
II.3.	In-plane X-ray diffraction of (PbSe) _{1+δ} VSe ₂ 15
II.4.	Out-of-plane X-ray diffraction of (PbSe) _{1+δ} VSe ₂ and its Rietveld analysis 16
II.5.	Characteristic X-ray intensity of Se per repeat unit in (PbSe) _{1+δ} (VSe ₂) _n for n = 1, 3-5. 17
II.6.	HAADF-STEM images of (PbSe) _{1+δ} VSe ₂ shows alternating layers of PbSe and VSe ₂ with turbostratic disorder 18
II.7.	Two of the eight possible lead combinations used in order to measure in-plane electrical resistivity 19

Figure	Page
II.8. Two of the possible four combinations used to measure the Hall coefficient	20
III.1. X-ray diffraction of $(\text{PbSe})_{1+\delta}(\text{VSe}_2)_n$ for $n = 1-3$ using Cu $K\alpha$ radiation ($\lambda = 0.15418$ nm)	28
III.2. Experimental, calculated, and difference patterns from the Rietveld refinement of the positions of atomic planes along the c-axis of $(\text{PbSe})_{1+\delta}\text{VSe}_2$	29
III.3. Normalized in-plane X-ray diffraction patterns of $(\text{PbSe})_{1+\delta}(\text{VSe}_2)_n$ for $n = 1-3$	30
III.4. HAADF-STEM images of $(\text{PbSe})_{1.11}\text{VSe}_2$ contain alternating PbSe bilayers and VSe_2 trilayers.....	31
III.5. Temperature-dependent resistivity of $(\text{PbSe})_{1+\delta}(\text{VSe}_2)_n$ for $n = 1-3$ and bulk VSe_2	33
III.6. Temperature dependence of the Hall coefficient for $(\text{PbSe})_{1+\delta}(\text{VSe}_2)_n$ $n = 1-3$ and bulk single crystal VSe_2	34
III.7. Temperature dependent single conducting band carrier mobility of $(\text{PbSe})_{1.11}\text{VSe}_2$, $(\text{SnSe})_{1.15}\text{VSe}_2$, ²⁴ and $(\text{BiSe})_{1+\delta}\text{VSe}_2$	35
III.8. Hall coefficients for different $(\text{MSe})_{1+\delta}(\text{VSe}_2)$ ($\text{M} = \text{Sn, Pb, Bi}$) ferecrystals and bulk VSe_2	37
IV.1. A series of diffraction scans $(\text{BiSe})_{1+\delta}\text{VSe}_2$ collected as a function of annealing temperature, as indicated at the right side of the scans	45
IV.2. Rietveld refinement of the $[(\text{BiSe})_{1+\delta}]_1[\text{VSe}_2]_1$ heterostructure determine the position of atomic planes along the c-axis.....	46
IV.3. Representative cross section HAADF-STEM images of the $[(\text{BiSe})_{1+\delta}]_1[\text{VSe}_2]_1$ heterostructure.....	47
IV.4. Resistivity data as a function of temperature for the $[(\text{BiSe})_{1+\delta}]_1[\text{VSe}_2]_1$ heterostructure compared to that reported for VSe_2 and $[(\text{SnSe})_{1.15}]_1(\text{VSe}_2)_1$	48
IV.5. Hall coefficients as a function of temperature for the $[(\text{BiSe})_{1+\delta}]_1[\text{VSe}_2]_1$ heterostructure compared to that reported for VSe_2 and $[(\text{SnSe})_{1.15}]_1(\text{VSe}_2)_1$	49

Figure	Page
V.1. Out-of-plane X-ray diffraction for $(\text{SnSe}_2)_{1+\delta}\text{VSe}_2$ with maxima that are indexed to $00l$ reflections.....	57
V.2. In-plane X-ray diffraction for $(\text{SnSe}_2)_{1+\delta}(\text{VSe}_2)_n$ $n = 1-3$	58
V.3. In-plane electrical resistivity and Hall coefficient measurements of $(\text{SnSe}_2)_{1+\delta}\text{VSe}_2$	59
V.4. In-plane electrical resistivity comparison between $(\text{PbSe})_{1.11}\text{VSe}_2$, $(\text{SnSe})_{1.15}\text{VSe}_2$, and $(\text{SnSe}_2)_{0.81}\text{VSe}_2$	60
V.5. Temperature dependent mobility and Hall coefficient measurements of $(\text{SnSe}_2)_{0.81}\text{VSe}_2$, $(\text{PbSe})_{1.11}\text{VSe}_2$, and $(\text{SnSe})_{1.15}\text{VSe}_2$	61
A.1. Band structures of monolayer (a) and bilayer (b) (VSe_2). Solid blue lines denote majority spins and dashed red lines denote minority spin bands.	67

LIST OF TABLES

Table		Page
A.1.	Rietveld refinement results from room temperature XRD data. Space group: P-3m1 (VSe ₂), Fm-3m (PbSe).	68

CHAPTER 1

INTRODUCTION

Authorship Statement

My advisor, David C. Johnson, was consulted in the preparation of this chapter.

Thin Films and Material Design

Modern materials are typically in the form of ceramics, nanomaterials, composite materials, and thin films and are ubiquitous in modern society. In particular, thin films offer access to a variety of desirable properties due to their unique structure, in which, they have a large surface area to volume ratio. This unique structure provides access to light and possibly flexible devices. Due to the discovery of graphene in 2004 by Geim et al. layered materials have become a focus of intense research interest.¹ Many compounds, such as graphene, hexagonal boron nitride (h-BN), and transition metal dichalcogenides (TMDs), show a change in properties as the thickness of the material reaches the monolayer limit. A well-known example of this is the TMD MoS₂ which, in the bulk form, is an indirect semiconductor. However, as the thickness of MoS₂ is reduced to the monolayer it becomes a direct bandgap semiconductor.² h-BN has a bulk bandgap of 4.0 eV and increases to a monolayer bandgap of 4.6 eV.³ A similar trend is computationally predicted in SnS, SnSe, GeS, and GeSe that have increased bandgaps at the monolayer limit.⁴ As modern technology progresses it is required that high-quality materials possess a wide range of desirable properties that is not possible in a single material device.² This is even evident in simple silicon solar cells that must be doped with boron and phosphorous. The large range of 2D materials and the diversity of their properties provide

an avenue for device design to access a large range of properties by layering these materials together in what is known as a van der Waals heterostructure.¹

Van der Waals Heterostructures

Van der Waals heterostructures are a set of thin film materials typically composed of individual films of 2D materials, such as graphene, h-BN, and TMDs, that are then stacked on top of one another (Figure I.1). These stacked layers are held together in the out-of-plane direction by van der Waals forces hence the name.¹ In an idealized sense, these heterostructures are similar to blocks of Legos in which you can design a material by placing the building blocks of the heterostructure on top of one another. One could then design the structure to exhibit certain properties determined by the layers and their interactions. However, designing structures this way is typically limited by the stability of the individual layers and is largely limited to semiconducting materials.

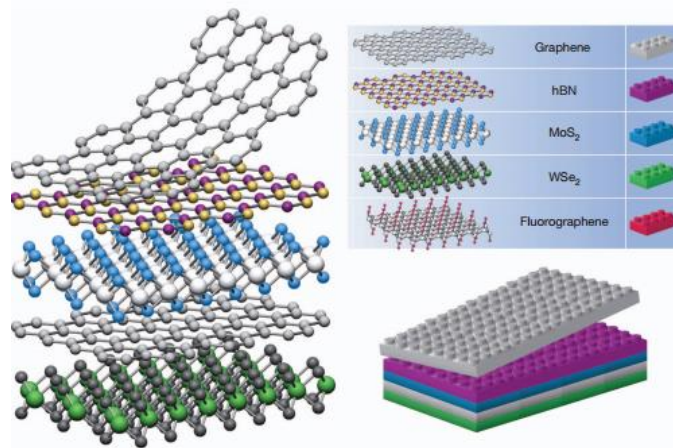


Figure I.1. A large variety of heterostructures can be formed by stacking layered materials together similar to a block of Legos. Copyright Geim, A. K.; Grigorieva, I. *Nature* **2013**, 499, 419–425.

Misfit Layered Compounds and Ferecrystals: Close cousins to VDWs Heterostructures

Misfit layered compounds (MLCs) are natural heterostructures of the form MTX_3 and were initially thought to be ternary compounds until they were discovered to have more complex structures, through the use of single crystal X-ray diffraction and electron microscopy.⁵ MLCs are actually composed of two types of layers. A distorted rock-salt, MX, with half the thickness of the cell edge of a face centered NaCl, and a transition metal dichalcogenide trilayer (TX_2 or X-T-X). These compounds have the general formula $[(MX)_{1+\delta}]_m(TX_2)_n$ where M is Sn, Pb, Bi, Sb, or a rare earth metal, T is Ti, V, Nb, Cr, or Ta, and X is S or Se.⁵⁻²⁰ Compounds of this type contain m layers of rock-salt and n layers of dichalcogenide. The c -axis is defined to be normal to the constituent layers and the name “misfit layered” compounds stems from the incommensurate a -lattice parameter that forms between layers. This mismatch in the a -lattice is described by the $1+\delta$ term and can be seen in Figure I.2.

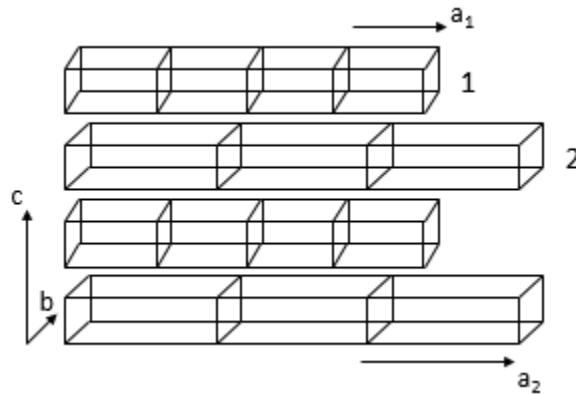


Figure I.2. Misfit layered compounds are formed with two layered materials that alternate in the c -direction. The layers distort to form a commensurate b -lattice and incommensurate a -lattice.

MLCs are synthesized using typical high temperature synthetic routes are limited to the thermodynamic products of the synthesis.⁵ This limitation restricts values of m and n with most common values being $m = n = 1$ or $m = 1$ and $n = 2$.^{5,21-30} There have been

reports of compounds with $m = 1.5$ or 2 and $n = 1$ and compounds with $m = 1$ and $n = 3$.^{22,31} The electrical properties are typically determined by the more conductive component of the MLC.⁵

A related set of compounds known as ferecrystals having the same general formula $[(MX)_{1+\delta}]_m(TX_2)_n$ where M is Sn, Pb, and Bi, T is Ti, V, Mo, Nb, Ta, W, or Mo, and X is Se or Te.³²⁻⁴⁰ These compounds are synthesized using a physical vapor deposition technique, termed Modulated Elemental Reactants (MER) and is discussed further in Chapter II, and then annealed at low temperatures. This technique unlocks access to kinetic products that may contain values of m and n that are not possible with typical MLC synthetic methods. The synthesis process for ferecrystals makes use of designed precursors with structure similar to the desired product. They are then annealed

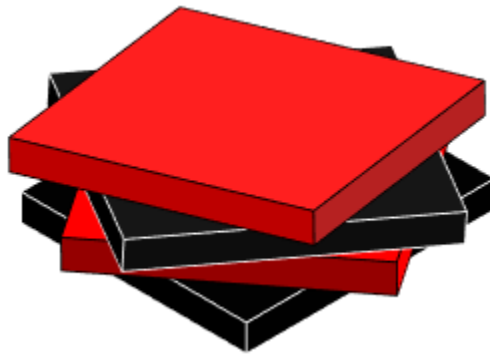


Figure I.3. Ferecrystals are formed with stacked blocks of layered materials that have incommensurate a- and b-lattice parameters. The blocks of material are randomly oriented about the c-axis.

at low temperatures ranging from 200-500 °C as opposed to the high temperatures typically required in the synthesis of MLCs. As a result of the designed precursors the formation process of the ferecrystal is nucleation limited as opposed to being diffusion limited that is found in common synthesis techniques. The layers nucleate independently resulting in turbostratic disorder between adjacent layers as depicted in Figure I.3. In

other words, layers within the ferecrystal have incommensurate a- and b-lattice parameters. This extensive turbostratic disorder is the origin of the term "ferecrystal" where *fere-* is derived from the Greek word for "almost."

The technique by which these ferecrystals are prepared, MER, offers the kinetic control that the synthetic method of MLCs cannot and provides a way to isolate a monolayer of a variety of metallic films that is not yet achieved by typical van der Waals heterostructures.^{34,39,41,42} The ability to control the values of m and n allows for a systematic approach to be performed in order to better understand material properties that may vary as a function of layer thickness.

Charge Density Waves

Charge density waves are a generalization of the Peierls' distortion that occurs in 1D metallic chains.⁴³ A simple example is illustrated below in figure I.4. Figure I.4.a shows a chain of hydrogen atoms with atomic spacing a , which leads to half-filled 1s-band. The lowest occupied MO, HOMO, LUMO, and high unoccupied MO are shown from top to bottom. As the temperature of the chain is cooled below the onset temperature of the CDW, T_{CDW} , pairs of atoms may move in such a way, illustrated, that leads to a lowering in energy of the conduction band and raising of energy of the valence band due to favorable and unfavorable interactions due to the change in structure. This phenomenon is expected in all idealized 1D metallic chains. However, as dimensionality is increased to quasi 2D the simple picture posed by Peierls' becomes complicated. The mechanism for the induced CDW has been proposed as nesting of Fermi surfaces, the surface of electron density in momentum space that separates the filled orbitals from the unfilled orbitals at $T = 0$ K. In the 1D case the Fermi surfaces experience complete

nesting while in the 2D case the Fermi surface becomes more complicated and may only experience partial nesting and becomes much less common. This phenomenon has been seen in two dimensional sheets of atoms and is common in metallic transition metal dichalcogenides, such as, TiSe_2 , TaSe_2 , NbSe_2 , and VSe_2 .⁴⁴⁻⁴⁹ This nesting is even more complicated in three dimensions, and as a consequence, less likely to occur. In other words, in order for a CDW to occur the energetic gain by opening a band gap must overcome the energetic cost of distorting the lattice. This particular condition is complicated when you increase the number of interacting atoms.

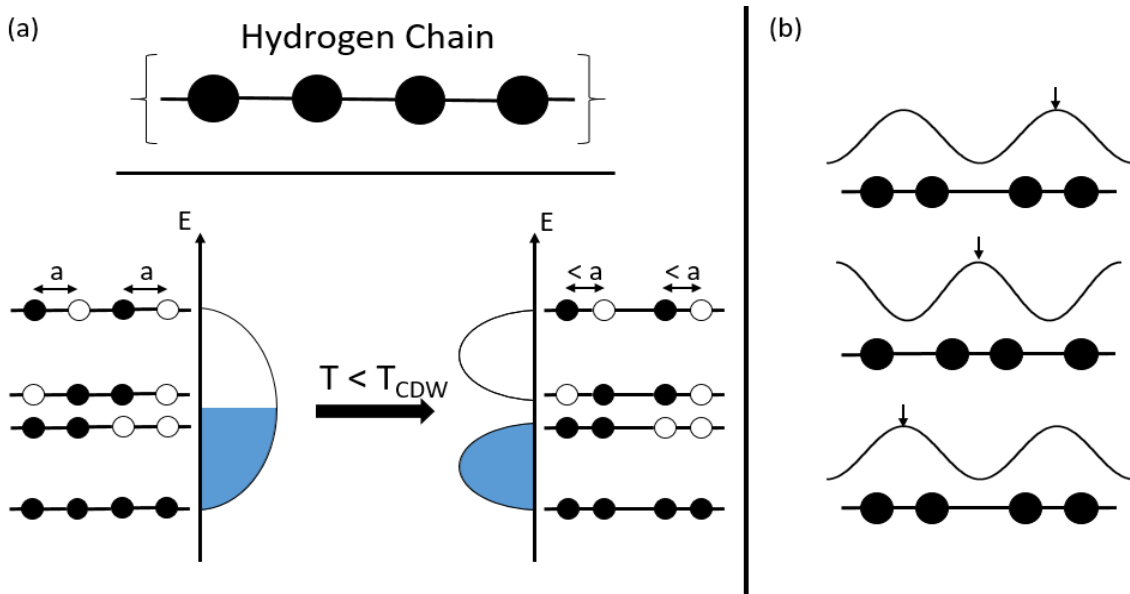


Figure I.4. (a) In a 1-dimensional chain of hydrogen atoms the half-filled s band can split decreasing the bond distance between atoms to form a unit cell with distance $2a$. (b) The hydrogen atoms can oscillate to induce charge movement.

Charge density waves are of particular interest due to the possibility of inducing superconductivity due to the modulation of the charge.⁴³ By inducing a voltage across the chain the atoms may react by oscillating and thereby moving the modulated charge as seen above in Figure I.4.b. A current issue that arises is the pinning of the charge density wave due to impurities that are present within the crystal. A simple picture of this

phenomenon is a marble (charge carrier) on a corrugated sheet of metal (lattice). The depth of the corrugation corresponds to the magnitude of the pinning and increased defects, while the tilt of the sheet of metal corresponds to the applied voltage. A consequence of this interaction is a non-linear conduction in response to an applied electric field.⁴³ An example being the marble interacting with the corrugation of the metal as it rolls along the surface.

In order to fully realize the use of CDW materials in devices it is imperative that we expand our understanding of the CDW transition and particularly how it behaves as the thickness of the CDW material is reduced. In other words, how does the CDW change as we approach the monolayer limit as opposed to the bulk limit? This question has been explored previously by determining how T_{CDW} is affected as the monolayer limit approached. In mechanically exfoliated $TiSe_2$ the onset temperature of the CDW transition is increased as the thickness of the exfoliated film is decreased.⁴⁹ In a similar study of $TaSe_2$ opposing results were reported. As the thickness of exfoliated flakes decreased the onset temperature also decreased.⁴⁸ Two studies were performed on VSe_2 each showing opposing results likely due to the different exfoliation methods the two studies performed.^{50,47} In all four studies mentioned above the monolayer limit was never achieved and was limited to about 4 trilayers in VSe_2 exfoliated films. Additionally precise control of thickness was not achieved. As mentioned above, the MER technique for growing ferecrystalline compounds allows for precise control of thickness and therefore offers a systematic approach to exploring the role of thickness in the CDW formation. The model system discussed in this thesis is VSe_2 containing ferecrystals, $[(MX)_{1+\delta}]_m(VSe_2)_n$.

VSe₂ and its Ferecrystals

VSe₂ is a layered transition metal dichalcogenide composed of a Se-V-Se trilayer (Figure I.5). It has a 1T-CdI₂ type trigonal structure with octahedrally coordinated V. Bulk VSe₂ was shown by Bayard et al. to have a resistivity anomaly at 80 K along with a negative Hall coefficient that increases in magnitude by a factor of 4 at the same temperature.⁵¹ The nature of this behavior has been attributed to a charge density wave transition.

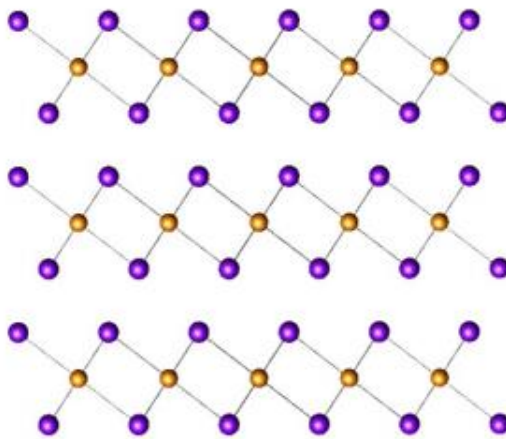


Figure I.5. An atomic layer of V atoms sandwiched by atomic layers of Se atoms from a single layer of VSe₂. These VSe₂ layers stack to form bulk VSe₂.

As mentioned above, later work produced conflicting results as to how T_{CDW} is affected by the thickness of VSe₂ exfoliated flakes. Early work on [(SnSe)_{1+δ}]_m(VSe₂)_n ferecrystals sought to further explore the nature of the CDW found VSe₂. Atkins et. al. was the first to produce and publish work on ferecrystalline (SnSe)_{1.15}VSe₂ showing an enhanced CDW around 115 K with a positive Hall coefficient that concomitantly increases in magnitude at the same temperature.³⁴ This increase in Hall coefficient is indicative of a decrease in carrier concentration indicative of a CDW transition. Further

work on $(\text{SnSe})_{1+\delta}(\text{VSe}_2)_n$ for $n = 1-4$ was published by Falmbigl et. al.³⁵ It was shown that for $n = 2-3$ the electrical behavior is very different compared to $n = 1$. Resistivity for $n = 4$ was not reported in this study. The change in resistivity was attributed to an increase in dimensionality as the $n = 1$ system is quasi two-dimensional while values of $n > 1$ are three-dimensional. Higher values of n showed bulk like resistivity behavior. In all systems the room temperature Hall coefficient was positive while for $n > 1$ there was a change in sign below 50 K likely due to the breakdown of single-band model typically used to determine carrier concentration from the Hall coefficient. The behavior of the Hall coefficient in $(\text{SnSe})_{1+\delta}(\text{VSe}_2)_n$ is likely due to charge transfer from the SnSe to the VSe₂ layer with additional affects from the n value. This work leads to the intuitive question as to how charge transfer affects the CDW in VSe₂ and if charge transfer can be reduced, enhanced, or completely stopped by material design using the MER method detailed in Chapter II.

Dissertation Overview

This dissertation explores the synthesis and structural and electrical properties of VSe₂ containing heterostructures. Chapter II outlines the synthetic method, known as modulated elemental reactants, that is used to target and synthesize multi-constituent heterostructures. Additionally, there is a thorough discussion of the techniques used to characterize the structural and electrical properties of the designed films. Three sets of kinetically stable VSe₂ heterostructures are discussed in Chapters III to V. Chapter III seeks to explore the uniqueness of the charge density wave that was previously observed in $(\text{SnSe})_{1.15}\text{VSe}_2$ by preparing a set of $(\text{PbSe})_{1+\delta}(\text{VSe}_2)_n$ for $n = 1 - 3$. Chapter IV explores the effect of charge transfer on the charge density wave by characterizing

$(\text{BiSe})_{1+\delta}\text{VSe}_2$. Chapter V replaces the rocksalt layer with 1T-SnSe₂ forming $(\text{SnSe}_2)_{1+\delta}\text{VSe}_2$ in an attempt to determine the role of structural interface on the charge density wave. These chapters are presented individually to explore the effects of interlayer interactions on the charge density wave observed in VSe₂ containing heterostructures. Chapter VI provides concluding remarks. The work presented within this dissertation was made possible through the help and joint effort of many individuals. Chapter I and II were prepared with the assistance of my thesis advisor David C. Johnson. Chapter III is published and co-authored with Matthias Falmbigl, Matti B. Alemayehu, Marco Esters, Suzannah R. Wood, and David C. Johnson. Chapter IV is published and co-authored with Michael Nellist, Jeffrey Ditto, Matthias Falmbigl, and David C. Johnson. Chapter V is in preparation for publication and the co-authors: Erik Hadland, James Sadighian, and David C. Johnson.

CHAPTER II

EXPERIMENTAL PROCEDURES

Authorship Statement

My advisor, David C. Johnson, was consulted in the preparation of this chapter.

Modulated Elemental Reactants Technique

The modulated elemental reactant (MER) technique was developed in the Dave Johnson laboratory in the 1990s. The MER technique provides access to kinetic materials that are not accessible via typical solid state synthesis techniques. Precursors are designed to closely match the nanoarchitecture of the desired final product. These “designed” precursors are nucleation limited rather than diffusion limited as in typical synthetic techniques. They are annealed at low temperature to enable nucleation of the material.¹

Precursors were prepared in a custom-built physical vapor deposition chamber pictured below (Figure II.1).² The chamber uses 3 3-kW Thermionic electron beam guns to evaporate Sn, V, Pb, and Bi and a Knudsen effusion cell to evaporate Se. Elemental vapor is deposited on a (100) oriented Si substrate and rate of deposition is controlled by INFICON Xtal quartz crystal microbalances (QCMs). QCMs are approximately 25 cm above the elemental sources. Elemental sources of Sn, V (99.8%), Se (99.999%), Pb (99.995%), and Bi are obtained from Alfa Aesar. The refractory metal, vanadium, is first melted in an arc melter in a He atmosphere prior to deposition. Sn, Pb, and Bi are placed in a graphite crucible prior to evaporation. V, Pb, and Bi are deposited at a rate of 0.04 nm/s, Sn at 0.03 nm/s, and Se at 0.05 nm/s. A QCM tooling factor of 68 is used for Se and 64 is used for all other elements to account for the spatial difference of the QCM and the Si substrate. A pre-programmed LabView controls a carousel to move substrates to

the desired elemental source and open/closes a set of shutters to control the desired deposition thickness to form the designed repeat structure of the material. This “repeat unit” is repeated until an approximate thickness of 50 nm is obtained. The electron beam is rastered over the vanadium source to prevent drilling that is commonly seen in refractory metals. This is unnecessary for Sn, Pb, and Bi as the sources completely melt.

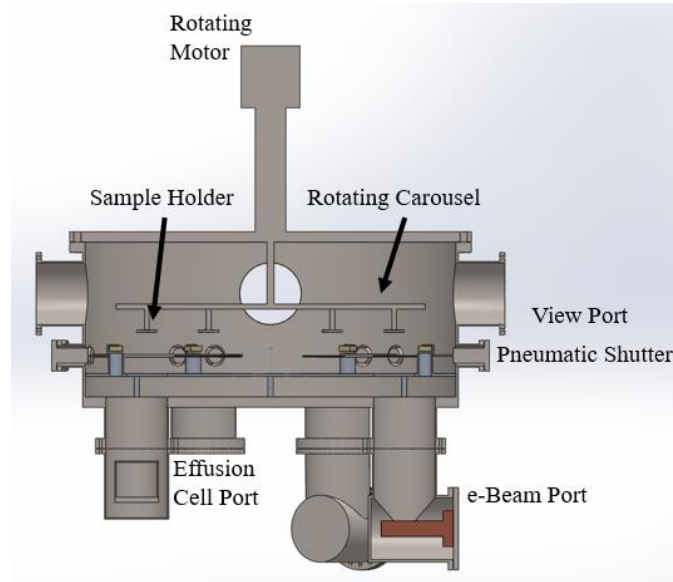


Figure II.1. Schematic of vacuum chamber used to synthesize designed precursors via physical vapor deposition.

The heterostructures $(MSe)_{1+\delta}VSe_2$ for $M = Pb$ and Bi were calibrated using a three-step process. First, a set precursors were synthesized by depositing an amount of M and V and scaling the Se such that a ratio of 1:1 and 1:2 were achieved for $M:Se$ and $V:Se$, respectively. The composition was determined using Electron Probe Micro Analysis (EPMA) and a plot of Se/M and Se/V vs. Se layer thickness was interpolated to determine the amount of Se that resulted in the desired ratio. Next, a set of precursors with a constant $M:Se$ and $V:Se$ ratio and constant $V:Se$ thickness were prepared. The $M|Se$ layer was scaled while maintaining the same $M:Se$ ratio. The $M:V$ ratio was

monitored as function of M|Se deposited to determine the parameters that yielded a ratio for M:V equal to the theoretical $1+\delta$ misfit parameter. Finally, a set of precursors were prepared with constant M:Se, V:Se, and M|Se:V|Se ratios and scaled total thickness in order to achieve the required thickness to form a complete rocksalt MSe bilayer and trigonal VSe₂ trilayer. An excess of Se was deposited in each layer to compensate for Se loss that occurs during the annealing process.

(MSe)_{1+ δ} VSe₂ (M = Pb and Bi) precursors were annealed at varying temperatures and time in order to determine the ideal annealing conditions for heterostructure formation. This “annealing study” was performed on a hotplate in an N₂ atmosphere with <0.5ppm O₂. The ideal annealing conditions were ones that maximized the intensity and minimized the full width at half maximum of 00*l* reflections.

The heterostructure (SnSe₂)_{1+ δ} VSe₂ was calibrated by targeting the ideal counts per second (cps) for each element as determined by X-ray Fluorescence (further details for XRF can be found in section II.4). A precursor with an arbitrary amount of Sn, Se and V is prepared and composition is measured using XRF. The deposition parameters for each element are scaled by the ratio of ideal kcps:measured kcps and a new precursor is prepared with the ideal deposition parameters, which yields a precursor with ideal kcps.

(SnSe₂)_{1+ δ} VSe₂ was first annealed on a hotplate in an N₂ atmosphere with <0.5 ppm O₂. The “pre-annealed” precursor was then sealed in an outgassed Pyrex ampule with bulk SnSe₂ at $\sim 10^{-6}$ torr. An annealing study was performed to determine the ideal temperature and time required to minimize intensity and full width at half maximum for 00*l* reflections while also producing *hk0* reflections that correspond to trigonal SnSe₂ and trigonal VSe₂.

Structural Analysis using X-ray Diffraction

The repeating unit of the heterostructure and total film thickness was determined using X-ray diffraction (XRD) and X-ray reflectivity (XRR), respectively. Out-of-plane XRD was performed on a Bruker D8 Discover diffractometer equipped with Cu K α , 0.154 nm, radiation, Bragg-Brentano geometry, and Göbel mirror. Due to the unique structure of the heterostructures the resulting maxima appear at angles that correspond to the repeating structure of the film, 00l planes, as dictated by Bragg's law (equation 1):

$$n\lambda = 2d\sin\theta \quad (1)$$

where n is some integer, λ is the wavelength of the incidental X-ray (0.154 nm), d is the spacing between reflecting planes, and θ is the angle of the incident beam. This equation can be derived from the path length difference between two scattered X-rays off parallel planes, $2d\sin\theta$, and in order to constructively interfere they must remain in phase (Figure II.2). Therefore this path length must be equal to an integer multiple of the incidental wavelength, $n\lambda$. Out-of-plane XRD is taken from 5° - 65° 2 θ .

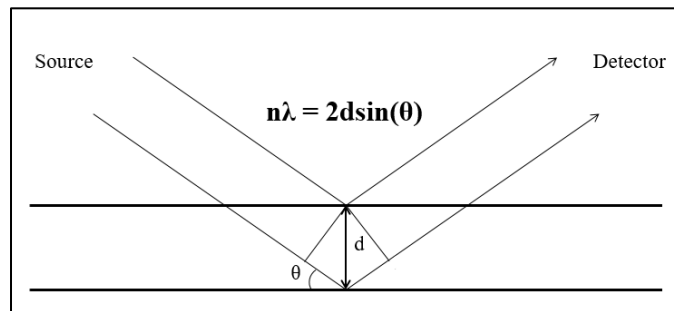


Figure II.2. Two photons that are in phase reflect off different planes separated by a distance d. To remain in phase the angle of incidental light and d must satisfy Bragg's Law.

XRR is performed on the same Bruker D8 Discover diffractometer as mentioned above. However, unlike XRD, XRR is not due to diffraction of incidental X-rays and is a consequence of constructive interference between reflecting X-rays at the air-film

interface and film-substrate interface. The resulting peaks appear at angles dictated by the modified Bragg's law and are termed Kiessig fringes.³

$$n\lambda = 2d(\sin^2\theta - \sin^2\theta_c)^{\frac{1}{2}} \quad (2)$$

The modified Bragg's law accounts for the extra distance traveled by the penetrating X-rays due to the critical angle, θ_c . It is important to note that if the film is more optically dense than the substrate a phase shift of π is observed and n becomes $n + \frac{1}{2}$. XRR is performed from $0^\circ - 11^\circ 2\theta$.

In-plane lattice parameters of the individual layers are determined using in-plane XRD ($hk0$ XRD) (Figure II.3). In-plane XRD is performed on a Rigaku SmartLab equipped with Cu $K\alpha$ radiation and at the Advance Photon Source at Argonne National Laboratory. Due to the structure of the heterostructures only $hk0$ reflections are observed, which allows for determination of in-plane lattice parameters.⁴

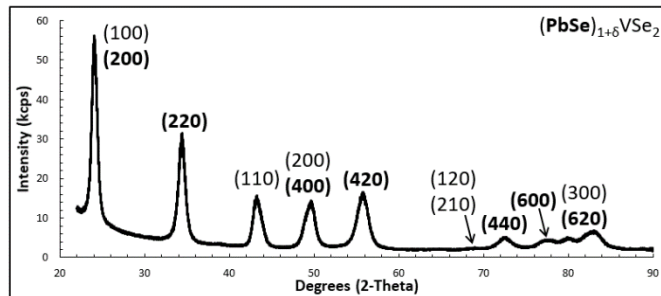


Figure II.3. In-plane X-ray diffraction of $(\text{PbSe})_{1+\delta}\text{VSe}_2$.

Rietveld Refinement

Rietveld analysis is performed on the off-specular X-ray diffraction patterns to further determine the structure of the heterostructure (Figure II.4). A Rietveld refinement employs a least squares algorithm to obtain a best fit between a structural model and an X-ray diffraction pattern. In order for the algorithm to converge a model that closely approximates the actual structure of the film is required. Due to the textured nature of the

film Rietveld refinements are only possible for out-of-plane XRD and therefore only yields structural information about the position of atomic planes along the c -axis.⁵

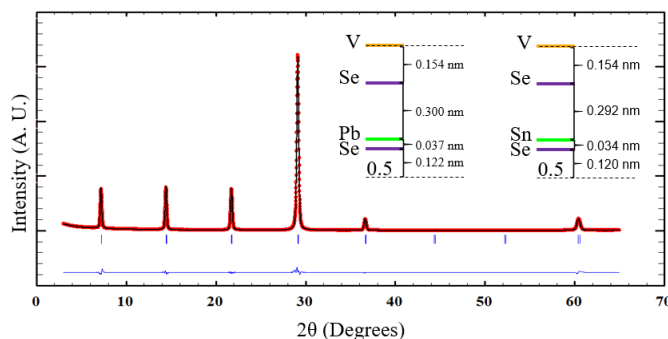


Figure II.4. Out-of-plane X-ray diffraction of $(\text{PbSe})_{1+\delta}\text{VSe}_2$ and its Rietveld analysis.

Compositional Analysis

Electron probe micro analysis (EPMA) focuses a beam of electrons at three different accelerating voltages onto the film and the resulting X-rays are measured and are characteristic of the elements that are present in the interacting volume. The electrons eject a core electron, which creates a vacancy that is then filled by an outer-shell electron resulting in the emission of a characteristic X-rays. The intensity of these X-rays are measured at each accelerating voltage for the sample and for a set of elemental standards corresponding to the elements present in the film.⁶ These intensities are modeled using StrataGEM and yields the elemental ratios that are present within the film.

X-ray fluorescence (XRF) is an analytical technique that focuses high-energy X-rays and measures secondary X-rays that, like EPMA, are characteristic of the elements present in the film. The high-energy X-rays eject a core electron that is then filled by an outer-shell electron resulting in the emission of a secondary X-ray. In the thin film limit, the intensity of secondary X-rays is directly proportional to the concentration of the element present within the film, assuming a homogeneous distribution of the element

(Figure II.5). It is important to note that XRF is not selective to the crystal structure present within the film and gives no information about where the measured elements are located.

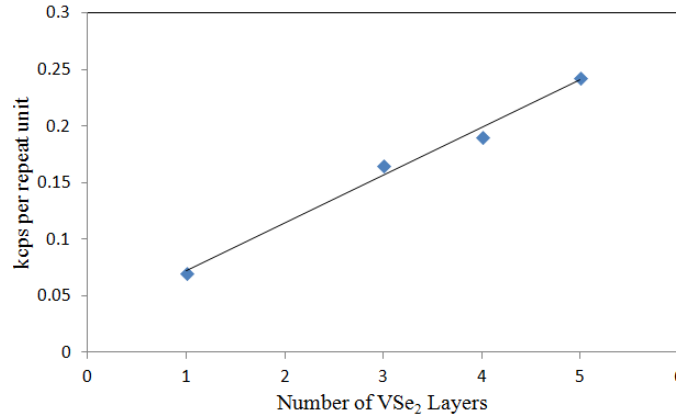


Figure II.5. Characteristic X-ray intensity of Se per repeat unit in $(\text{PbSe})_{1+\delta}(\text{VSe}_2)_n$ for $n = 1, 3-5$.

Scanning Transmission Electron Microscopy

While XRD provides a picture of the average structure of the film, electron microscopy provides an avenue for investigating the local structure of the heterostructure (Figure II.6). A thin cross-section of the film is produced using an FEI Helios Nanolab D600 Dual Beam focused ion beam (FIB) using a method described by Schaffer et al.⁷ This cross section is then imaged using a high angle annular dark-field scanning transmission electron microscope (HAADF-STEM). In HAADF-STEM electrons are rastered over the sample and very high angle, incoherently scattered electrons (Rutherford scattering) are collected with an annular dark-field detector. The number of electrons scattered depends directly on the atomic number (Z-contrast) and atoms appear brighter in the resulting images. HAADF-STEM is performed on an FEI Titan 80-300.

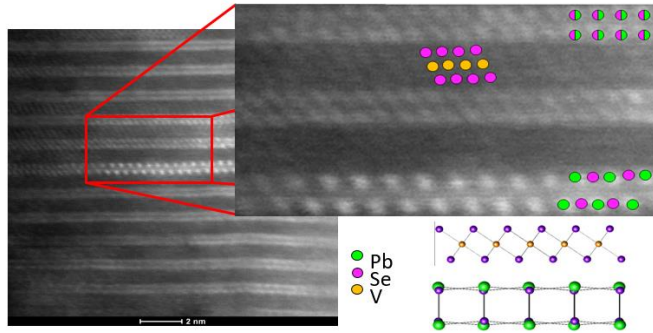


Figure II.6. HAADF-STEM images of $(\text{PbSe})_{1+\delta}\text{VSe}_2$ shows alternating layers of PbSe and VSe_2 with turbostratic disorder.

Transport Property Measurements

In-plane resistivity and Hall effect measurements were taken on a custom-built instrument using the van der Pauw technique.⁸ The van der Pauw method allows for the electrical characterization of arbitrary shaped lamellae, assuming the lamella meets three criteria:

1. The lamellae is approximately two-dimensional,
2. The lamellae is free of isolated pin-holes,
3. The electrical contacts are an order of magnitude smaller in area than the lamellae, and ideally as small as possible.

For our purposes, a cross-shaped geometry was used in order to allow for uniform current (Figure II.7). Samples are deposited through a cross-shaped shadow mask and collected on a fused silica substrate. Copper leads are contacted to the sample with indium at each point of the cross. For resistivity measurements, voltage leads are contacted at adjacent points along with current leads. A known current is applied and the resulting voltage is

measured. This measurement is conducted in all 8 possible configurations allowing for an average resistivity to be calculated:

$$\rho = \frac{\pi d}{\ln 2} \frac{R_{AB,CD} + R_{BC,DA}}{2} f \quad (3)$$

Where d is the film thickness, R is the sheet resistance, and f is the symmetry constant for the cross pattern.

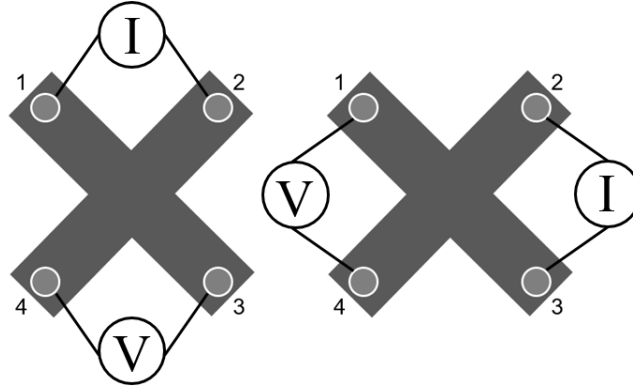


Figure II.7. Two of the eight possible lead combinations used in order to measure in-plane electrical resistivity.

Hall effect measurements place voltage leads at opposite corners of the cross and the current at the remaining two corners (Figure II.8). A current is sourced across the two leads and a magnetic field is applied in the out-of-plane direction, the moving electrons experience a Lorentz force. The direction of this force is governed by the “right-hand rule” for electrons and the “left-hand rule” for holes. This induces a separation of negatively charged and positively charged particles. This induced voltage is then measured. The Hall coefficient is then calculated using the Hall voltage, V_H , the applied current, I , applied magnetic field, B , and the thickness of the film:

$$R_H = \frac{V_H d}{IB}. \quad (4)$$

Under the assumption that the conducting band in the film is singular and rigid then a carrier concentration can be calculated:

$$V_H = \frac{IB}{ned} \quad (5)$$

where n is the carrier concentration and e is the elemental charge of the carrier.

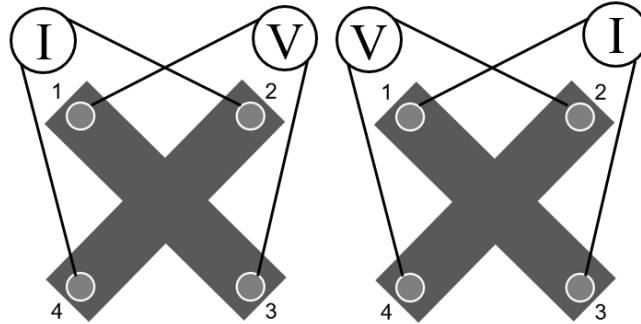


Figure II.8. Two of the possible four combinations used to measure the Hall coefficient.

Bridge

The technique explained throughout this chapter are employed throughout the remainder of this dissertation. In order to understand what follows it is imperative that one understands the techniques by which these materials are analyzed. These techniques are used to provide insight into the structure of these of heterostructures and their electrical behavior.

CHAPTER III
CHARGE DENSITY WAVE TRANSITION IN $(\text{PbSe})_{1+\Delta}(\text{VSe}_2)_N$
WITH $N = 1, 2, \text{ AND } 3$

Authorship Statement

This work appeared in *Chemistry of Materials* in 2017, volume 29, issue 13, pages 5646 – 5653. I am the primary author of this work. Matti B. Alemayehu and Matthias Falmbigl assisted with sample synthesis. Matthias Falmbigl also assisted with diffraction analysis. Marco Esters performed DFT calculations. Suzannah R. Wood assisted in figure generation. David C. Johnson is my advisor and consulted in preparation of this manuscript. Reprinted with permission from Charge Density Wave Transition in $(\text{PbSe})_{1+\delta}(\text{VSe}_2)_n$ Compounds with $n = 1, 2, \text{ and } 3$ Omar K. Hite, Matthias Falmbigl, Matti B. Alemayehu, Marco Esters, Suzannah R. Wood, and David C. Johnson *Chemistry of Materials* **2017** 29 (13), 5646-5653. Copyright 2017 American Chemical Society.

Introduction

The isolation of graphene¹ and the discovery that its properties differ from those of bulk graphite has led to a surge of research on single layer and very thin layers of quasi-two-dimensional systems such as h-boron nitride (h-BN)^{2,3} and transition metal dichalcogenides⁴ and their heterostructures⁵ in a search for emergent properties not present in the bulk constituents. For MoS_2 a transition was observed from an indirect to a direct band gap semiconductor as the materials dimensions are reduced from bulk to a single sheet.⁶ It has been shown computationally that SnS, SnSe, GeS, and GeSe have increased band gaps as the number of layers is reduced from the bulk to monolayer.⁷ A

similar trend in band gaps is seen for h-BN, where the bulk 4.0 eV band gap increases to a 4.6 eV band gap in the monolayer.⁸ Emergent properties have also been observed in heterostructures,^{9–12} including ultrafast charge transfer in MoS₂/WS₂ consistent with a type II band alignment having spatially direct absorption, but spatially indirect emission.¹³ Other examples include long-lived interlayer excitons in a MoSe₂-WSe₂ heterostructure with experimentally observed type II band alignment,¹⁴ and epitaxial single-layers of MoS₂ on a Au(111) surface showing a dramatic change in their band structure around the center of the Brillouin zone.¹⁵

The majority of the systems being investigated are semiconducting because isolation of single sheets of metallic systems has been challenging as they are not stable in air.¹¹ There are a number of interesting properties in metallic systems, however, that are being explored as a function of thickness towards the 2D limit, including superconductivity, and charge density waves (CDW). It has been demonstrated that the onset temperature of superconductivity in 2H-NbSe₂ decreases as the number of NbSe₂ layers is decreased.^{16–18} Studies on mechanically exfoliated TiSe₂ have shown that as thickness of the exfoliated film is decreased the onset temperature of the CDW is increased.²⁶ Others have shown that the onset temperature of the CDW in TaSe₂ is decreased as the thickness of the mechanically exfoliated film is decreased.²⁷ It was shown both computationally and experimentally, that the ferromagnetism of VS₂ is enhanced as the VS₂ approaches the monolayer limit.^{19,20} VSe₂ exhibits a CDW transition in the bulk²¹ but there is disagreement on how this CDW changes as the number of VSe₂ layers are reduced in this n-type metal.^{22–25} The onset of the CDW in thin layers of VSe₂ prepared via liquid exfoliation transitions from 100 K²¹ in the bulk single crystal to 135 K

as thickness is reduced to 4-8 trilayers of VSe₂.²² An opposite trend has been reported for micromechanically exfoliated nanoflakes, however, where the onset temperature decreases to 81 K at the lowest thickness measured, 11.6 nm.²³ The thin nanoflakes are n-type conductors, as is bulk VSe₂, but the carrier concentration increases as the nanoflake thickness is decreased. These exfoliation techniques were not able to precisely control the thickness of the VSe₂ flakes nor were they able to reach the monolayer limit. Studies of [(SnSe)_{1.15}]_m(VSe₂)_n prepared by annealing designed precursors have shown that compounds with a single layer of VSe₂ separated by *m* layers of SnSe are p-type metals with a CDW that depends on the thickness of SnSe and exhibit a dramatic change in electrical resistivity and charge carrier concentration at the CDW transition temperature.²⁸ In contrast, increasing the VSe₂ layer thickness to two or more layers results in low temperature n-type metals and the suppression of the pronounced effect in transport properties at the CDW transition temperature similar to bulk VSe₂.²⁵ These compounds grown at low temperatures from designed precursors have been called ferecrystals, from the Latin root *fer-* meaning “almost”, due to their extensive turbostratic disorder. The influence of surface contaminations and/or the substrate on the charge density wave transition has not been explored or discussed in the literature.

In order to explore the impact of neighboring layers on the CDW of VSe₂ heterostructures, we replaced SnSe with the isovalent PbSe in a sequence of (PbSe)_{1+δ}(VSe₂)_n compounds. The compounds were prepared using modulated elemental reactant precursors and electrical properties were measured as a function of temperature. Diffraction data is consistent with *n* layers of VSe₂ separating a single rock salt structured PbSe layer. The *n* = 1 ferecrystal is metallic with a positive Hall coefficient indicative of

p-type conduction, while for the $n = 2$ and 3 compounds, the Hall coefficient switches sign, indicating a change of the majority carriers to electrons equivalent to bulk VSe_2 .²¹ Both the resistivity and Hall coefficient of the $n = 1$ compound increase as the temperature is lowered below 100 K, becoming a factor of 3.7 and 8 higher, respectively, by 20 K. This anomaly is very similar to the CDW transition observed in $([\text{SnSe}]_{1.15})_m\text{VSe}_2$ compounds. The temperature dependencies of the resistivity and Hall coefficient of the $n = 2$ and 3 compounds are very similar to bulk VSe_2 . There is a change in the slope of the resistivity and the Hall coefficient as a function of temperature at 100 K, suggesting that a CDW similar to the bulk occurs if there is more than one VSe_2 layer. The different sign of the Hall coefficient and large changes in resistivity and Hall coefficient indicates, the electronic structure of $(\text{PbSe})_{1+\delta}\text{VSe}_2$ with a single VSe_2 layer is distinctly different than heterostructures with thicker VSe_2 layers. The changes in properties when PbSe replaces SnSe , although only an isovalent substitution, indicates that the interactions between constituents can be used to tune the electrical properties of heterostructures.

Experimental Methods

The ferecrystalline compounds, $(\text{PbSe})_{1+\delta}(\text{VSe}_2)_n$ where $1 \leq n \leq 3$, were synthesized using the modulated elemental reactants (MER) technique.²⁹ Precursors were prepared by sequentially evaporating elemental sources of Pb (99.995%, Alfa Aesar), V (99.8%, Alfa Aesar), and Se (99.999%, Alfa Aesar) on (100) oriented Si wafers in specific sequences for each compound in a custom built high-vacuum physical vapor deposition chamber, details provided elsewhere.²⁹ Precursors were annealed at 250 °C for 1 hour in a N_2 glove box with a concentration of oxygen below 0.6 ppm. Methods used to

determine the optimal annealing temperatures for converting the precursors into the desired product are described in the literature.²⁴

Specular X-ray diffraction (XRD) was performed to determine the *c*-axis lattice parameter of the $(\text{PbSe})_{1+\delta}(\text{VSe}_2)_n$ compounds on a Bruker D8 Discover diffractometer equipped with Cu K_α radiation ($\lambda = 0.15418$ nm), Göbel mirrors, and Bragg-Brentano θ - 2θ optics geometry. In-plane XRD of the $n = 1$ and 3 compounds were taken at the Advanced Photon Source, Argonne National Laboratories (BM 33-C) ($\lambda = 0.12653$ nm). In-plane XRD of the $n = 2$ compound was done on a Rigaku SmartLab diffractometer equipped with Cu K_α radiation.

Compositional analysis was performed with electron probe micro-analysis (EPMA) on a Cameca SX-100. Accelerating voltages of 7.5, 13, and 18 keV were used and overall composition was calculated as a function of the three accelerating voltages using the technique for thin films developed by Donovan *et al.*³⁰

Samples were prepared for High-angle Annular Dark-field Scanning Transmission Electron Microscopy (HAADF-STEM) on a FEI Helios 600 dual-beam using a technique described by Schaffer *et al.*³¹ HAADF-STEM was taken on a FEI Titan 80-300 FEG-TEM at the Center for Advanced Materials Characterization in Oregon (CAMCOR).

Electrical resistivity and Hall measurements were determined using the van der Pauw technique³² in a temperature range of 20 - 295 K. Samples were prepared on fused Quartz crystal slides in a $1 \text{ cm} \times 1 \text{ cm}$ cross geometry. Further details on how temperature-dependent resistivity and Hall measurements were conducted are described elsewhere.³³

Results and Discussion

Precursors for each of the compounds $(\text{PbSe})_{1+\delta}(\text{VSe}_2)_n$ with $n = 1 - 3$ were prepared by depositing sequences of elemental layers where the elemental Pb|Se and V|Se bilayers were calibrated to match the composition of the desired product such that each Pb|Se bilayer formed two (001) planes of rock salt structured PbSe and each V|Se bilayer formed a single Se-V-Se dichalcogenide structured trilayer. The calibration was a three-step process. The composition of the Pb|Se and V|Se bilayers were calibrated by preparing a set of samples with a fixed metal thickness and varying thicknesses of Se, and determining the composition with EPMA. The resulting graphs of Se:Pb and Se:V ratio versus Se layer thickness were interpolated to obtain the ratio of thicknesses that resulted in the respective desired compositions. To determine the thickness ratio between the Pb and V layers to obtain the targeted misfit parameter of 1.11, a set of samples were prepared by depositing Pb|Se|V|Se sequences where the thickness of the Pb|Se bilayer at the previously determined Pb/Se thickness ratio was scaled while holding the thickness and thickness ratio of the V|Se bilayer constant. The change in composition as a function of the thickness of the Pb|Se bilayer was interpolated to find the thickness required to obtain the desired misfit parameter. The last step was to hold the Pb|Se, V|Se and Pb|Se/V|Se ratios constant while scaling the total thickness, using the quality of the resulting annealed sample diffraction patterns to determine the thickness such that each Pb|Se bilayer forms two (001) planes of rock salt structured PbSe and the V|Se layer forms a single Se-V-Se dichalcogenide structured trilayer. X-ray diffraction (XRD) scans were taken on the annealed precursors in order to determine the total thickness that yields

maximum peak intensity and minimum peak FWHM in the resulting product, as described previously by Atkins *et al.*³⁴

Sequences with the nanoarchitecture of the desired products, for example the sequence of layers Pb|Se-V|Se-V|Se for $(\text{PbSe})_{1+\delta}(\text{VSe}_2)_2$, were repeatedly deposited until the desired total sample thickness of about 45 nm was reached. These precursors were annealed at 250 °C to self-assembly of the targeted products. This temperature was determined using the approach of Atkins *et al.*³⁴ Figure III.1 shows the specular XRD patterns of the $n = 1 - 3$ compounds. Each peak can be indexed to a $00l$ reflection of the $(\text{PbSe})_{1+\delta}(\text{VSe}_2)_n$ compounds indicating crystallographically aligned layers with the c -axis perpendicular to the substrate. Using Bragg's Law, the c -axis lattice parameters were determined to be 1.225(1) nm, 1.835(3) nm, and 2.445(4) nm for $n = 1, 2,$ and $3,$ respectively. The change in thickness as n is increased yields the thickness of a VSe_2 layer from the slope and the thicknesses of the PbSe layer from the intercept. The PbSe bilayer thickness of 0.617(5) nm is slightly thicker than the 0.607-0.612 nm found in a series of $[(\text{PbSe})_{1.14}]_m(\text{NbSe}_2)_n$ compounds³³ and the 0.61(1) nm found for the PbSe bilayer thickness in $(\text{PbSe})_{1+\delta}(\text{TiSe}_2)_n$ ferecrystals.³⁵ The thickness of the VSe_2 trilayer is 0.610(2) nm, which is slightly thicker than the 0.596(1) nm reported for the VSe_2 sub-unit in $(\text{SnSe})_{1.15}(\text{VSe}_2)_n$ compounds.¹³

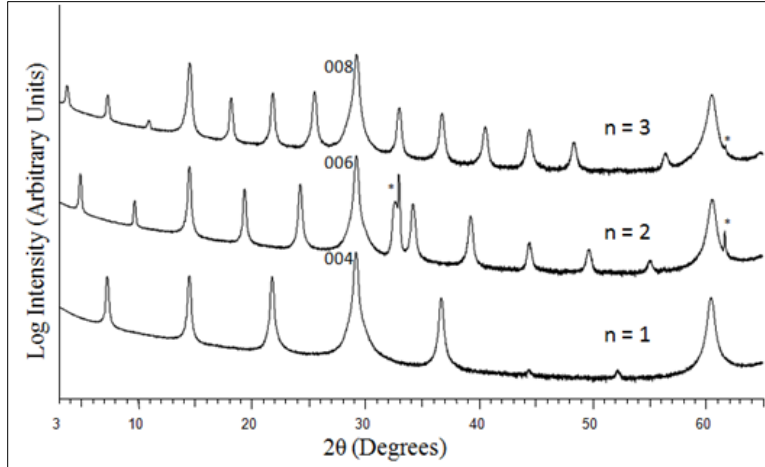


Figure III.1. X-ray diffraction of $(\text{PbSe})_{1+\delta}(\text{VSe}_2)_n$ for $n = 1-3$ using Cu $K\alpha$ radiation ($\lambda = 0.15418$ nm). Maxima can be indexed to 00l reflections of the respective compound, with the appropriate index given the figure for the reflection at the $\sim 29^\circ$ 2θ . Asterisks (*) indicate substrate or stage reflections.

A Rietveld refinement of the $n = 1$ out-of-plane XRD was performed to determine relative positions of the atomic planes along the c -axis. Figure III.2 contains the fitted intensities along with a schematic of the atomic plane positions compared to those previously determined for $(\text{SnSe})_{1.15}\text{VSe}_2$.¹⁴ The refinement revealed puckering of the PbSe layer, which separates the Pb and Se atomic planes from one another by 0.0367(2) nm. This puckering is typical for bilayers of rock salt structured constituents and has been seen previously in both SnSe and PbSe containing misfit layered compounds and ferecrystals.^{25,36} The magnitude of this puckering is within the range reported previously, 0.020 nm to 0.065 nm, in the relatively few atomic level structures that have been previously determined.³⁷⁻⁴³ It is larger than the puckering observed in $(\text{PbSe})_{1.00}\text{MoSe}_2$ (0.025(1) nm) and $(\text{PbSe})_{0.99}\text{WSe}_2$ (0.021(1) nm) ferecrystals⁴⁴ but smaller than the 0.062(5) nm found in the $(\text{PbSe})_{1.18}(\text{TiSe}_2)_2$ ferecrystal.⁴⁵ The extent of the puckering may be related to the amount of charge transfer between the constituents, as a negatively charged environment in the dichalcogenide layer would attract the

positive Pb and repel the negative Se ions. The gap between the PbSe and VSe₂ layers was found to be 0.300(5) nm which is very similar to the 0.306(5) nm observed in (SnSe)_{1.15}VSe₂.²⁵ The distance between V and Se planes along the *c*-axis in VSe₂ was found to be 0.153(2) nm, which is the same as the 0.154(2) nm reported for the (SnSe)_{1.15}(VSe₂) compound.²⁵

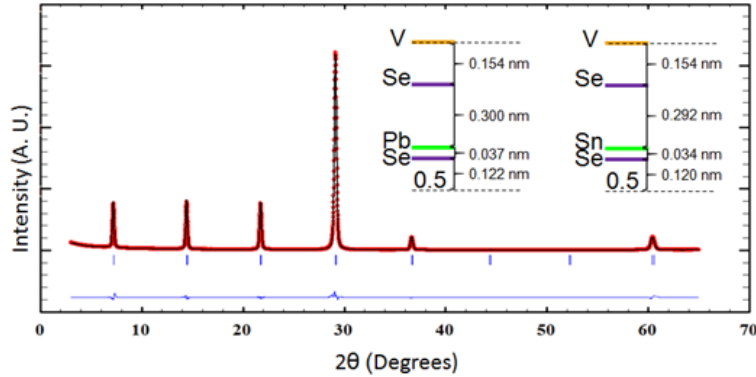


Figure III.2. Experimental, calculated, and difference patterns from the Rietveld refinement of the positions of atomic planes along the *c*-axis of (PbSe)_{1+ δ} VSe₂. The inset figures contain the interplane distances obtained for (PbSe)_{1+ δ} VSe₂ and those for (SnSe)_{1.15}VSe₂ are presented for comparison.²⁵

In-plane *hk0* XRD scans were collected on all compounds (Figure III.3), and the reflections in each scan can be indexed as either reflections from a hexagonal in-plane structure for VSe₂ or reflections from a square in-plane structure for PbSe. The reflections for each constituent can easily be distinguished as relative intensities of the VSe₂ peaks (for example the (110) reflection) proportionally increase relative to the PbSe reflections (for example the (220) reflection) as the number of VSe₂ layers increase. The in-plane *a*-axis lattice parameter for the VSe₂ constituent remains the same within error and are 0.343(1) nm, 0.346(5) nm, and 0.339(1) nm for *n* = 1, 2, and 3, respectively. These values are all within the uncertainty of the 0.334(8) nm²⁸ and 0.341(1) nm[24] previously reported for (SnSe)_{1.15}VSe₂. The square in-plane *a*-lattice parameter of the

PbSe constituent additionally remains the same with values of 0.605(1) nm, 0.604(3) nm, and 0.607(1) nm for $n = 1, 2,$ and $3,$ respectively. All of these values are slightly smaller than the 0.6122(3) nm reported for $(\text{PbSe})_{1.18}\text{TiSe}_2$ ⁴⁵ and the 0.618(2) nm reported for in $(\text{PbSe})_{1.00}\text{MoSe}_2$ and $(\text{PbSe})_{0.99}\text{WSe}_2$. The small changes in the in-plane lattice parameters of the constituents results in a misfit parameter that varies as the thickness of the VSe_2 constituent increases. The misfit parameter, $(1+\delta)$, was 1.11(1) for the $n = 1$ compound, 1.14(2) for the $n = 2$ compound and 1.08(1) for the $n = 3$ compound. The values for the misfit fall within the range of misfit values reported in the literature (0.99 to 1.29).^{39-41,46-59}

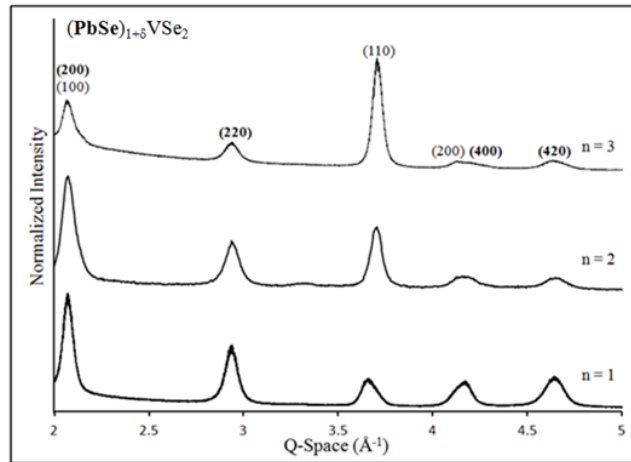


Figure III.3. Normalized in-plane X-ray diffraction patterns of $(\text{PbSe})_{1+\delta}(\text{VSe}_2)_n$ for $n = 1-3$. Scans are individually normalized to the highest intensity reflection. The numbers above the $n = 3$ scan reflections are the indices using hexagonal VSe_2 and square PbSe (bold font).

HAADF-STEM images of $(\text{PbSe})_{1.11}(\text{VSe}_2)$ show a regular repeating structure of a single plane of VSe_2 separated by single planes of PbSe . A representative image is shown in Figure III.4. The visible areas aligned along a zone axis support the interpretation of the XRD data, as zone axes consistent with a distorted rocksalt structure are observed for PbSe layers and zone axis images of the VSe_2 layer are consistent with

octahedral coordination of the vanadium atoms, which are situated between Se planes. The disorder in the orientation of the layers from layer to layer indicates that there is no long-range order. This is consistent with the XRD data, which show that there is long range order due to alternating VSe₂ and PbSe layers along (00*l*), that each layer is crystalline with distinct (*hk0*) diffraction from each of the constituents, and that there is no common in-plane axis between the constituents. The crystalline nature of each of the constituent layers with lack of long-range order between planes is a consequence of the mechanism of the self-assembly from the precursor.⁶⁰

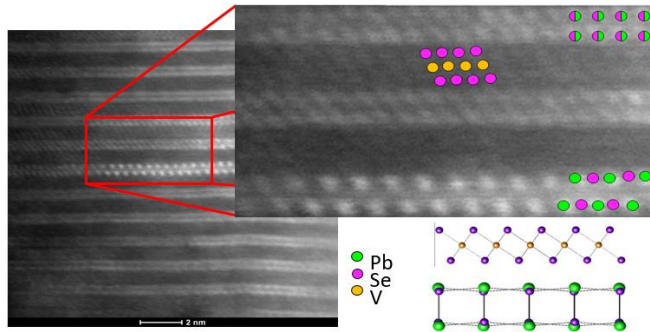


Figure III.4. HAADF-STEM images of (PbSe)_{1.11}VSe₂ contain alternating PbSe bilayers and VSe₂ trilayers. The different crystallographic orientations of the PbSe layers are a result of turbostratic disorder. The expanded image shows a PbSe layer with [100] crystallographic orientation (top) and a [110] crystallographic orientation (bottom). The VSe₂ layer is consistent with octahedral coordination of V.

Temperature dependent resistivity measurements were conducted on all samples and the data is plotted in Figure III.5 along with data previously reported for bulk VSe₂.²¹ The absolute value of the room temperature resistivity and the temperature dependence of the resistivity above 150 K for all samples indicate that they are metallic. The magnitude of the resistivity systematically decreases as the percentage of the metallic constituent VSe₂ is increased, which is consistent with conduction occurring primarily through the VSe₂ layer as observed in the analogous (PbSe)_{1.12}(NbSe₂)_n compounds.³³ The

temperature dependence of the $n = 3$ sample is similar to that of bulk VSe_2 , with a slightly decreased temperature dependence suggesting weaker electron-phonon scattering compared to bulk VSe_2 . The temperature dependence of the $n = 2$ sample shows a further decrease in the slope, suggesting even weaker electron-phonon scattering. The weaker electron-phonon scattering reflects the changes in phonon modes and phonon energies as the VSe_2 block is reduced in thickness. The $n = 2$ and 3 heterostructures both show a change in slope of the resistivity that is very similar to that seen as a result of a CDW in bulk VSe_2 . The temperature dependence of the $n = 1$ sample is distinctly different than bulk VSe_2 and the $n = 2$ and 3 heterostructures, with the resistivity abruptly increasing at approximately 110 K as temperature is lowered. The resistivity ultimately reaches a value of more than 5 times higher at 20 K than would be extrapolated from the high temperature behavior. The change in resistivity of $(\text{PbSe})_{1.11}\text{VSe}_2$ is very similar to that reported by Falmbigl *et al.* for $(\text{SnSe})_{1.15}(\text{VSe}_2)$,²⁵ which has been attributed to a charge density wave (CDW) based on resistivity, Hall coefficient and heat capacity measurements.⁶¹ The overall increase in resistivity in the $(\text{PbSe})_{1.11}\text{VSe}_2$ compound is approximately double that of the analogous SnSe compound, indicating that a higher percentage of the charge carriers are localized and/or that there is a significant difference in the change of the carrier mobility below the CDW. This may reflect structural differences at the interface between the constituents (in $n = 1$ the VSe_2 and PbSe layers alternate and for the other compounds PbSe is separated by 2 or 3 VSe_2 layers) or a different Fermi level caused by a difference in charge transfer between the SnSe (bulk E_g , 1.38 eV⁶²) or PbSe (bulk E_g , 0.23 eV⁶³) layer and the VSe_2 layers. The difference in charge transfer could be a consequence of the different misfit parameters

between the Sn and Pb compounds and/or due to different Fermi energies for the PbSe bilayer relative to the SnSe bilayer with respect to the monolayer of VSe₂.⁶⁴ A similar increase in charge transfer was seen when substituting PbSe for SnSe in NbSe₂ containing heterostructures.³³

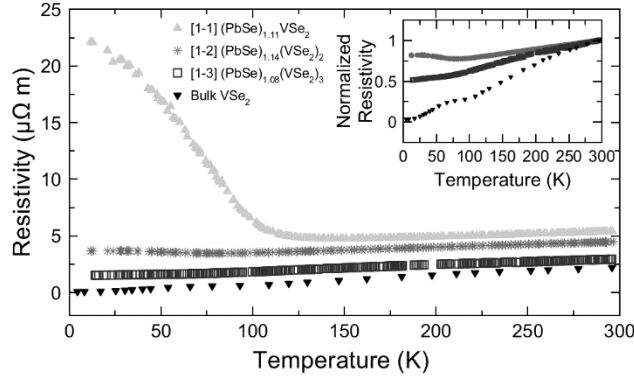


Figure III.5. Temperature-dependent resistivity of $(\text{PbSe})_{1+\delta}(\text{VSe}_2)_n$ for $n = 1-3$ and bulk VSe_2 .²¹ Resistivity normalized to room temperature resistivity for the $n = 2$ and 3 heterostructures and bulk VSe_2 is displayed in the inset to highlight the anomalies observed in the CDW of bulk VSe_2 .

Temperature dependent Hall measurements were conducted on all samples to provide further insight to the unusual resistivity behavior in $(\text{PbSe})_{1.11}\text{VSe}_2$, and the data obtained is plotted in Figure III.6 along with that measured for a single crystal of VSe_2 .²¹ The Hall coefficient for a single crystal of VSe_2 is negative along the entire temperature range, suggesting that electrons are the primary carrier, and has a change in slope at approximately 110 K that was attributed to a CDW.²¹ The $n = 3$ sample also has a negative Hall coefficient that decreases as temperature is decreased and has a change in slope at approximately the same temperature as the bulk single crystal. The $n = 2$ sample has a small positive Hall coefficient at room temperature but decreases with decreasing temperature with a slope similar to the bulk single crystal, becoming negative at ~ 230 K. It also has a change of slope at about 100 K. The change in sign of the Hall coefficient suggests that at least two bands are contributing to the electrical transport, which suggests

that the PbSe layer contributes to the conduction. And a similar result was found by Falmbigl *et. al.* investigating $([\text{Sn}_{1-x}\text{Bi}_x\text{Se}]_{1.15})_1(\text{VSe}_2)_1$ alloys.⁶⁵ The temperature dependence of the resistivity and Hall coefficient suggest that the $n = 2$ and 3 compounds are very similar to the bulk, in contrast to the properties measured on liquid and mechanically exfoliated VSe_2 thin layers.^{22,23} $(\text{PbSe})_{1.11}\text{VSe}_2$, however, has a positive Hall coefficient over the entire temperature range and, like $(\text{SnSe})_{1.15}\text{VSe}_2$ ²⁵ has an abrupt increase in the Hall coefficient at 110 K, the same temperature where the resistivity begins to increase. The Hall coefficient increases by about a factor of 8 as temperature is decreased to 20 K, and using the single conducting band approximation the change in carrier concentration shows that 1.06 holes per vanadium atom are localized over the CDW. This value is almost twice as large as of the analogous $(\text{SnSe})_{1.15}\text{VSe}_2$, which was reported at 0.54 holes per vanadium atom.⁶¹ This calculated change in carrier concentration accounts for most of the change in resistivity. The changes in the Hall coefficient and resistivity of the $n = 1$ sample as a function of temperature are consistent with a CDW transition.

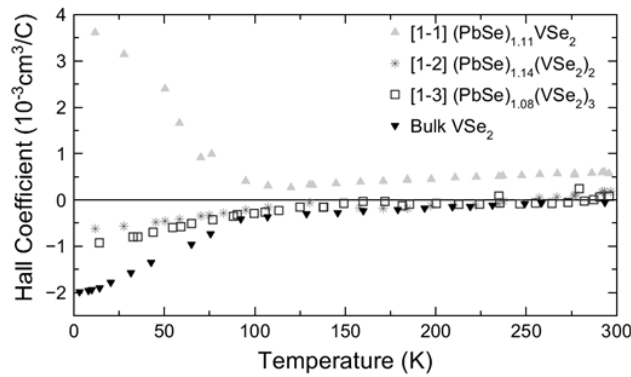


Figure III.6. Temperature dependence of the Hall coefficient for $(\text{PbSe})_{1+\delta}(\text{VSe}_2)_n$ $n = 1-3$ and bulk single crystal VSe_2 .²¹

Figure III.7 contains the temperature-dependent single conducting band carrier mobility calculated using $\mu = R_H/\rho$ for $(\text{PbSe})_{1.11}\text{VSe}_2$ prepared in this study as well as those of bulk VSe_2 , $(\text{SnSe})_{1.15}\text{VSe}_2$ and $(\text{BiSe})_{1+\delta}\text{VSe}_2$. The single band mobility values for the $n = 2$ and 3 compounds were not calculated due to the change in sign of the Hall coefficient in the $n = 2$ compound, which indicates that more than a single band is involved in conduction. The room temperature mobility of the $n = 1$ compounds is very similar, suggesting that the VSe_2 layers are the primary conductor in the compounds.

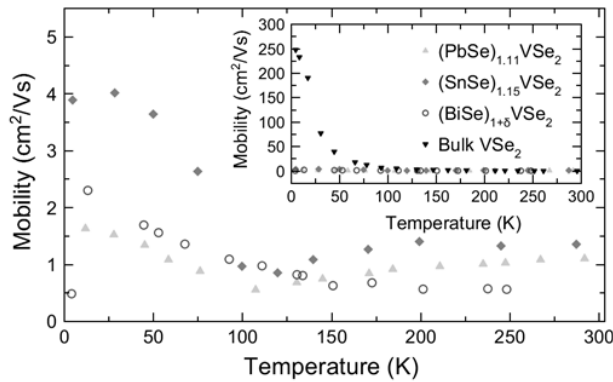


Figure III.7. Temperature dependent single conducting band carrier mobility of $(\text{PbSe})_{1.11}\text{VSe}_2$, $(\text{SnSe})_{1.15}\text{VSe}_2$,²⁴ and $(\text{BiSe})_{1+\delta}\text{VSe}_2$.⁶⁶ The inset compares the mobility of the three compounds to bulk VSe_2 .²¹

While the changes in mobility of the holes in $n = 1$ compounds as temperature is lowered are all much smaller than observed for the electrons in bulk VSe_2 , there is a larger increase in mobility as the temperature is lowered in $(\text{SnSe})_{1.15}(\text{VSe}_2)$ (a factor of 3) than in either $(\text{PbSe})_{1.11}\text{VSe}_2$ or $(\text{BiSe})_{1+\delta}\text{VSe}_2$ (a factor of 1.2). There is a small decrease in mobility at the onset of the CDW in both $(\text{PbSe})_{1.11}(\text{VSe}_2)$ and $(\text{SnSe})_{1.15}(\text{VSe}_2)$, which may be an indicator of CDW formation in these compounds as this feature is not seen in $(\text{BiSe})_{1+\delta}\text{VSe}_2$. The differences in the changes in carrier concentration and mobility of carriers in $(\text{PbSe})_{1.11}\text{VSe}_2$ compared to $(\text{SnSe})_{1.15}\text{VSe}_2$ indicates that CDW formation is a complex process and is sensitive to the degree of charge transfer in these systems.

The change in electrical resistivity and the sign of the Hall coefficient as the number of VSe₂ layers in the repeat unit is increased prompted us to perform DFT calculations on both a single layer and a double layer of VSe₂. The calculations were done using the bulk 1T crystal structure of VSe₂, separating either the single layer or the double layers from one another by vacuum, and allowing the system to relax. The resulting band structures (contained in the supplemental information) are similar to those reported previously^{67,68} and indicate that 1T-VSe₂ should be a metal. Unlike what was reported for MoS₂ where the Mo has trigonal prismatic coordination,⁶⁹ there are only very small differences in the band structure calculated for the single and double layer of VSe₂ due to the octahedral local coordination of vanadium atoms and the 1T stacking. Changing the position of the Fermi level in either the single or double layer of VSe₂ results in changes in the density of states, but the calculations do not indicate that one or the other have a distinct feature in the band structure that makes them more likely to have a charge density wave transition. Figure III.8 contains a plot of the temperature dependence of the Hall coefficients of (PbSe)_{1.11}VSe₂, (SnSe)_{1.15}VSe₂,²⁵ and (BiSe)_{1+δ}VSe₂,⁶⁶ all of which contain single VSe₂ trilayers separated by a monochalcogenide bilayer, and the temperature dependence of the Hall coefficients of bulk VSe₂.²¹ The compounds containing SnSe and PbSe are distinctly different from bulk VSe₂ and the compound containing BiSe. However, resistivity and Hall data reported by Alemayehu *et al.* for a series of (GeSe₂)_m(VSe₂)_n heterostructures⁷⁰ indicates that CDW's occur for a number of different n values, suggesting that a monolayer of VSe₂ is not a necessary condition for the formation of a CDW. The observed differences in transport properties cannot be explained as only being due to a structurally isolated VSe₂

monolayer, as all of the ferecrystalline compounds contain isolated monolayers of VSe_2 and $(\text{GeSe}_2)_m(\text{VSe}_2)_n$ contains isolated blocks of n VSe_2 layers. The electronic structure is heavily influenced by the position of the Fermi level, which can be altered in ferecrystals without purposefully introducing local impurities in the VSe_2 layers via charge transfer from the adjacent constituent, a phenomenon referred to as modulation doping. The observed differences in transport properties, however, cannot be explained solely by significant charge transfer between constituents, but that other factors like electron localization need to be taken into consideration.

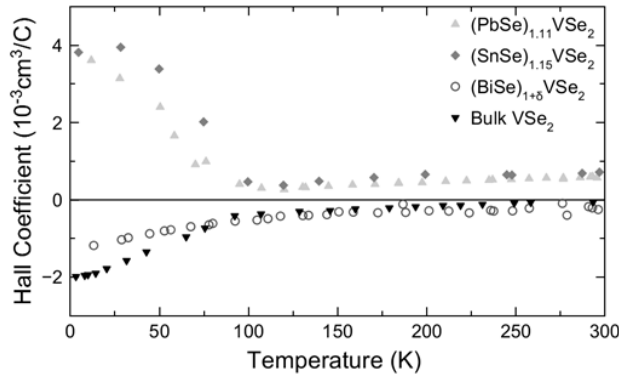


Figure III.8. Hall coefficients for different $(\text{MSe})_{1+\delta}(\text{VSe}_2)$ ($\text{M} = \text{Sn}, \text{Pb}, \text{Bi}$) ferecrystals and bulk VSe_2 .²¹

Conclusions

The compounds $(\text{PbSe})_{1+\delta}(\text{VSe}_2)_n$ with $n = 1 - 3$ were prepared from designed precursors. Diffraction and electron microscopy data indicate that the compounds consist of bilayers of PbSe separated from one another by n Se-V-Se trilayers. All the compounds are metallic, with discontinuities in the temperature dependence of their resistivity and Hall coefficients, suggestive of charge density waves. Both the carrier type and the charge density wave transition of the compound with $n = 1$ (holes, abrupt change in resistivity) were distinctly different than found for the $n = 2$ and 3 compounds (electrons, change in slope of resistivity). The increased change of the resistivity and Hall

coefficient through the charge density wave transition for $(\text{PbSe})_{1.11}\text{VSe}_2$ relative to $(\text{BiSe})_{1+\delta}\text{VSe}_2$ and bulk VSe_2 demonstrates the importance of the companion layer in controlling properties. The extent of charge transfer between constituent layers, the magnitude of the structural misfit at the interface between constituents, the magnitude of electron-electron correlation, and the degree of isolation of the single VSe_2 layers from one another may all contribute to the magnitude and the transition temperature of the charge density wave.

Bridge

In order to determine if the charge density wave reported in $(\text{SnSe})_{1.15}\text{VSe}_2$ was unique to a SnSe-VSe_2 heterostructure, SnSe was replaced with the isoelectronic PbSe . It was found that $(\text{PbSe})_{1.11}\text{VSe}_2$ has a higher resistivity increase as temperature is lowered than the analogous SnSe heterostructure. It has been previously reported that in $(\text{MSe})_{1+\delta}\text{NbSe}_2$, $\text{M} = \text{Sn, Pb, PbSe}$ donated more charge to NbSe_2 than SnSe . This increase in charge transfer from PbSe to VSe_2 leads to an enhanced charge density wave as evidenced by resistivity and Hall coefficient measurements. To further investigate the effect of charge transfer on the charge density wave in VSe_2 , PbSe was replaced with BiSe , which should donate up to one further electron. The work done on $(\text{BiSe})_{1+\delta}\text{VSe}_2$ is discussed in the following chapter.

CHAPTER IV
TRANSPORT PROPERTIES OF VSE₂ MONOLAYERS SEPARATED BY
BILAYERS OF BISE

Authorship Statement

This work appeared in Journal of Materials Research in 2015, volume 31, issue 7, pages 886 - 992. I am the primary author of this work. Mike Nellist assisted with sample synthesis. Matthias Falmbigl and Mike Nellist also assisted with diffraction analysis. Jeffery Ditto collected electron microscopy data and images. David C. Johnson is my advisor and consulted in preparation of this manuscript.

Introduction

Research on two dimensional atomic crystals and heterostructures has grown enormously in the last decade, sparked by the properties of monolayers being different than properties of the bulk, to become one of the leading sub-fields in condensed matter physics and materials science.^{1,2} The wavefunction of a monolayer extends beyond its surface, decaying exponentially into the materials (or vacuum) both above and below it. The surface (if vacuum) or interface (in a heterostructure) interactions result in structural distortions, new phenomena, new physics and challenging chemistry. For example, MoS₂ transitions from an indirect to a direct band gap semiconductor,³ the onset temperature of superconductivity in 2H-NbSe₂ decreases as the number of NbSe₂ layers is decreased and in extremely thin samples of NbSe₂ superconductivity no longer persists,⁴ and ultrathin layers of PbSe distort from the bulk rock salt structure, with both a puckering distortion in and a pairing interaction between layers.⁵ While stability issues have limited the ability to prepare monolayer films of many materials via a cleaving approach,⁶ the ability to

reasonably predict the structure of potential heterostructures made from 2-D atomic constituents makes them attractive candidates for theoretical investigations that predict properties as a function of nanoarchitecture. There are already quite a few predictions of interesting properties reported in the literature.^{7,8}

The interaction at the interfaces between monolayers also provides interesting experimental opportunities to both tailor existing properties and potentially obtain properties not found in either of the constituent materials. It has already been shown that the properties of graphene strongly depend on the substrate on which it is grown.⁹ Ultra low thermal conductivity results from rotational disorder between layers.¹¹ Several reports of samples containing thin layers of VSe₂ differ with respect to the effect of layer thickness on the charge density wave that occurs at 100K in the bulk single crystals.¹² If prepared via liquid exfoliation, the CDW increases to 135 K¹³ as thickness is reduced to 4-8 trilayers of VSe₂. In VSe₂ micromechanically exfoliated nanoflakes, the CDW onset temperature was reported to decrease to 81 K at 11.6 nm, the lowest thickness measured.¹⁴ In turbostratically disordered single layers of VSe₂ separated by layers of SnSe prepared using a self-assembly approach, a CDW has been reported that has an opposite carrier type (holes) than the bulk (electrons),¹⁵ which does not occur when the VSe₂ thickness is increased beyond a monolayer.¹⁶ An understanding of how to control properties based on the interaction between layers is developing as more heterostructures and their properties are reported.

The change in carrier type and CDW reported for SnSe-VSe₂ heterostructures relative to bulk VSe₂ prompted us to prepare a new heterostructure consisting of alternating layers of BiSe and VSe₂. BiSe was chosen as a companion layer due to the

prior literature on BiSe-dichalcogenide misfit compounds, which showed that the transport properties of $(\text{BiSe})_{1.10}\text{NbSe}_2$ and $(\text{BiSe})_{1.09}\text{TaSe}_2$ are very similar to those of the analogous Sn compound.¹⁷ Localization of the additional valence electron of the Bi within the BiX subsystem has been proposed as a reason for the similar transport properties.¹⁸ The charge is localized in Bi-Bi bonds at anti-phase boundaries, which are thought to systematically occur due to the mutual accommodation of the lattice mismatch to form a commensurate structure.^{17,19} We find that the VSe_2 layer(s) in a superlattice containing single layers of BiSe and VSe_2 is structurally similar to what was previously reported for $[(\text{SnSe})_{1.15}]_1(\text{VSe}_2)_1$. The in-plane diffraction pattern and layer positions from Rietveld refinement of the specular diffraction pattern are consistent with BiSe having a rocksalt type structure. HAADF-STEM images, however, reveal extensive turbostratic disorder and the presence of anti-phase boundaries seen previously in BiSe containing misfit layer compounds. This suggests that the presence of anti-phase boundaries are not dependent on forming an ordered long range distortion of both constituent structures to form a coherent crystal. Despite the similarity of the structure of the VSe_2 single layers, no CDW is observed in the BiSe- VSe_2 heterostructure. The BiSe- VSe_2 heterostructure has a negative Hall coefficient, indicating n-type carriers predominate, which is similar to bulk VSe_2 .¹² Since $[(\text{SnSe})_{1.15}]_m(\text{VSe}_2)_1$ heterostructures have positive Hall coefficients, indicating that holes are the predominant carrier, the change of carrier type in the BiS - VSe_2 heterostructure prevents formation of the CDW.

Experimental

The compound $[(\text{BiSe})_{1+\delta}]_1(\text{VSe}_2)_1$ was synthesized using the modulated elemental reactants (MER) technique in a custom built high-vacuum physical vapor

deposition chamber.²⁰ Elemental sources of Bi (99.995%) and V (99.8%), obtained from Alfa Aesar, were evaporated at a rate of 0.4 Å/s using Thermionics 3kW electron-beam guns onto (100) oriented Si wafers. Se (99.999%) was deposited at a rate of 0.5 Å/s utilizing a Knudsen effusion cell. Rates were monitored using quartz crystal monitors positioned 25 cm above the elemental sources. A custom-made LabView program controlled the rotation of the carousel with the mounted Si wafers over the desired elemental sources to obtain the desired deposition sequence. Pneumatically powered shutters allow a precise control of atomic composition based on the opening time of the shutter. The Se-Bi-Se-V layering sequence was repeated until a total thickness of 45-55 nm of the modulated precursor was obtained. To determine optimal annealing conditions for self-assembly the precursors were annealed between 200 °C - 550 °C for 20 minutes. X-ray diffraction, discussed below, was used to determine optimal temperature.

To form the ferecrystalline products, the precursors were annealed for 20 minutes in a N₂ glove box with oxygen content below 0.6 ppm and the resulting products characterized using X-ray scattering. X-ray diffraction (XRD) were performed to determine repeat unit thickness of the film. XRD measurements were performed on a Bruker D8 Discover diffractometer equipped with Cu K α radiation, Göbel mirrors, and Bragg-Brentano optics geometry. Locked coupled θ -2 θ scans were taken from 0-9° 2 θ for XRR and 5-65° 2 θ for XRD. Samples were prepared for STEM on a FEI Helios 600 dual-beam using methods developed by Schaffer *et al.*²¹ High-angle Annular Dark-field Scanning Transmission Electron Microscopy (HAADF-STEM) images were taken on a FEI Titan 80-300 FEG-TEM at the Center for Advanced Materials Characterization in Oregon (CAMCOR).

The Van der Pauw technique²² was used to determine temperature-dependent resistivity and Hall coefficient of the sample in a temperature range of 20-295 K. Samples for electrical resistivity and Hall measurements were deposited on fused Quartz crystal slides. Using a shadow mask, a 1 cm x 1 cm cross geometry was deposited and indium contacts were placed on the points of the cross. By sourcing a current between two adjacent contacts and measuring the voltage on the remaining two contacts, an average sheet resistance at a fixed temperature can be found.

$$\rho = \frac{\pi d}{\ln 2} R_{Avg,Sheet} f$$

Resistivity, ρ , can be found by converting the average sheet resistance, R , into resistivity by using thickness (d) of the sample and the cross pattern symmetry (f). The Hall coefficient was also determined using the Van der Pauw technique by sourcing a current of 100 mA between two opposing contacts, applying a magnetic field of 0 - 1.6 T, and measuring the voltage induced by the magnetic field between the two remaining opposing contacts. The Hall coefficient, R_H , is the slope of the least squares fit for the measured voltage vs. applied magnetic field curve.

Results and Discussion

The [(BiSe)_{1+ δ}]₁[VSe₂]₁ heterostructure was synthesized using modulated elemental reactants approach. In this approach, precursors consisting of a sequence of elemental layers are repeatedly deposited on a nominally room temperature substrate and then annealed to self-assemble the desired heterostructure. The sequence of elemental layers, in this case Bi-Se-V-Se was chosen to resemble that in the targeted heterostructure. The relative thicknesses of the elemental layers in the Bi-Se bilayer was calibrated to yield a one to one stoichiometry and the absolute thickness was calibrated to

yield two (100) monolayers of a rock salt structured BiSe. The relative thicknesses of the elemental layers in the V-Se bilayer was calibrated to yield a one to two stoichiometry and the absolute thickness was calibrated to a single layer of a Se-V-Se dichalcogenide structure. The precursors were deposited using a previously described deposition system.²⁰ Initial ratio of deposition thicknesses and absolute thicknesses both Bi-Se and V-Se elemental bilayers to obtain a bilayer layer of BiSe and a structural monolayer of VSe₂ were taken from previous studies.^{15,23} The initial samples self-assembled in to the desired [(BiSe)_{1+δ}]₁[VSe₂]₁ compound after annealing at 350°C for 20 minutes, but broader and less intense 00 l diffraction maxima than seen in previous ferecrystals^{11,15,25} were observed in a specular XRD scan. The lattice parameter was close, however, to the expected one, and only 00 l reflections were observed in the specular scan, suggesting the formation of the desired compound crystallographically aligned with the c -axis perpendicular to the substrate. We varied the initial Bi composition in the BiSe component by 5% both above and below the ideal composition. The c -axis lattice parameter varied from 1.178(1) nm when Bi was deficient to 1.180(1) nm when there was excess Bi, and in both extremes the quality of XRD scans decreased, having larger line widths and less intensity than at the ideal composition. The Bi content that gave the largest intensity and smallest line-width was used in subsequent studies. The c -axis lattice parameters in all of the samples are smaller than the 1.203 Å observed for [(SnSe)_{1.15}]₁(VSe₂)₁.¹⁵

An annealing study was performed to determine optimal formation conditions and the resulting specular XRD scans are shown in Figure IV.1. The as-deposited scan contains only broad (001) and (004) reflections. After 20 minutes of annealing at 250°C,

the first six (00*l*) reflections are observed, indicating the self-assembly of the targeted heterostructure. The intensity of these reflections increases and the line width decreases with increasing annealing temperature until 500°C. After annealing at 550°C, the line-widths begin to broaden due to evaporation of the components. An annealing period of 20 minutes at 500°C was therefore chosen as the optimal annealing conditions.

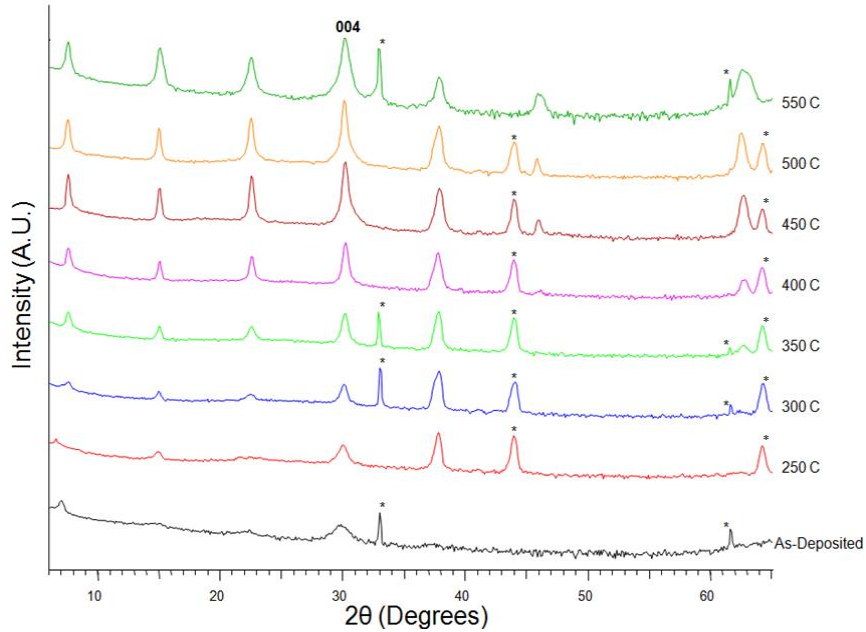


Figure IV.1. A series of diffraction scans collected as a function of annealing temperature, as indicated at the right side of the scans. All of the diffraction peaks from the sample can be indexed as (00*l*) reflections and the (004) reflection is indexed in the figure. Diffraction artifacts from the stage and Si substrate are marked with * symbols.

The specular diffraction pattern, Rietveld refinement and difference between them for the $[(\text{BiSe})_{1+\delta}]_1[\text{VSe}_2]_1$ heterostructure are shown in Figure IV.2. The refined position of the atomic planes along the *c*-axis of the refined structure is compared to the previously reported structure for $[(\text{SnSe})_{1.15}]_1(\text{VSe}_2)_1$ in the image below the data. The positions of the atomic planes are consistent with the expected heterostructure. The refined V-Se distance is 0.152(1) nm in the BiSe-VSe₂ heterostructure, which is very similar to the 0.152(1) nm reported for $[(\text{SnSe})_{1.15}]_1(\text{VSe}_2)_1$.¹⁵ The Bi and Se atoms in the

BiSe layer are no longer in the same plane as would be expected for a rock salt structure, with the Bi closer to the Se layer in VSe₂ by 0.025(1) nm. This “puckering” distortion is smaller than most reported, which range between 0.020 - 0.060(1) nm in previously reported rock salt-dichalcogenide misfit structures.[18] In [(SnSe)_{1.15}]₁(VSe₂)₁, the Sn and Se planes are 0.034(1) nm apart,¹⁵ while a puckering of 0.0293(1) nm¹⁷ and 0.291(1) nm¹⁹ have been reported in the misfit layer compound (BiSe)_{1.09}TaSe₂. A two selenium layers of the BiSe constituent are separated by 0.260(1) nm, which is slightly smaller than the 0.2751(1) nm and 0.2820(1) nm found by Zhou *et. al.*¹⁷ in (BiSe)_{1.09}TaSe₂. This separation is much larger than the 0.24(1) nm found in [(SnSe)_{1.15}]₁(VSe₂)₁.¹⁵ Gap between Bi layer of the BiSe and VSe₂ is 0.286(1) nm which is shorter than the 0.292(1) nm found in [(SnSe)_{1.15}]₁(VSe₂)₁.¹⁵ In (BiSe)_{1.09}TaSe₂, a gap of 0.3232 nm is found between the BiSe and the Se plane of TaSe₂.¹⁹ A gap of 0.289(1) nm was reported in a recent paper containing the structure of a BiSe-NbSe₂ heterostructure.²⁶ The refined model is consistent with the targeted BiSe-VSe₂ heterostructure.

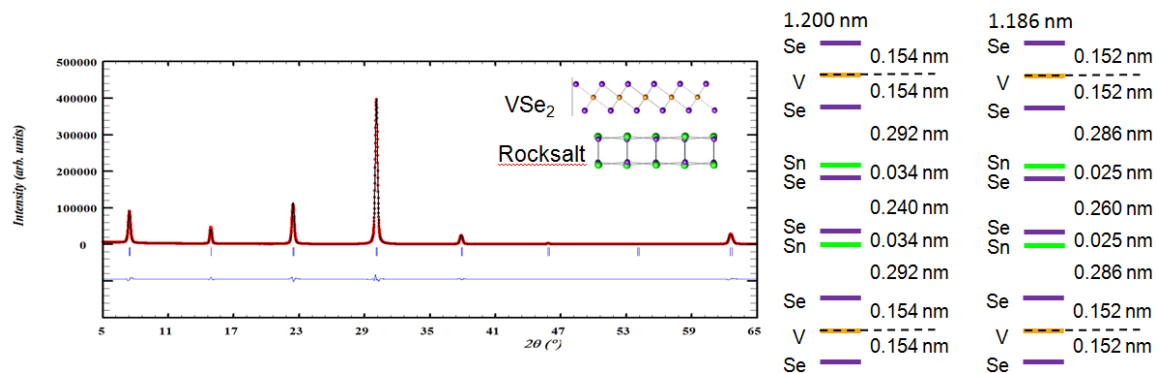


Figure IV.2. Rietveld refinement of the [(BiSe)_{1+δ}]₁[VSe₂]₁ heterostructure determine the position of atomic planes along the c-axis. The model to the right shows projected positions of the atoms onto the c-axis and their relative distances.

To obtain additional information about the [(BiSe)_{1+δ}]₁[VSe₂]₁ heterostructure, cross section HAADF-STEM images were collected and representative images are

contained in Figure IV.3. The structure from the top to the bottom of the film, Figure IV.3.a, contains alternating layers of VSe₂ and BiSe consistent with the targeted heterostructure. Occasionally, there are missing layers of BiSe suggesting that the precursor used for this STEM sample was deficient in Bi. These missing layers of BiSe, which reduce the coherence of the structure perpendicular to the substrate, are the likely cause of the line broadening observed in the specular diffraction patterns as composition was varied. In higher resolution images, some of the layers are aligned along the [111] and [100]/[010] zone axes, but the majority of the layers are not, consistent with prior reports of extensive rotational disorder between layers for samples prepared using modulated elemental reactants.²⁴ Several images contained regions where some of the BiSe layers were aligned along a zone axis, as shown in Figure IV.3.b. Clearly visible in these layers is a periodic anti-phase boundary, similar to that previously reported for (BiSe)_{1.09}TaSe₂.^{17,19}

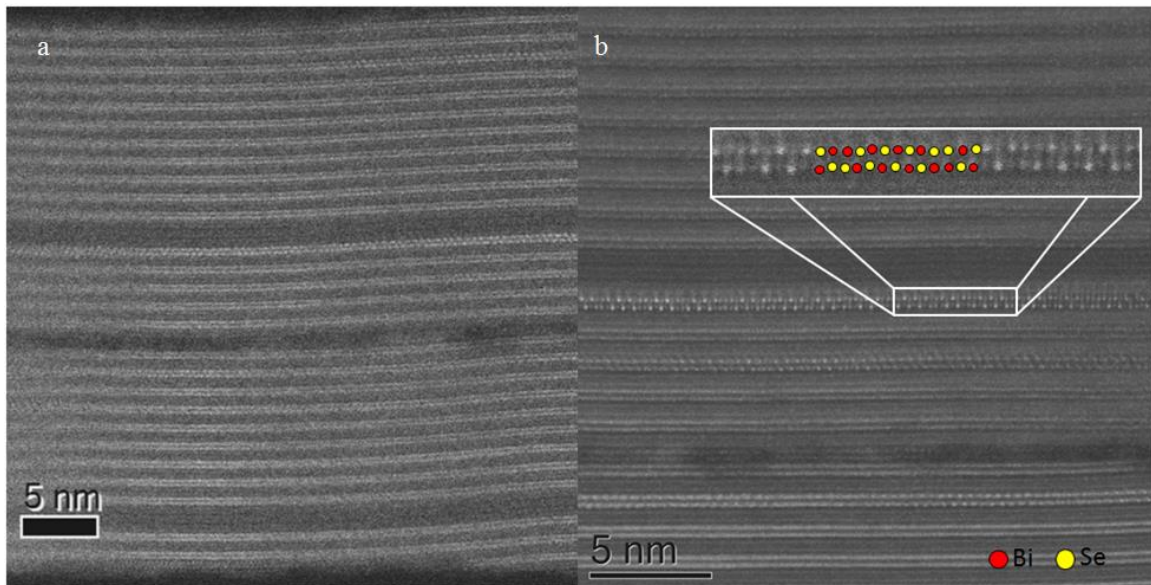


Figure IV.3. (a) Representative cross section HAADF-STEM images of the [(BiSe)_{1+ δ }]₁[VSe₂]₁ heterostructure. (b) Appearance of anti-phase boundaries apparent in BiSe bilayer.}

Resistivity as a function of temperature is shown in Figure IV.4 for the $[(\text{BiSe})_{1+\delta}]_1[\text{VSe}_2]_1$ heterostructure prepared in this study along with that of bulk VSe_2 ¹² and $[(\text{SnSe})_{1.15}]_1(\text{VSe}_2)_1$.¹⁵ The resistivity of the $[(\text{BiSe})_{1+\delta}]_1[\text{VSe}_2]_1$ heterostructure looks like that of a metal both in magnitude and in its temperature dependence. It has a very similar room temperature resistivity as $[(\text{SnSe})_{1.15}]_1(\text{VSe}_2)_1$ ¹⁵ and 2.5 times higher resistivity than bulk VSe_2 . It has a more temperature independent resistivity than bulk VSe_2 , which is consistent with prior comparisons of heterostructures made using modulated elemental reactants with crystalline misfit layered compounds.²⁵ There is no evidence for the prominent charge density wave transition found for $[(\text{SnSe})_{1.15}]_1(\text{VSe}_2)_1$ ¹⁵ in the resistivity data for the $[(\text{BiSe})_{1+\delta}]_1[\text{VSe}_2]_1$ heterostructure.

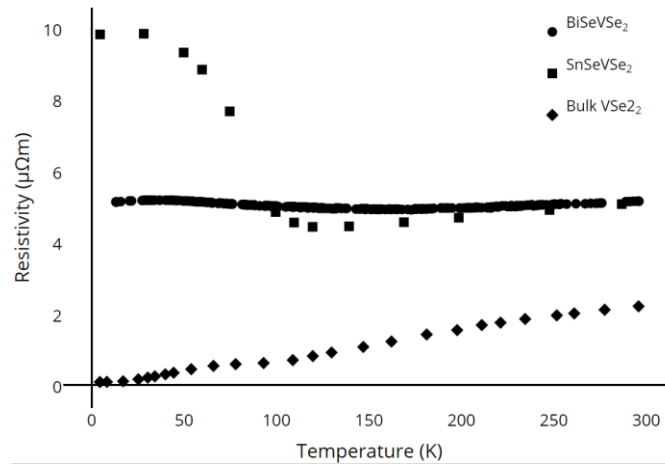


Figure IV.4. Resistivity data as a function of temperature for the $[(\text{BiSe})_{1+\delta}]_1[\text{VSe}_2]_1$ heterostructure compared to that reported for VSe_2 ¹² and $[(\text{SnSe})_{1.15}]_1(\text{VSe}_2)_1$.¹⁵

To obtain more information on the differences between the electrical properties of the $[(\text{BiSe})_{1+\delta}]_1[\text{VSe}_2]_1$ heterostructure, Hall coefficients were measured as a function of temperature as shown in Figure IV.5. The measured Hall coefficient for the $[(\text{BiSe})_{1+\delta}]_1[\text{VSe}_2]_1$ heterostructure is negative, similar in magnitude and temperature dependence as that reported for bulk VSe_2 ¹² and for SnSe-VSe_2 heterostructures prepared

with thicker VSe₂ layers.¹⁶ This contrasts with the positive Hall coefficient previously reported for [(SnSe)_{1.15}]₁(VSe₂)₁.¹⁵

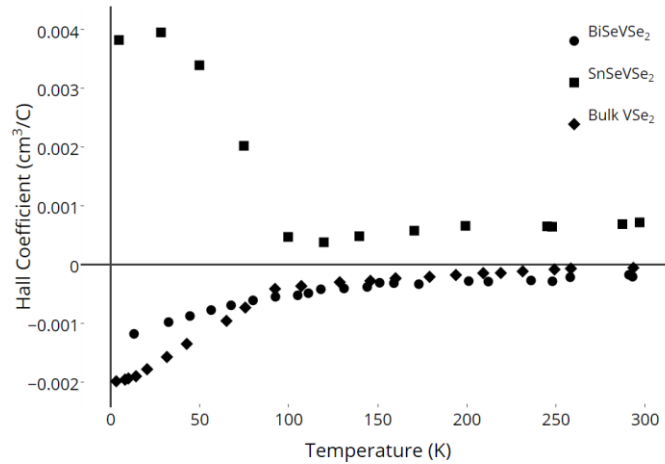


Figure IV.5. Hall coefficients as a function of temperature for the [(BiSe)_{1+δ}]₁[VSe₂]₁ heterostructure compared to that reported for VSe₂¹² and [(SnSe)_{1.15}]₁(VSe₂)₁.¹⁵

The resistivity and Hall data reported here for the [(BiSe)_{1+δ}]₁[VSe₂]₁ heterostructure is distinctly different than that reported for the analogous SnSe compound as shown in Figures IV.4 and IV.5. [(SnSe)_{1.15}]₁(VSe₂)₁¹⁵ is a p-type conductor and has a significant increase in resistivity and in the Hall coefficient consistent with a charge density wave transition. The [(BiSe)_{1+δ}]₁[VSe₂]₁ heterostructure is an n-type conductor and the temperature dependence of its Hall coefficient looks very similar to that of VSe₂. The higher resistivity of the the [(BiSe)_{1+δ}]₁[VSe₂]₁ heterostructure likely results from a higher concentration of defects than the equilibrium grown single crystal of VSe₂.

There are several potential reasons for the difference in transport behavior between the [(BiSe)_{1+δ}]₁[VSe₂]₁ and the [(SnSe)_{1.15}]₁[VSe₂]₁ heterostructures. One unlikely explanation is that the V centers of the VSe₂ layer in the [(BiSe)_{1+δ}]₁[VSe₂]₁ heterostructure adopt a trigonal prismatic coordination rather than the expected octahedral coordination found in the [(SnSe)_{1.15}]₁[VSe₂]₁ heterostructure and in bulk

VSe₂. The similarity of the bond distances between the V and Se layers in both heterostructures argues against this, although there is no direct evidence for the coordination of the V in the VSe₂ layer. A second possibility is that a difference in the alignment of the electronic bands and the Fermi level of the SnSe and BiSe constituent with those of the VSe₂ monolayer results in a different amount of charge transfer. The distortion of both the SnSe and BiSe bilayers in the [(MSe)_{1+δ}]₁[VSe₂]₁ heterostructures relative to their bulk structures indicates the importance of the interface in determining the structure and consequently the electronic structure. The periodic anti-phase boundary in the BiSe bilayer has been proposed by Wiegers to localize potential conduction electrons in Bi-Bi bonds at the anti-phase boundary in BiX containing misfit layer compounds as a means of rationalizing the trivalent nature of Bi determined from bond valence sum calculations with the similar electronic properties of analogous Sn containing misfit layer compound.¹⁸ A higher conductivity of the BiSe layer relative to that of SnSe might electronically couple with the VSe₂ layers on either side of it more strongly, changing the electronic structure. The periodic changes in the interface potential resulting from the regular anti-phase boundaries in the BiSe layer might also prevent the formation of the CDW. The lack of CDW in crystalline misfit layer compounds has been proposed to result from the strong interaction between layers overwhelming the weaker electron-phonon interactions underlying charge density wave formation.

The modular design criteria inherent to heterostructures enables one to propose potential heterostructures to systematically test physical phenomena. For example, preparing a repeating structure consisting of a single structural unit of VSe₂-BiSe-MoSe₂-BiSe would maintain the same interfaces adjacent to the VSe₂ layer, but the

semiconducting MoSe₂ layer would reduce the through plane conductivity. If electron localization is the driving force for the formation of anti-phase boundaries in the BiSe bilayer, a VSe₂-BiSe-VSe₂-M_{1-x}M'_xSe heterostructure where M and M' had different valences would enable the titration of the charge density. The changing charge density might also be expected to change the frequency of the anti-phase boundary. Comparing a VSe₂-BiSe heterostructure with a VSe₂-Bi₂Se₃ or a VSe₂-PbSe heterostructure would probe the effect of the anti-phase boundary on the CDW. Interest in heterostructures will continue to expand as theory and experiment are able to test ideas and concepts via systematic changes in nanostructure and nanoarchitecture.

Conclusions

The single structural layer of VSe₂ in the [(BiSe)_{1+δ}]₁[VSe₂]₁ heterostructure has very similar structural properties to that found in the analogous [(SnSe)_{1.15}]₁[VSe₂]₁ heterostructure, but the heterostructures have very different electrical properties. The [(BiSe)_{1+δ}]₁[VSe₂]₁ heterostructure is metallic with electrons as majority carriers while the analogous [(SnSe)_{1.15}]₁[VSe₂]₁ heterostructure has holes as the majority carriers. The [(SnSe)_{1.15}]₁[VSe₂]₁ heterostructure has large resistance and Hall coefficient change with temperature as a consequence of a charge density wave transition, while the [(BiSe)_{1+δ}]₁[VSe₂]₁ heterostructure has an almost temperature independent resistivity and a Hall coefficient sign (negative), magnitude and temperature dependence that is very similar to bulk VSe₂. The major structural difference between the two heterostructures is in the MSe constituent. The bilayer of SnSe adopts a rock salt structure while the BiSe bilayer has periodic anti-phase boundaries resulting in a larger *a*-axis lattice parameter. The anti-phase boundaries are thought to both localize electrons in Bi-Bi bonds and

potentially effectively scatter charge carriers, resulting in a low mobility. Systematic changes in heterostructure constituents and nanoarchitecture are suggested to further probe the effect of interfaces and charge transfer between constituents on properties.

Bridge

With the replacement of PbSe with BiSe in $(MSe)_{1+\delta}VSe_2$ the charge density wave previously seen becomes severely dampened. However, STEM images show antiphase boundaries within BiSe, which localize the extra electron of the bismuth to the Bi-Bi pair. This change in interface from a rocksalt to an orthorhombic structure with antiphase boundaries may have a significant effect on the charge density wave of the adjacent VSe_2 . To further explore the effects of the interface on the charge density wave in VSe_2 , BiSe was replaced with trigonal $SnSe_2$. The structure of the $(SnSe_2)_{1+\delta}(VSe_2)_n$ for $n = 1-3$ and electrical properties for $n = 1$ are discussed in the following chapter.

CHAPTER V

INFLUENCE OF INTERFACIAL STRUCTURE ON THE CHARGE DENSITY WAVE IN VSE2 HETEROSTRUCTURES WITH 1T-SNSE2

Authorship Statement

This work is currently unpublished but a manuscript for publication is expected to be prepared by myself with consultation from my advisor, David C. Johnson. I am the primary author of this work. James Sadighian aided in collection of X-ray diffraction and analysis. David C. Johnson is my advisor and consulted in preparation of this manuscript.

Introduction

Isolation of graphene in 2004 by Novoselov et al.¹ not only led to the awarding of the Nobel Prize in Physics but kickstarted many efforts into the study of 2D-materials. The resulting research has shown that the transition from a 3-dimensional bulk to a 2-dimensional monolayer often results in changes in chemical and physical properties. A well-known example is MoS₂, which transitions from an indirect band gap in the bulk to a direct band gap in a monolayer. The indirect band gap has been attributed to the interaction of the d-orbitals of the S atoms with the S atoms of adjacent layers. Since this interaction no longer exists in the isolated monolayer, the transition now becomes a direct transition.² A similar transition has been seen in hexagonal boron nitride (h-BN) where the bulk band gap of 4.0 eV increases to 4.6 eV in the monolayer.³ However, much of the work on the 2D-materials is limited to semiconducting films due to stability issues present in thin metallic films, which readily oxidize when exposed to atmosphere.⁴

Heterostructures allow for isolation of materials, such as metallic monolayers, that are not necessarily stable in atmosphere, by surrounding air-sensitive layers with several

oxidation resistant layers. Heterostructures also allow for systematic changes in constituents and/or nanoarchitecture that enables a more complete understanding of exotic properties such as superconductivity and charge density waves. Due in part to the challenges in making finite thickness layers of metallic layered compounds, there are considerable differences in the reported onset temperature of the charge density wave transition in VSe₂. For example, micromechanically exfoliated VSe₂ layers have a measured onset temperature of 81 K at 11.6 nm while liquid exfoliated films between 4-8 trilayers report an onset temperature of 135 K.^{5,6} In a series of papers of heterostructures containing VSe₂ Falmbigl et al. and Hite et al. reported that the CDW changes significantly in character in (SnSe)_{1.15}(VSe₂)_n and (PbSe)_{1+δ}(VSe₂)_n when *n* is increased from 1 (monolayer) to 2 (bilayer), respectively.^{7,8} However, only a small change in overall resistivity and Hall coefficient was seen for *n* = 1 when switching from SnSe to PbSe and is likely due to differing degrees of charge transfer from the rocksalt to the dichalcogenide layer.

In an attempt to understand the role of the MSe_x layer on the CDW in VSe₂ heterostructures, we prepared the compounds (SnSe₂)_{1+δ}(VSe₂)_n where *n* = 1 - 3. These compounds contain a repeating unit of one 1T-SnSe₂ and *n* 1T-VSe₂ layers. Temperature dependent resistivity in (SnSe₂)_{1+δ}(VSe₂)₁ reveals metallic like behavior above T = 120 K with a large upturn in resistivity below 120 K similar to the CDW transition found in (SnSe)_{1.15}(VSe₂)₁ and (PbSe)_{1+δ}(VSe₂)₁. A positive Hall coefficient is observed and a concomitant upturn in Hall coefficient is also seen at 120 K further supporting the existence of a CDW similar to that observed in (SnSe)_{1.15}(VSe₂)₁ and (PbSe)_{1+δ}(VSe₂)₁. Further resistivity measurements for *n* = 2 and 3 are underway.

Experimental

(SnSe₂)_{1+δ}VSe₂ was synthesized in a custom built Physical Vapor Deposition (PVD)⁹ using the Modulated Elemental Reactant (MER)⁹ technique. Precursors were sequentially deposited on (100) oriented silicon wafers using elemental sources of Sn (Alfa Aesar, 99.98%), V (Alfa Aesar, 99.8%), and Se (Alfa Aesar, 99.999%). The sequence Se-Sn-Se-V was deposited in order to best match the desired stacking sequence of the final product. Precursors were annealed in N₂ atmosphere for 1 minute at 350 °C before being placed in a close ended Pyrex tube with an ampule of solid SnSe₂ and pumped to ~10⁻⁶ torr and the tube was then sealed and further annealed for 1 hour at 250 °C.

X-ray fluorescence (XRF) was performed on a Rigaku Primus II was used to determine the intensity in counts per second (cps) of emitted X-rays. The intensity of these emitted X-rays are then compared to an ideal intensity determined by previously made heterostructures containing one or more of the desired layers. For more details on XRF see Chapter II.4. Specular X-ray diffraction (00*l*-XRD) was performed on a Bruker Discover diffractometer, equipped with Cu K_α radiation ($\lambda = 0.15418$ nm), Göbel mirrors, and Bragg-Brentano θ -2 θ optics geometry, in order to determine the c-lattice parameter of the (SnSe₂)_{1+δ}VSe₂ repeat unit. In-plane X-ray diffraction (*hk*0-XRD) was performed on a Rigaku SmartLab, equipped with Cu K_α radiation ($\lambda = 0.15418$ nm), to determine the in-plane lattice parameters of the SnSe₂ and VSe₂ layers. Annealed precursors were prepared for High-Angle Annular Dark-Field Scanning Transmission Electron Microscopy (HAADF-STEM) on an FEI Helios 600 dual-beam using techniques

described elsewhere.¹⁰ HAADF-STEM was performed on an FEI Titan 80-300 FEG-TEM at the Center for Advanced Materials Characterization in Oregon (CAMCOR).

Resistivity measurements were performed using the van der Pauw method¹¹ with temperature ranging from 20-295 K. Samples were prepared for electrical characterization on fused quartz crystal slides in a 1 cm × 1 cm cross geometry. Further details on how electrical characterization was performed can be found elsewhere.¹²

Results and Discussion

Precursors for each of the compounds $(\text{SnSe}_2)_{1+\delta}(\text{VSe}_2)_n$ for $n = 1-3$ were prepared by depositing sequences of elemental layers that match the target heterostructure. For example, for $n = 1$ a designed precursor was prepared by sequentially depositing Se-Sn-Se-V and repeating this to achieve a desired thickness of approximately 50 nm. Precursors were calibrated using a new method that employs X-ray fluorescence. By determining a target intensity of secondary X-rays that corresponds to a theoretical complete layer of material the deposition time can be scaled to match this intensity. The target intensity for VSe_2 was determined by comparing X-ray intensity to the previously synthesized $(\text{SnSe})_{1.15}\text{VSe}_2$. Using the same system, $(\text{SnSe})_{1.15}\text{VSe}_2$, the target intensity for Sn atoms required to form a complete trilayer of SnSe_2 can be calculated by equation (1):

$$I_{\text{SnSe}_2} = \frac{1+\delta}{1.15} I_{\text{SnSe}} \quad (1)$$

where I_{SnSe} is the intensity of Sn required to make a complete SnSe bilayer, 1.15 is the misfit parameter for the SnSe- VSe_2 heterostructure, and $1+\delta$ is the theoretical misfit parameter for the SnSe_2 - VSe_2 heterostructure calculated from bulk in-plane lattice parameters of SnSe_2 and VSe_2 . Similarly, Se intensity was also calculated. These

designed precursors were allowed to self-assemble by annealing on hotplate for 1 min at 350 °C followed by annealing in a sealed ampule at 250 °C for 1 hour.

Out-of-plane X-ray diffraction is shown in Figure V.1 and was performed on annealed $(\text{SnSe}_2)_{1+\delta}(\text{VSe}_2)_n$ heterostructures for $n = 1-3$. Diffraction peaks were indexed to 00 l reflections of a one trilayer Se-Sn-Se stacked on n trilayers of Se-V-Se. Repeat units (c -lattice parameter) of 1.226(2) nm, 1.886(3) nm, and 2.495(2) nm were found for $n = 1, 2,$ and 3 , respectively. The increase in c -lattice parameter as n is increased corresponds to c -lattice of 0.614 nm for each VSe_2 layer (bulk = 0.610 nm¹³). By solving for $n = 0$, a c -lattice parameter for SnSe_2 was found to be 0.654 nm (bulk = 0.614 nm¹⁴). Further refinement of the structure is not possible due to the current SnSe impurity discussed briefly below.

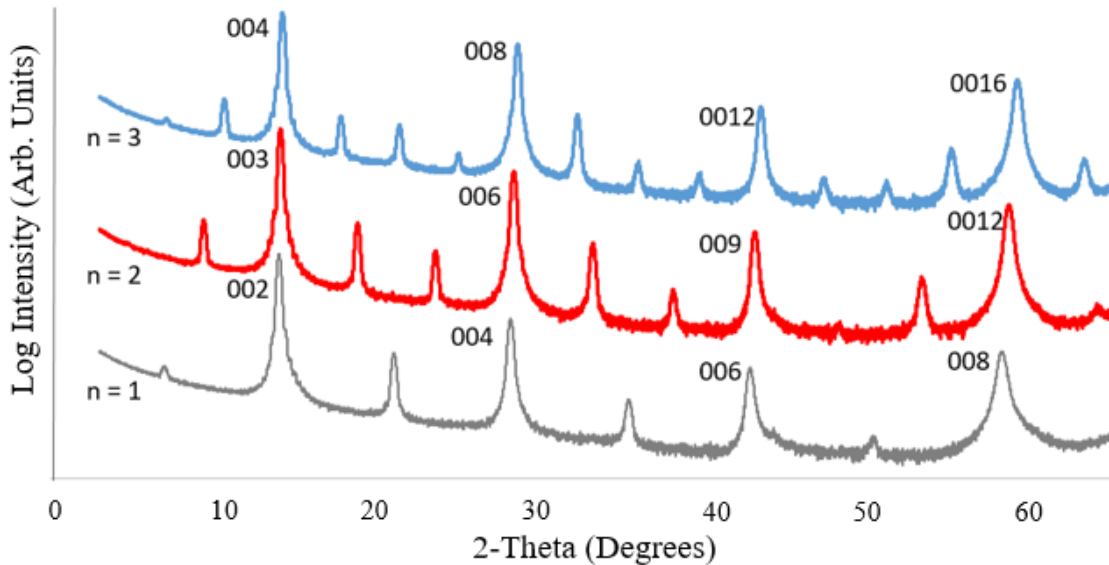


Figure V.1. Out-of-plane X-ray diffraction for $(\text{SnSe}_2)_{1+\delta}\text{VSe}_2$ with maxima that are indexed to 00 l reflections.

To further parse the structure of $(\text{SnSe}_2)_{1+\delta}\text{VSe}_2$, in-plane diffraction was performed for $n = 1 - 3$ revealing maxima, as seen in Figure V.2, that can be indexed to trigonal SnSe_2 and trigonal VSe_2 . Relative intensities for VSe_2 $hk0$ peaks increase with

the increase in the number of VSe₂ layers, n , per repeat unit. The a -lattice parameters for SnSe₂ were 0.378(2) nm, 0.382(1) nm, and 0.381(2) nm for $n = 1, 2,$ and $3,$ respectively, as compared to the bulk value of 0.381 nm¹⁴. The a -lattice parameters for VSe₂ were 0.340(2) nm, 0.338(1) nm, and 0.338(2) nm for $n = 1, 2,$ and $3,$ respectively, as compared to the bulk value of 0.336 nm¹³. The measured a -lattice parameter falls within what has been measured previously in VSe₂ containing ferecrystals, which range from 0.341(1) nm, 0.341(3) – 0.34630(3) nm, and 0.343(6) nm were found in (SnSe)_{1.15}VSe₂, [(SnSe)_{1.15}]_mVSe₂, and (PbSe)_{1.11}VSe₂, respectively.^{7,8,29,30} Misfit parameters, $1+\delta$, describing the ratio in area taken up by individual SnSe₂ and VSe₂ unit cells in the ab -plane were determined to be 0.809(3), 0.783(2), and 0.787(3) for $n = 1, 2,$ and $3,$ respectively. Misfit parameter values of 0.99-1.29¹⁵⁻²⁸ have been seen previously in compounds containing a rocksalt and a dichalcogenide. A misfit parameter of 0.778 would be calculated using the bulk values and the slightly higher values are likely due to

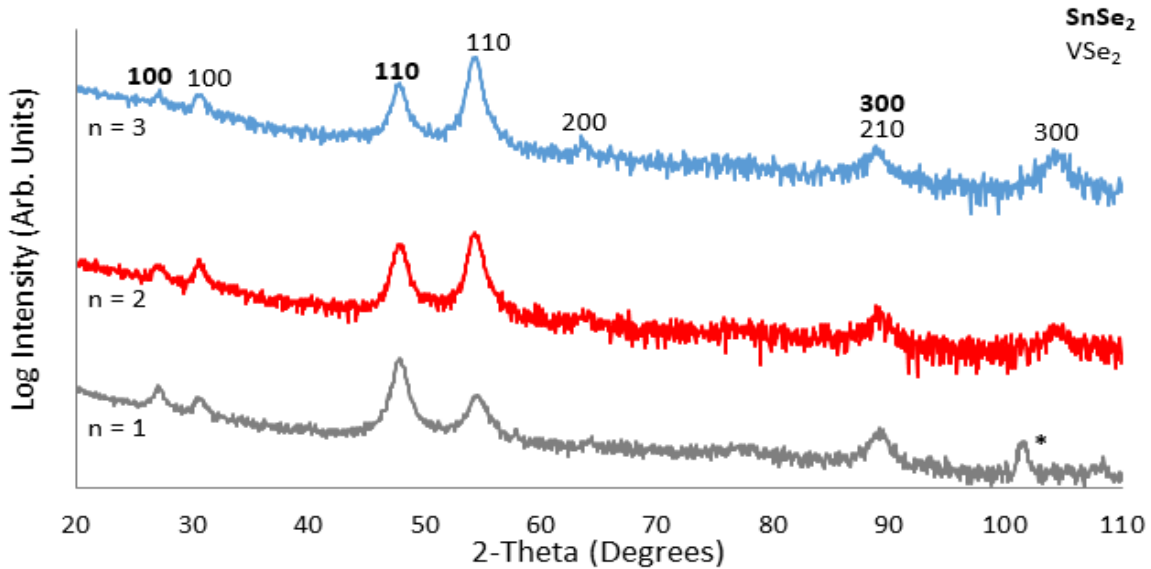


Figure V.2. In-plane X-ray diffraction for (SnSe₂)_{1+δ}(VSe₂)_n $n = 1-3$. Maxima can be indexed to $hk0$ peaks of 1T-SnSe₂ and 1T-VSe₂. A SnSe impurity peak is marked by an asterisk.

some degree of charge transfer and interplay of the van der Waals forces that hold the layers together.

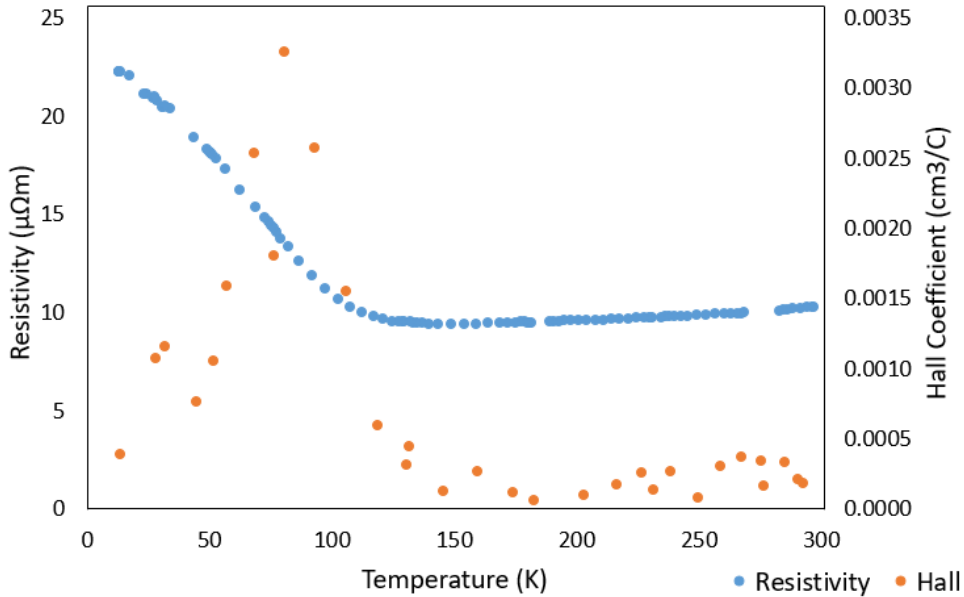


Figure V.3. In-plane electrical resistivity and Hall coefficient measurements of $(\text{SnSe}_2)_{1+\delta}\text{VSe}_2$. An upturn in both resistivity and Hall coefficient at approximately 120 K indicate the presence of a charge density wave.

Temperature dependent resistivity and Hall coefficient for $n = 1$ are shown in Figure V.3. At temperatures above 150 K p-type metallic behavior is observed but below 150 K an upturn in resistivity is seen along with an upturn in Hall coefficient. This upturn in resistivity supported by the localization of charge carriers provides evidence for the existence of a CDW as has been seen in VSe_2 compounds. This behavior has also been seen in other VSe_2 containing heterostructures, however, it is not known at this point how much SnSe currently exists within the heterostructure, which may be influencing the electrical properties.

A comparison of resistivity as measured previously^{7,8,29} in different VSe₂ heterostructures is seen in Figure V.4. It has been previously discussed^{7,8,30,29} that the increase in resistivity relative to the bulk is likely due to two phenomenon: charge transfer between layers that does not occur in the bulk and a reduction of dimensionality from the 3D bulk to the quasi-2D layer that is present in the heterostructure. However, a charge density wave of similar behavior for the $n = 1$ compound is seen in (GeSe₂)-(VSe₂)₂ and a charge density wave is not seen in BiSe-VSe₂.^{29,31} The behavior of the (SnSe₂)_{0.81}VSe₂ heterostructure has an onset temperature of 120 K similar to both the analogous PbSe and SnSe heterostructures. The similarity in resistivity behavior shows that interfacial interactions between layers has a minimal effect on the overall electric behavior of the system. This is likely a consequence of turbostratic disorder that removes any long range interactions between orbitals of adjacent layers.

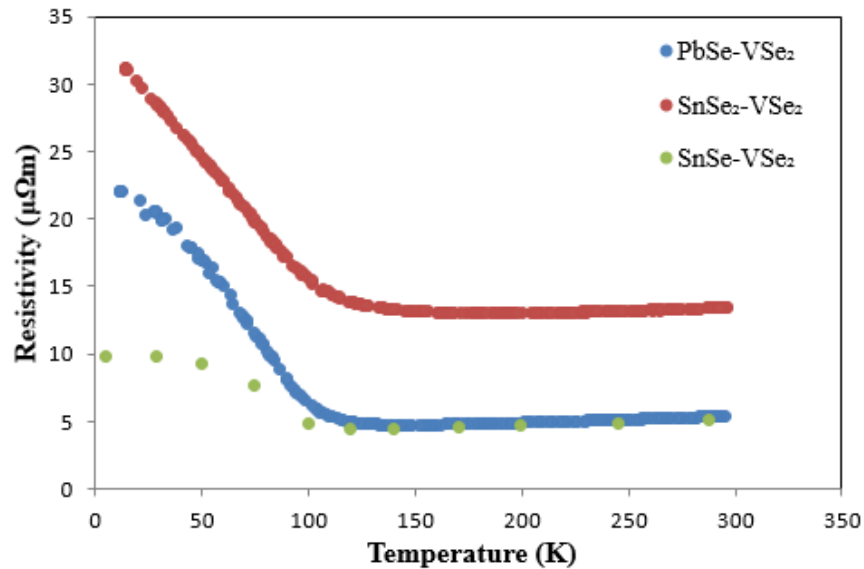


Figure V.4. In-plane electrical resistivity comparison between (PbSe)_{1.11}VSe₂, (SnSe)_{1.15}VSe₂, and (SnSe₂)_{0.81}VSe₂.^{7,8,29}

Mobility and Hall coefficient as a function temperature for $(\text{SnSe}_2)_{0.81}\text{VSe}_2$, $(\text{PbSe})_{1.11}\text{VSe}_2$, and $(\text{SnSe})_{1.15}\text{VSe}_2$ are shown in Figure V.5. At temperatures above 150 K SnSe-VSe_2 has the most mobile carriers while SnSe_2 has the least mobile carriers. This difference in “high” temperature mobility may be due to greater phonon scattering at the interface between MSe_x and VSe_2 of mobile carriers. Additional phonon scattering of carriers in $\text{SnSe}_2\text{-VSe}_2$ may be due to the presence of additional grain boundaries as a consequence of the SnSe impurity. At temperatures below the critical temperature of the charge density wave both mobility and Hall coefficient increase compared to room temperature values. The behavior of the $\text{SnSe}_2\text{-VSe}_2$ is similar to SnSe-VSe_2 , which further supports that the SnSe impurity is likely influencing the electrical behavior of the $\text{SnSe}_2\text{-VSe}_2$ heterostructure.

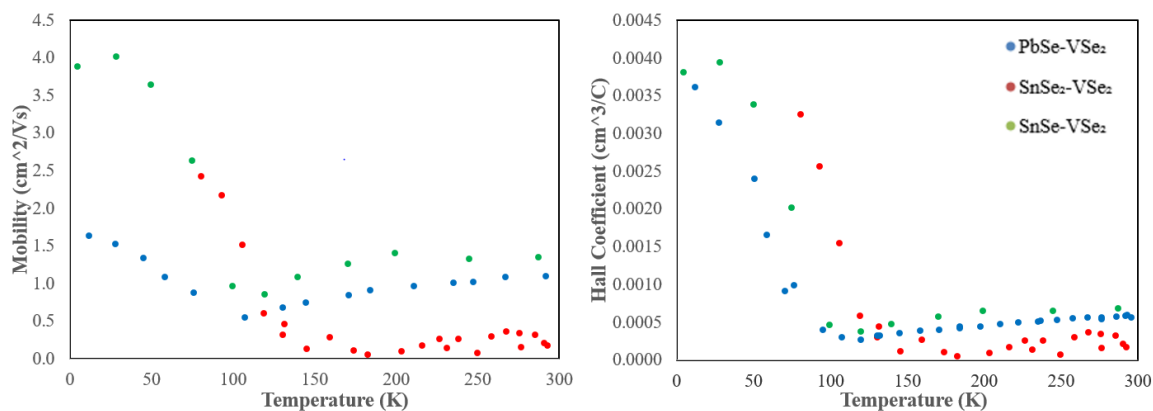


Figure V.5. Temperature dependent mobility and Hall coefficient measurements of $(\text{SnSe}_2)_{0.81}\text{VSe}_2$, $(\text{PbSe})_{1.11}\text{VSe}_2$, and $(\text{SnSe})_{1.15}\text{VSe}_2$.^{7,8,29}

Conclusion

The compounds $(\text{SnSe}_2)_{1+\delta}(\text{VSe}_2)_n$ with $n = 1-3$ were prepared using the modulated elemental reactants technique on a custom-built physical vapor deposition chamber. Diffraction shows films that consist of 1T- SnSe_2 separated by n layers of VSe_2 . However,

diffraction for $n = 1$ shows a SnSe impurity. Resistivity and Hall coefficient measurements were performed on $(\text{SnSe}_2)_{0.81}\text{VSe}_2$ which revealed metallic behavior with p-type conductance. An increase in resistivity is seen at temperatures below 120 K and has been attributed to a charge density wave. The nature of the resistivity and Hall are similar to analogous SnSe and PbSe compounds. This work further shows the importance of VSe₂ isolation by a semiconducting compound in enhancing the charge density wave. Additionally, the interface appears to play a minimal role on the electric behavior and is likely due to the rotational disorder inherent within the films that presents long range interactions between orbitals in adjacent layers.

CHAPTER VI
CONCLUDING REMARKS

Authorship Statement

My advisor, David C. Johnson, was consulted in the preparation of this chapter.

Remarks

Structure and electronic properties of several VSe₂ heterostructures were synthesized using the modulated elemental reactants technique and discussed. The modulated elemental reactants technique allows for precise synthetic control of compounds known as ferecrystals. Precursors are composed of alternating layers of elements that closely match the superlattice structure of the desired ferecrystal. This unique technique produces materials that are no longer limited by diffusion and only need to be annealed at relatively low temperatures in order to induce nucleation. This control allows for systematic changes in the layered structure of the ferecrystal to further explore the effects of interlayer interactions on the overall electronic properties of the ferecrystal. This was utilized to further investigate the charge density wave that was previously reported in the (SnSe)_{1.15}VSe₂ heterostructure.

Prior to this work Atkins and Falmbigl et al. reported a resistance anomaly at approximately 115 K that was attributed to a charge density wave in (SnSe)_{1.15}VSe₂. With increasing layers of VSe₂ in the SnSe-VSe₂ heterostructure this charge density wave was severely dampened as a result of increased dimensionality of the VSe₂. During this time (SnSe)_{1.15}VSe₂ was the only known VSe₂ heterostructure to have a charge density wave. To determine if the charge density wave in (SnSe)_{1.15}VSe₂ was unique to this heterostructure, SnSe was replaced with PbSe. PbSe is a layered materials with rocksalt

structure and is isovalent to SnSe. $(\text{PbSe})_{1+\delta}(\text{VSe}_2)_n$ for $n = 1 - 3$ was synthesized and structural analysis showed that the heterostructure was composed of an alternating structure of a distorted rocksalt PbSe and 1T-VSe₂. For $n = 1$, a resistance anomaly at 115 K was observed similarly to the analogous $(\text{SnSe})_{1.15}\text{VSe}_2$ heterostructure. Additionally, the overall change in resistivity as temperature was lowered was higher for the PbSe containing heterostructure as compared to the analogous SnSe heterostructure. It is suspected that this charge density wave enhancement is due to the increased charge transfer from the PbSe layer to the VSe₂ layer. Higher values of n show resistivity behavior that is approaching bulk resistivity and change in carrier type from p to n-type. To further explore the effects of charge transfer on the charge density wave in VSe₂, PbSe was replaced with BiSe.

$(\text{BiSe})_{1+\delta}\text{VSe}_2$ was prepared to determine how increased charge transfer to the VSe₂ layer influences. Electrical resistivity measurements show behavior as a function of temperature to be similar to that of bulk VSe₂. Additionally, Hall coefficient measurements show the heterostructure to be *n*-type similar to bulk. HAADF-STEM show the presence of antiphase boundaries that likely localize the additional electron the BiSe and prevent further charge transfer. The presence of the antiphase boundaries may also allow coupling between adjacent VSe₂ layers and thereby removing the quasi two-dimensionality of the VSe₂ monolayer.

In order to understand the effects of interfacial interactions between layers and remove the coupling between adjacent VSe₂ layers, the rocksalt structure was replaced with semiconducting 1T-SnSe₂. It was found to have electrical behavior similar to that of both SnSe and PbSe containing heterostructures. However, in-plane XRD shows peak

that can be indexed to a SnSe impurity that may be influencing the behavior of the electrical resistivity. Further work is need to be performed on this system to remove the SnSe impurity.

This work demonstrates the possibility of isolating a metallic monolayer within a a heterostructure and using adjacent layers to control the electrical behavior of the entire heterostructure. The electrical behavior is largely determined by the composition of the metallic layer and the number of layers found therein. However, future studies will be needed to further understand the role of dimensionality in the electrical behavior of layered metallic systems.

APPENDIX

SUPPORTING INFORMATION FOR CHARGE DENSITY WAVE TRANSITION IN $(\text{PBSE})_{1+\Delta}(\text{VSE}_2)_N$ COMPOUNDS WITH $N = 1, 2, \text{ AND } 3$

Band Structure Calculations on 1T-VSe₂ Monolayers and Bilayers

Density functional theory (DFT) calculations were performed using the Vienna *ab initio* simulation package (vasp).¹⁻⁴ The interactions of the electrons with the ionic core were described using the projector augmented wave (PAW) method.^{5,6} To describe exchange and correlation, the functionals of Perdew-Burke-Ernzerhof (PBE) were used.⁷ A cutoff energy of 500 eV was used to expand the wave functions. To reduce interactions between periodic images, vacuum of 25 Å was added between VSe₂ monolayers and bilayers. For structural relaxations, a Γ -centered $18 \times 18 \times 1$ k-point mesh was used. Since interactions between VSe₂ layers are of van-der-Waals type, dispersion corrections were added using Dion's method in the vdW-DF corrected optPBE functionals.⁸⁻¹¹

The in-plane lattice parameters are 0.337 nm for the monolayer and 0.338 nm for the bilayer, which is slightly smaller than in the ferecrystals, but consistent with prior theoretical results.^{12,13} The distance between the V and Se layers in the monolayer is 0.158 nm, which is consistent with experimental results. For the bilayer, the distances between the V and Se layers are slightly asymmetric: 0.158 nm for the Se layers adjacent to the vacuum, and 0.157 nm for the remaining layers. The distance between the two VSe₂ trilayers is 0.316 nm. Both the monolayer and the bilayer are ferromagnetic with a magnetization of 0.64 and 0.66 $\mu_B/\text{f.u.}$, respectively.

The band structures of a pristine VSe₂ monolayer and bilayer are shown in Figure A.1. The majority spin bands for the monolayer are metallic with a hole-like Fermi surface near the K point, whereas the minority spin bands are semi-metallic with a valence band

maximum at the Γ point and a conduction band minimum at the M point. The bilayer shows additional bands because of the additional VSe_2 trilayer that are mostly degenerate with the bands of the other VSe_2 trilayer. However, near the Γ point the additional band is raised in energy for the band right below (majority spin) and above (minority spin) the Fermi level. Just like the monolayer, the majority spin bands are metallic with a hole-like Fermi surface near the K point, and the minority spin bands are semi-metallic with a valence band maximum at the Γ point and a conduction band minimum at the M point. The results suggest that VSe_2 monolayers and bilayers should have similar electrical properties with isovalent charge donors such as SnSe and PbSe . The temperature dependence of the electrical resistivity and the Hall coefficient show similar behavior in $[(\text{PbSe})_{1.12}]_1[\text{VSe}_2]_1$ and $[(\text{SnSe})_{1.15}]_1[\text{VSe}_2]_1$, but the sign of the Hall coefficient is positive for $[(\text{SnSe})_{1.15}]_1[\text{VSe}_2]_n$ and negative for $[(\text{PbSe})_{1.12}]_1[\text{VSe}_2]_n$ ($n > 1$), indicating significant interactions between with VSe_2 layer beyond simple charge transfer. Further research must be conducted to investigate the nature of these interactions.

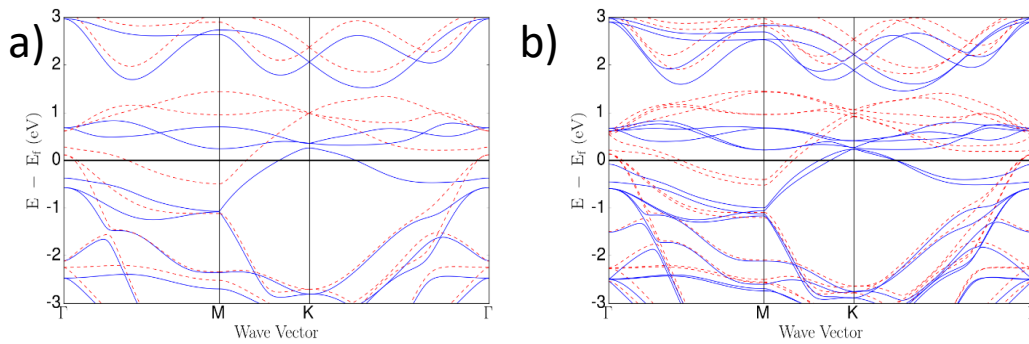


Figure A.1. Band structures of monolayer (a) and bilayer (b). Solid blue lines denote majority spins and dashed red lines denote minority spin bands.

Rietveld Refinement Details

The X-ray pattern (00*l*-reflections) for (PbSe)_{1.11}VSe₂ was refined via the Rietveld method employing the FullProf program.¹⁴ Refinement details are found in Table A.1.

Parameter/Compound	
Composition from refinement	(PbSe) _{1.02} VSe ₂
Radiation	Bruker D8, Cu K _α
2θ range (degrees)	5 ≤ 2θ ≤ 65
<i>c</i> (nm)	12.2572(2)
Reflections in refinement	8
Number of variables	7
$R_F = \sum F_o - F_c / \sum F_o$	0.0171
$R_I = \sum I_o - I_c / \sum I_o$	0.0180
$R_{wp} = [\sum w_i y_{oi} - y_{ci} ^2 / \sum w_i y_{oi} ^2]^{1/2}$	0.0794
$R_P = \sum y_{oi} - y_{ci} / \sum y_{oi} $	0.0550
$R_e = [(N - P + C) / (\sum w_i y_{oi}^2)]^{1/2}$	0.0191
$\chi^2 = (R_{wp} / R_e)^2$	17.3
Atom parameters	
V in 1 <i>a</i> (0)	
Occ.	1.0
Se1 in 2 <i>c</i> (<i>z</i>), <i>z</i>	0.1254(1)
Occ.	2.0
Pb in 2 <i>c</i> (<i>z</i>), <i>z</i>	0.3706(1)
Occ.	1.02
Se2 in 2 <i>c</i> (<i>z</i>), <i>z</i>	0.4005(3)
Occ.	1.02
Relevant distances [nm]	
V- Se1	0.1537
Se1- Pb	0.3005
Pb- Se2	0.0367

Table A.1. Rietveld refinement results from room temperature XRD data. Space group: P-3m1 (VSe₂), Fm-3m (PbSe).

REFERENCES CITED

Chapter I

- (1) Geim, A. K.; Grigorieva, I. V. Van Der Waals Heterostructures. *Nature* **2013**, *499*, 419–425.
- (2) Wang, H.; Yuan, H.; Sae Hong, S.; Li, Y.; Cui, Y. Physical and Chemical Tuning of Two-Dimensional Transition Metal Dichalcogenides. *Chem. Soc. Rev.* **2015**, *44*, 2664–2680.
- (3) Fujimoto, Y.; Koretsune, T.; Saito, S. Electronic Structures of Hexagonal Boron-Nitride Monolayer: Strain-Induced Effects. *J. Ceram. Soc. Japan* **2014**, *122*, 346–348.
- (4) Gomes, L. C.; Carvalho, A. Phosphorene Analogues: Isoelectronic Two-Dimensional Group-IV Monochalcogenides with Orthorhombic Structure. *Phys. Rev. B* **2015**, *92*, 085406.
- (5) Wiegiers, G. A. Misfit Layer Compounds: Structures and Physical Properties. *Prog. Solid State Chem.* **1996**, *24*, 1–139.
- (6) Yarmoshenko, Y. M.; Trofimova, V. A.; Shamin, S. N.; Solovyev, N. V.; Kurmaev, E. Z.; Ettema, A. R. H. F.; Haas, C. The X-Ray Emission Spectra and Electronic-Structure of the Misfit Layer Compounds $(\text{BiS})_{1.08}\text{NbS}_2$ and $(\text{PbS})_{1.14}\text{TaS}_2$. *J. Phys. Condens. Matter* **1994**, *6*, 3993–3998.
- (7) Meerschaut, A.; Guemas, L.; Auriel, C.; Rouxel, J. Preparation, Structure Determination and Transport Properties of a New Misfit Layer Compound: Lead Niobium Sulfide $((\text{PbS})_{1.14}(\text{NbS}_2)_2)$. *Eur. J. Solid State Inorg. Chem.* **1990**, *27*, 557–570.
- (8) Wiegiers, G. A.; Meetsma, A.; Haange, R. J.; van Smaalen, S.; de Boer, J. L.; Meerschaut, A.; Rabu, P.; Rouxel, J. The Incommensurate Misfit Layer Structure of $(\text{PbS})_{1.14}\text{NbS}_2$, “ PbNbS_3 ” and $(\text{LaS})_{1.14}\text{NbS}_2$, “ LaNbS_3 ”: An X-Ray Diffraction Study. *Acta Crystallogr. B* **1990**, *46*, 324–332.
- (9) Wiegiers, G. A.; Meetsma, A.; de Boer, J. L.; van Smaalen, S.; Haange, R. J. X-ray Crystal Structure Determination of the Triclinic Misfit Layer Compound $(\text{SnS})_{1.20}\text{TiS}_2$. *J. Phys. Condens. Matter* **1991**, *3*, 2603–2612.
- (10) Meerschaut, A.; Auriel, C.; Rouxel, J. Structure Determination of a New Misfit Layer Compound $(\text{PbS})_{1.18}(\text{TiS}_2)_2$. *J. Alloys Compd.* **1983**, *183*, 129–137.
- (11) Wiegiers, G. A.; Haange, R. J. Electrical Transport Properties of the Misfit Layer Compounds $(\text{SnS})_{1.20}\text{TiS}_2$ and $(\text{PbS})_{1.18}\text{TiS}_2$. *Eur. J. Solid State Inorg. Chem.* **1991**, *28*, 1071–1078.

- (12) Meerschaut, A. Misfit Layer Compounds. *Curr. Opin. Solid State Mater. Sci.* **1996**, *1*, 250–259.
- (13) De Boer, J. L.; Meetsma, A.; Zeinstra, T. J.; Haange, R. J.; Wiegers, G. A. Structures of the Misfit Layer Compounds $(\text{LaS})_{1.13}\text{TaS}_2$, “ LaTaS_3 ” and $(\text{CeS})_{1.5}\text{TaS}_2$, “ CeTaS_3 .” *Acta Crystallogr. C* **1991**, *47*, 924–930.
- (14) Wulff, J.; Meetsma, A.; Haange, R. J.; de Boer, J. L.; Wiegers, G. A. Structure and Electrical Transport Properties of the Misfit-Layer Compound $(\text{BiS})_{1.08}\text{TaS}_2$. *Synth. Met.* **1990**, *39*, 1–12.
- (15) Auriel, C.; Roesky, R.; Meerschaut, A.; Rouxel, J. Structure Determination and Electrical Properties of a New Misfit Layered Selenide $[(\text{PbSe})_{1.10}\text{NbSe}_2]$. *Mater. Res. Bull.* **1993**, *28*, 247–254.
- (16) Van Smaalen, S.; Meetsma, A.; Wiegers, G. A.; de Boer, J. L. Determination of the Modulated Structure of the Inorganic Misfit Layer Compound $(\text{PbS})_{1.18}\text{TiS}_2$. *Acta Crystallogr. B* **1991**, *47*, 314–325.
- (17) Wiegers, G. A.; Meetsma, A.; Haange, R. J.; de Boer, J. L. Structure and Physical Properties of $(\text{SnS})_{1.18}\text{NbS}_2$, “ SnNbS_3 ”, a Compound with Misfit Layer Structure. *Mater. Res. Bull.* **1988**, *23*, 1551–1559.
- (18) Meetsma, A.; Wiegers, G. A.; Haange, R. J.; de Boer, J. L. The Incommensurate Misfit Layer Structure of $(\text{SnS})_{1.17}\text{NbS}_2$, “ SnNbS_3 ”. I. A Study by Means of X-Ray Diffraction. *Acta Crystallogr. A* **1989**, *45*, 285–291.
- (19) Meerschaut, A.; Roesky, R.; Lafond, A.; Deudon, C.; Rouxel, J. Misfit Layered Compounds: Polytypism, Multilayer Stages, Non-Stoichiometry and Electronic Structure, Self-Misfit Compounds. *J. Alloys Compd.* **1995**, *219*, 157–160.
- (20) Wiegers, G. A.; Haange, R. J. Electrical Transport and Magnetic Properties of the Misfit Layer Compound $(\text{LaS})_{1.14}\text{NbS}_2$. *J. Phys. Condens. Matter* **1990**, *455*.
- (21) Rouxel, J.; Meerschaut, A.; Wiegers, G. a. Chalcogenide Misfit Layer Compounds. *J. Alloys Compd.* **1995**, *229*, 144–157.
- (22) Palewski, T. Rare Earth Compounds with Incommensurate Layered Structures. *Wiadomości Chem.* **2003**, *57*, 827–854.
- (23) Oosawa, Y.; Gotoh, Y.; Akimoto, J.; Tsunoda, T.; Sohma, M.; Onoda, M. Three Types of Ternary Selenides with Layered Composite Crystal Structures Formed in the Pb-Nb-Se System. *Japanese J. Appl. Physics, Part 2 Lett.* **1992**, *31*, L1096-L1099.
- (24) Gotoh, Y.; Goto, M.; Kawaguchi, Y.; Onoda, M. Preparation and Characterization of a New Composite-Layered Sulfide, $(\text{PbS})_{1.12}\text{VS}_2$, “ PbVS_3 .” *Mater. Res. Bull.* **1990**, *25*, 307–314.

- (25) Ruscher, C. H.; Haas, C.; Smaalen, S. van; Wiegers, G. A. Investigation of the Optical Reflectivity of Misfit Layer Compounds: $(MS)_nTS_2$ (T=Ta, Nb; M=Sn, Pb, Sm, Tb, La; $1.08 < n < 1.23$). *J. Phys. Condens. Matter* **1994**, *6*, 2117–2128.
- (26) Roesky, R.; Gressier, P.; Meerschaut, A.; Widder, K.; Geserich, H. P.; Scheiber, G. Optical Properties and Electronic Structure of the Misfit Layer Compounds 'LnNb₂X₅' (Ln Identical to Y, La or Nd; X Identical to S or Se). *J. Phys. Condens. Matter* **1994**, *6*, 3437–3442.
- (27) Ren, Y.; Haas, C.; Wiegers, G. A. Photoelectron Spectroscopy Study of the Electronic Structure of the Incommensurate Intergrowth Compounds $(SbS)_{1.15}(TiS_2)_n$ with $n=1, 2$. *J. Phys. Condens. Matter* **1995**, *7*, 5949–5958.
- (28) Hernan, L.; Morales, J.; Pattanayak, J.; Tirado, J. L. Preparation and Characterization of New Misfit Layer Selenides SnVSe₃ and SnNb₂Se₅. *Chem Lett* **1991**, *20*, 1981–1984.
- (29) Giang, N.; Xu, Q.; Hor, Y. S.; Williams, A. J.; Dutton, S. E.; Zandbergen, H. W.; Cava, R. J. Superconductivity at 2.3 K in the Misfit Compound $(PbSe)_{1.16}(TiSe_2)_2$. *Phys. Rev. B* **2010**, *82*, 24503.
- (30) Trump, B. A.; Livi, K. J. T.; McQueen, T. M. The New Misfit Compound $(BiSe)_{1.15}(TiSe_2)_2$ and the Role of Demensionality in the $Cu_x(BiSe)_{1+\delta}(TiSe_2)_n$ Series. *J. Solid State Chem.* **2014**, *209*, 6–12.
- (31) Ohno, Y. Electron Tunneling from a Metallic TS₂ Layer underneath an Ultra-Thin MS Layer with Semiconducting Properties for Misfit-Layer Compounds. *Surf. Sci.* **2006**, *600*, 598–609.
- (32) Atkins, R.; Dolgos, M.; Fiedler, A.; Grosse, C.; Fischer, S. F.; Rudin, S. P.; Johnson, D. C. Synthesis and Systematic Trends in Structure and Electrical Properties of $[(SnSe)_{1.15}]_m(VSe_2)_1$, $m = 1, 2, 3$, and 4. *Chem. Mater.* **2014**, *26*, 2862–2872.
- (33) Atkins, R.; Wilson, J.; Zschack, P.; Grosse, C.; Neumann, W.; Johnson, D. C. Synthesis of $[(SnSe)_{1.15}]_m(TaSe_2)_n$ Ferecrystals: Structurally Tunable Metallic Compounds. *Chem. Mater.* **2012**, *24*, 4594–4599.
- (34) Atkins, R.; Disch, S.; Jones, Z.; Haeusler, I.; Grosse, C.; Fischer, S. F.; Neumann, W.; Zschack, P.; Johnson, D. C. Synthesis, Structure and Electrical Properties of a New Tin Vanadium Selenide. *J. Solid State Chem.* **2013**, *202*, 128–133.
- (35) Falmbigl, M.; Fiedler, A.; Atkins, R. E.; Fischer, S. F.; Johnson, D. C. Suppressing a Charge Density Wave by Changing Dimensionality in the Ferecrystalline Compounds $[(SnSe)_{1.15}]_1(VSe_2)_n$. *Nano Lett.* **2015**, *15*, 943–948.
- (36) Merrill, D. R.; Moore, D. B.; Ditto, J.; Sutherland, D. R.; Falmbigl, M.; Winkler, M.; Pernau, H.-F.; Johnson, D. C. The Synthesis, Structure, and Electrical Characterization of $(SnSe)_{1.2}TiSe_2$. *Eur. J. Inorg. Chem.* **2015**, *2015*, 83–91.

- (37) Bauers, S. R.; Merrill, D. R.; Moore, D. B.; Johnson, D. C. Carrier Dilution in TiSe₂ Based Intergrowth Compounds for Enhanced Thermoelectric Performance. *J. Mater. Chem. C* **2015**, *3*, 10451–10458.
- (38) Hite, O. K.; Nellist, M.; Ditto, J.; Falmbigl, M.; Johnson, D. C. Transport Properties of VSe₂ Monolayers Separated by Bilayers of BiSe. *J. Mater. Res.* **2016**, *31*, 886–892.
- (39) Alemayehu, M. B.; Mitchson, G.; Hanken, B. E.; Asta, M.; Johnson, D. C. Charge Transfer between PbSe and NbSe₂ in [(PbSe)_{1.14}]_m(NbSe₂)₁ Ferecrystalline Compounds. *Chem. Mater.* **2014**, *26*, 1859–1866.
- (40) Alemayehu, M. B.; Ta, K.; Falmbigl, M.; Johnson, D. C. Structure, Stability, and Properties of the Intergrowth Compounds ([SnSe]_{1+δ})_m(NbSe₂)_n. *J. Am. Chem. Soc.* **2015**, *137*, 4831–4839.
- (41) Alemayehu, M. B.; Falmbigl, M.; Ta, K.; Grosse, C.; Westover, R. D.; Bauers, S. R.; Fischer, S. F.; Johnson, D. C. Structural and Electrical Properties of ([SnSe]_{1+δ})_m(NbSe₂)₁ Compounds: Single NbSe₂ Layers Separated by Increasing Thickness of SnSe. *Chem. Mater.* **2015**, *27*, 867–875.
- (42) Moore, D. B.; Beekman, M.; Disch, S.; Zschack, P.; Häusler, I.; Neumann, W.; Johnson, D. C. Synthesis, Structure, and Properties of Turbostratically Disordered (PbSe)_{1.18}(TiSe₂)₂. *Chem. Mater.* **2013**, *25*, 2404–2409.
- (43) Thorne, R. E. Charge-Density-Waves Conductors. *Phys. Today* **1996**, *63*, 42.
- (44) Mutka, H.; Housseau, N.; Pelissier, J.; Ayroles, R.; Roucau, C. Effects of Defects on Charge Density Waves in Layered Dichalcogenides. *Solid State Commun.* **1984**, *50*, 161–164.
- (45) Morris, R. C. Connection between Charge-Density Waves and Superconductivity in NbSe₂. *Phys. Rev. Lett.* **1975**, *34* (18), 1164–1166.
- (46) LeBlanc, a.; Nader, a. Resistivity Anisotropy and Charge Density Wave in 2H - NbSe₂ and 2H - TaSe₂. *Solid State Commun.* **2010**, *150* (29-30), 1346–1349.
- (47) Yang, J.; Wang, W.; Liu, Y.; Du, H.; Ning, W.; Zheng, G.; Jin, C.; Han, Y.; Wang, N.; Yang, Z.; Tian, M.; Zhang, Y. Thickness Dependence of the Charge-Density-Wave Transition Temperature in VSe₂. *Appl. Phys. Lett.* **2014**, *105* (6), 063109.
- (48) Samnakay, R.; Wickramaratne, D.; Pope, T. R.; Lake, R. K.; Salguero, T. T.; Balandin, A. A. Zone-Folded Phonons and the Commensurate-Incommensurate Charge-Density-Wave Transition in 1 T -TaSe₂ Thin Films. *Nano Lett.* **2015**, *15*, 2965–2973.
- (49) Goli, P.; Khan, J.; Wickramaratne, D.; Lake, R. K.; Balandin, A. A. Charge Density Waves in Exfoliated Thin Films of Van Der Waals Materials: Evolution of Raman Spectrum in TiSe₂. *Nano Lett.* **2012**, *12*, 5941–5945.

- (50) Xu, K.; Chen, P.; Li, X.; Wu, C.; Guo, Y.; Zhao, J.; Wu, X.; Xie, Y. Ultrathin Nanosheets of Vanadium Diselenide: A Metallic Two-Dimensional Material with Ferromagnetic Charge-Density-Wave Behavior. *Angew. Chemie Int. Ed.* **2013**, *52*, 10477–10481.
- (51) Bayard, M.; Sienko, M. J. Anomalous Electrical and Magnetic Properties of Vanadium Diselenide. *J. Solid State Chem.* **1976**, *19*, 325–329.

Chapter II

- (1) Smeller, M. M.; Heideman, C. L.; Lin, Q.; Beekman, M.; Anderson, M. D.; Zschack, P.; Anderson, I. M.; Johnson, D. C. Structure of Turbostratically Disordered Misfit Layer Compounds [(PbSe)_{0.99}]₁[WSe₂]₁, [(PbSe)_{1.00}]₁[MoSe₂]₁, and [(SnSe)_{1.03}]₁[MoSe₂]₁. *Z. Anorg. Allg. Chem.* **2012**, *638*, 2632–2639.
- (2) Fister, L.; Li, X.-M.; McConnell, J.; Novet, T.; Johnson, D. C. Deposition System for the Synthesis of Modulated, Ultrathin-Film Composites. *J. Vac. Sci. Technol. A* **1993**, *11*, 3014–3019.
- (3) Ming, X.; Tao, Y.; Wen-xue, Y.; Ning, Y.; Cui-xiu, L.; Xhen-hong, M.; Wu-yan, L.; Kun, T. Accurate Determination of Film Thickness by Low-Angle X-Ray Reflectivity. *Chinese Phys. Soc.* **2000**, *9*, 833–836.
- (4) Ofuji, M.; Inaba, K.; Omote, K.; Hoshi, H.; Takanishi, Y.; Ishikawa, K.; Takezoe, H. Grazing Incidence In-Plane X-Ray Diffraction Study on Oriented Copper Phthalocyanine Thin Films. *Japan Soc. Appl. Phys.* **2002**, *41*, 5467–5471.
- (5) Fullerton, E. E.; Schuller, I. K.; Vanderstraeten, H.; Bruynseraede, Y. Structural Refinement of Superlattices from X-Ray Diffraction. *Phys. Rev. B* **1992**, *45*, 9292–9310.
- (6) Phung, T. M.; Jensen, J. M.; Johnson, D. C.; Donovan, J. J.; Mccburnett, B. G. Determination of the Composition of Ultra-Thin Ni-Si Films on Si: Constrained Modeling of Electron Probe Microanalysis and X-Ray Reflectivity Data. *X-Ray Spectrom.* **2008**, *37*, 608–614.
- (7) Schaffer, M.; Schaffer, B.; Ramasse, Q. Sample Preparation for Atomic-Resolution STEM at Low Voltages by FIB. *Ultramicroscopy* **2012**, *114*, 62–71.
- (8) van der Pauw, L. J. A Method of Measuring the Resistivity and Hall Coefficient of Lamellae of Arbitrary Shape. *Philips Tech. Rev.* **1958**, *26*, 220–224.

Chapter III

- (1) Novoselov, K. S.; Geim, A. K.; Morozov, S. V.; Jiang, D.; Zhang, Y.; V, D. S.; Grigorieva, I. V.; Firsov, A. A. Electrical Field Effect in Atomically Thin Carbon Films. *Science* **2004**, *306*, 666–669.
- (2) Kim, K. K.; Hsu, A.; Jia, X.; Kim, S. M.; Shi, Y.; Hofmann, M.; Nezich, D.; Rodriguez-nieva, J. F.; Dresselhaus, M.; Palacios, T.; Kong, J. Synthesis of

Monolayer Hexagonal Boron Nitride on Cu Foil Using Chemical Vapor Deposition. *Nano Lett.* **2011**, *12*, 161–166.

- (3) Peng, Q.; Ji, W.; De, S. Mechanical Properties of the Hexagonal Boron Nitride Monolayer: Ab Initio Study. *Comput. Mater. Sci.* **2012**, *56*, 11–17.
- (4) Duan, X.; Wang, C.; Pan, A.; Yu, R.; Duan, X. Two-Dimensional Transition Metal Dichalcogenides as Atomically Thin Semiconductors: Opportunities and Challenges. *Chem. Soc. Rev.* **2015**, *44*, 8859–8876.
- (5) Tan, C.; Zhang, H. Two-Dimensional Transitional Metal Dichalcogenide Nanosheet-Based Composites. *Chem. Soc. Rev.* **2015**, *44*, 2713–2731.
- (6) Wang, H.; Yuan, H.; Sae Hong, S.; Li, Y.; Cui, Y. Physical and Chemical Tuning of Two-Dimensional Transition Metal Dichalcogenides. *Chem. Soc. Rev.* **2015**, *44*, 2664–2680.
- (7) Gomes, L. C.; Carvalho, A. Phosphorene Analogues: Isoelectronic Two-Dimensional Group-IV Monochalcogenides with Orthorhombic Structure. *Phys. Rev. B* **2015**, *92*, 085406.
- (8) Fujimoto, Y.; Koretsune, T.; Saito, S. Electronic Structures of Hexagonal Boron-Nitride Monolayer: Strain-Induced Effects. *J. Ceram. Soc. Japan* **2014**, *122*, 346–348.
- (9) Wang, M.-X.; Li, P.; Xu, J.-P.; Liu, Z.-L.; Ge, J.-F.; Wang, G.-Y.; Yang, X.; Xu, Z.-A.; Ji, S.-H.; Gao, C. L.; Qian, D.; Luo, W.; Liu, C.; Jia, J.-F. Interface Structure of a Topological Insulator/superconductor Heterostructure. *New J. Phys.* **2014**, *16*, 123043.
- (10) Xu, J.-P.; Wang, M.-X.; Liu, Z. L.; Ge, J.-F.; Yang, X.; Liu, C.; Xu, Z. A.; Guan, D.; Gao, C. L.; Qian, D.; Liu, Y.; Wang, Q.-H.; Zhang, F.-C.; Xue, Q.-K.; Jia, J.-F. Experimental Detection of a Majorana Mode in the Core of a Magnetic Vortex inside a Topological Insulator-Superconductor $\text{Bi}_2\text{Te}_3/\text{NbSe}_2$ Heterostructure. *Phys. Rev. Lett.* **2015**, *114*, 017001.
- (11) Geim, A. K.; Grigorieva, I. V. Van Der Waals Heterostructures. *Nature* **2013**, *499*, 419–425.
- (12) Furchi, M. M.; Pospischil, A.; Libisch, F.; Burgdörfer, J.; Mueller, T. Photovoltaic Effect in an Electrically Tunable van Der Waals Heterojunction. *Nano Lett.* **2014**, *14*, 4785–4791.
- (13) Hong, X.; Kim, J.; Shi, S.-F.; Zhang, Y.; Jin, C.; Sun, Y.; Tongay, S.; Wu, J.; Zhang, Y.; Wang, F. Ultrafast Charge Transfer in Atomically Thin MoS_2/WS_2 Heterostructures. *Nat. Nanotechnol.* **2014**, *9*, 682–686.
- (14) Rivera, P.; Schaibley, J. R.; Jones, A. M.; Ross, J. S.; Wu, S.; Aivazian, G.; Klement, P.; Seyler, K.; Clark, G.; Ghimire, N. J.; Yan, J.; Mandrus, D. G.; Yao, W.; Xu, X.

Observation of Long-Lived Interlayer Excitons in Monolayer MoSe₂-WSe₂ Heterostructures. *Nat. Commun.* **2015**, *6*, 6242.

- (15) Grønberg, S. S.; Ulstrup, S.; Bianchi, M.; Dendzik, M.; Sanders, C. E.; Lauritsen, J. V.; Hofmann, P.; Miwa, J. A. Synthesis of Epitaxial Single-Layer MoS₂ on Au(111). *Langmuir* **2015**, *31*, 9700–9706.
- (16) El-Bana, M. S.; Wolverson, D.; Russo, S.; Balakrishnan, G.; Paul, D. M.; Bending, S. J. Superconductivity in Two-Dimensional NbSe₂ Field Effect Transistors. *Supercond. Sci. Technol.* **2013**, *26*, 125020.
- (17) Frindt, R. F. Superconductivity in Ultrathin NbSe₂ Layers. *Phys. Rev. Lett.* **1972**, *28*, 299–301.
- (18) Grosse, C.; Alemayehu, M. B.; Falmbigl, M.; Mogilatenko, A.; Chiatti, O.; Johnson, D. C.; Fischer, S. F. Superconducting Ferecrystals: Turbostratically Disordered Atomic-Scale Layered (PbSe)_{1.14}(NbSe₂)_n Thin Films. *Sci. Rep.* **2016**, *6*, 33457.
- (19) Gao, D.; Xue, Q.; Mao, X.; Wang, W.; Xu, Q.; Xue, D. Ferromagnetism in Ultrathin VS₂ Nanosheets. *J. Mater. Chem. C* **2013**, *1*, 5909–5916.
- (20) Zhang, H.; Liu, L.-M.; Lau, W.-M. Dimension-Dependent Phase Transition and Magnetic Properties of VS₂. *J. Mater. Chem. A* **2013**, *1*, 10821–10828.
- (21) Bayard, M.; Sienko, M. J. Anomalous Electrical and Magnetic Properties of Vanadium Diselenide. *J. Solid State Chem.* **1976**, *19*, 325–329.
- (22) Xu, K.; Chen, P.; Li, X.; Wu, C.; Guo, Y.; Zhao, J.; Wu, X.; Xie, Y. Ultrathin Nanosheets of Vanadium Diselenide: A Metallic Two-Dimensional Material with Ferromagnetic Charge-Density-Wave Behavior. *Angew. Chemie Int. Ed.* **2013**, *52*, 10477–10481.
- (23) Yang, J.; Wang, W.; Liu, Y.; Du, H.; Ning, W.; Zheng, G.; Jin, C.; Han, Y.; Wang, N.; Yang, Z.; Tian, M.; Zhang, Y. Thickness Dependence of the Charge-Density-Wave Transition Temperature in VSe₂. *Appl. Phys. Lett.* **2014**, *105*, 063109.
- (24) Atkins, R.; Disch, S.; Jones, Z.; Haeusler, I.; Grosse, C.; Fischer, S. F.; Neumann, W.; Zschack, P.; Johnson, D. C. Synthesis, Structure and Electrical Properties of a New Tin Vanadium Selenide. *J. Solid State Chem.* **2013**, *202*, 128–133.
- (25) Falmbigl, M.; Fiedler, A.; Atkins, R. E.; Fischer, S. F.; Johnson, D. C. Suppressing a Charge Density Wave by Changing Dimensionality in the Ferecrystalline Compounds ([SnSe]_{1.15})₁(VSe₂)_n. *Nano Lett.* **2015**, *15*, 943–948.
- (26) Goli, P.; Khan, J.; Wickramaratne, D.; Lake, R. K.; Balandin, A. A. Charge Density Waves in Exfoliated Films of van der Waals Materials: Evolution of Raman Spectrum in TiSe₂. *Nano Lett.* **2012**, *12*, 5941–5945.
- (27) Samnakay, R.; Wickramaratne, D.; Pope, T. R.; Lake, R. R.; Salguero, T. T.; Balandin, A. A. Zone-Folded Phonons and the Commensurate-Incommensurate

Charge-Density-Wave Transition in 1T-TaSe₂ Thin Films. *Nano Lett.* **2015**, *15*, 2965-2973.

- (28) Atkins, R.; Dolgos, M.; Fiedler, A.; Grosse, C.; Fischer, S. F.; Rudin, S. P.; Johnson, D. C. Synthesis and Systematic Trends in Structure and Electrical Properties of [(SnSe)_{1.15}]_m(VSe₂)₁, m = 1, 2, 3, and 4. *Chem. Mater.* **2014**, *26*, 2862–2872.
- (29) Fister, L.; Li, X.-M.; McConnell, J.; Novet, T.; Johnson, D. C. Deposition System for the Synthesis of Modulated, Ultrathin-Film Composites. *J. Vac. Sci. Technol. A* **1993**, *11*, 3014.
- (30) Phung, T. M.; Jensen, J. M.; Johnson, D. C.; Donovan, J. J.; MCBurnett, B. G. Determination of the Composition of Ultra-Thin Ni-Si Films on Si: Constrained Modeling of Electron Probe Microanalysis and X-Ray Reflectivity Data. *X-Ray Spectrom.* **2008**, *37*, 608–614.
- (31) Schaffer, M.; Schaffer, B.; Ramasse, Q. Sample Preparation for Atomic-Resolution STEM at Low Voltages by FIB. *Ultramicroscopy* **2012**, *114*, 62–71.
- (32) Van der Pauw, L. J. A Method of Measuring the Resistivity and Hall Coefficient of Lamellae of Arbitrary Shape. *Philips Tech. Rev.* **1958**, *26*, 220–224.
- (33) Alemayehu, M. B.; Mitchson, G.; Hanken, B. E.; Asta, M.; Johnson, D. C. Charge Transfer between PbSe and NbSe₂ in [(PbSe)_{1.14}]_m(NbSe₂)₁ Ferecrystalline Compounds. *Chem. Mater.* **2014**, *26*, 1859–1866.
- (34) Atkins, R.; Wilson, J.; Zschack, P.; Grosse, C.; Neumann, W.; Johnson, D. C. Synthesis of [(SnSe)_{1.15}]_m(TaSe₂)_n Ferecrystals: Structurally Tunable Metallic Compounds. *Chem. Mater.* **2012**, *24*, 4594–4599.
- (35) Bauers, S. R.; Merrill, D. R.; Moore, D. B.; Johnson, D. C. Carrier Dilution in TiSe₂ Based Intergrowth Compounds for Enhanced Thermoelectric Performance. *J. Mater. Chem. C* **2015**, *3*, 10451–10458.
- (36) Merrill, D. R.; Moore, D. B.; Ditto, J.; Sutherland, D. R.; Falmbigl, M.; Winkler, M.; Pernau, H.-F.; Johnson, D. C. The Synthesis, Structure, and Electrical Characterization of (SnSe)_{1.2}TiSe₂. *Eur. J. Inorg. Chem.* **2015**, *2015*, 83–91.
- (37) De Boer, J. L.; Meetsma, A.; Zeinstra, T. J.; Haange, R. J.; Wiegers, G. A. Structures of the Misfit Layer Compounds (LaS)_{1.13}TaS₂, “LaTaS₃” and (CeS)_{1.5}TaS₂, “CeTaS₃.” *Acta Crystallogr. C* **1991**, *47*, 924–930.
- (38) Van Smaalen, S.; Meetsma, A.; Wiegers, G. A.; de Boer, J. L. Determination of the Modulated Structure of the Inorganic Misfit Layer Compound (PbS)_{1.18}TiS₂. *Acta Crystallogr. B* **1991**, *47*, 314–325.
- (39) Wiegers, G. A. Misfit Layer Compounds: Structures and Physical Properties. *Prog. Solid State Chem.* **1996**, *24*, 1–139.

- (40) Wiegers, G. A.; Meetsma, A.; de Boer, J. L.; van Smaalen, S.; Haange, R. J. X-Ray Crystal Structure Determination of the Triclinic Misfit Layer Compound $(\text{SnS})_{1.20}\text{TiS}_2$. *J. Phys. Condens. Matter* **1991**, *3*, 2603–2612.
- (41) Wiegers, G. A.; Meetsma, A.; Haange, R. J.; van Smaalen, S.; de Boer, J. L.; Meerschaut, A.; Rabu, P.; Rouxel, J. The Incommensurate Misfit Layer Structure of $(\text{PbS})_{1.14}\text{NbS}_2$, “ PbNbS_3 ” and $(\text{LaS})_{1.14}\text{NbS}_2$, “ LaNbS_3 ”: An X-Ray Diffraction Study. *Acta Crystallogr. B* **1990**, *46*, 324–332.
- (42) Wiegers, G. A.; Meetsma, A.; van Smaalen, S.; Haange, R. J.; de Boer, J. L. Structural Relationship between the Orthorhombic, Monoclinic and Triclinic Misfit Layer Compounds $(\text{MS})_n\text{TS}_2$ ($\text{M} = \text{Sn, Pb, Rare-Earth-Metals, T} = \text{Ti, V, Cr, Nb, Ta; } 1.13 < n < 1.21$). *Solid State Commun.* **1990**, *75*, 689–692.
- (43) Meerschaut, A.; Guemas, L.; Auriel, C.; Rouxel, J. Preparation, Structure Determination and Transport Properties of a New Misfit Layer Compound: Lead Niobium Sulfide $((\text{PbS})_{1.14}(\text{NbS}_2)_2)$. *Eur. J. Solid State Inorg. Chem.* **1990**, *27*, 557–570.
- (44) Smeller, M. M.; Heideman, C. L.; Lin, Q.; Beekman, M.; Anderson, M. D.; Zschack, P.; Anderson, I. M.; Johnson, D. C. Structure of Turbostratically Disordered Misfit Layer Compounds $[(\text{PbSe})_{0.99}]_1[\text{WSe}_2]_1$, $[(\text{PbSe})_{1.00}]_1[\text{MoSe}_2]_1$, and $[(\text{SnSe})_{1.03}]_1[\text{MoSe}_2]_1$. *Z. Anorg. Allg. Chem.* **2012**, *638*, 2632–2639.
- (45) Moore, D. B.; Beekman, M.; Disch, S.; Zschack, P.; Häusler, I.; Neumann, W.; Johnson, D. C. Synthesis, Structure, and Properties of Turbostratically Disordered $(\text{PbSe})_{1.18}(\text{TiSe}_2)_2$. *Chem. Mater.* **2013**, *25*, 2404–2409.
- (46) Ren, Y.; Baas, J.; Meetsma, A.; de Boer, J. L.; Wiegers, G. A. Vacancies and Electron Localization in the Incommensurate Intergrowth Compound $(\text{La}_{0.95}\text{Se})_{1.21}\text{VSe}_2$. *Acta Crystallogr. B* **1996**, *52*, 398–405.
- (47) Gotoh, Y.; Onoda, M.; Akimoto, J.; Oosawa, Y. Preparation and Characterization of New Sb-Containing Ternary Sulfides with Layered Composite Crystal Structure. *Jpn. J. Appl. Phys.* **1992**, *30*, L1039–L1041.
- (48) Gotoh, Y.; Onoda, M.; Akimoto, J.; Goto, M.; Oosawa, Y. The Layered Composite Crystal Structure of the Ternary Sulfide, $(\text{BiS})_{1.07}\text{TaS}_2$, “ BiTaS_3 .” *Jpn. J. Appl. Phys.* **1992**, *31*, 3946–3950.
- (49) Gotoh, Y.; Goto, M.; Kawaguchi, Y.; Onoda, M. Preparation and Characterization of a New Composite-Layered Sulfide, $(\text{PbS})_{1.12}\text{VS}_2$, “ PbVS_3 .” *Mater. Res. Bull.* **1990**, *25*, 307–314.
- (50) Wiegers, G. A.; Haange, R. J. Electrical Transport Properties of the Misfit Layer Compounds $(\text{SnS})_{1.20}\text{TiS}_2$ and $(\text{PbS})_{1.18}\text{TiS}_2$. *Eur. J. Solid State Inorg. Chem.* **1991**, *28*, 1071–1078.

- (51) Wiegers, G. A.; Meetsma, A.; Haange, R. J.; de Boer, J. L. Structure and Physical Properties of $(\text{SnS})_{1.18}\text{NbS}_2$, “ SnNbS_3 ”, a Compound with Misfit Layer Structure. *Mater. Res. Bull.* **1988**, *23*, 1551–1559.
- (52) Wulff, J.; Meetsma, A.; Haange, R. J.; de Boer, J. L.; Wiegers, G. A. Structure and Electrical Transport Properties of the Misfit-Layer Compound $(\text{BiS})_{1.08}\text{TaS}_2$. *Synth. Met.* **1990**, *39*, 1–12.
- (53) Yarmoshenko, Y. M.; Trofimova, V. A.; Shamin, S. N.; Solovyev, N. V.; Kurmaev, E. Z.; Ettema, A. R. H. F.; Haas, C. The X-Ray Emission Spectra and Electronic-Structure of the Misfit Layer Compounds $(\text{BiS})_{1.08}\text{NbS}_2$ and $(\text{PbS})_{1.14}\text{TaS}_2$. *J. Phys. Condens. Matter* **1994**, *6*, 3993–3998.
- (54) Meerschaut, A. Misfit Layer Compounds. *Curr. Opin. Solid State Mater. Sci.* **1996**, *1*, 250–259.
- (55) Meerschaut, A.; Auriel, C.; Rouxel, J. Structure Determination of a New Misfit Layer Compound $(\text{PbS})_{1.18}(\text{TiS}_2)_2$. *J. Alloys Compd.* **1983**, *183*, 129–137.
- (56) Meerschaut, A.; Deudon, C. Crystal Structure Studies of the $3\text{R-Nb}_{1.09}\text{S}_2$ and the 2H-NbSe_2 Compounds: Correlation between Nonstoichiometry and Stacking Type (= Polytypism). *Mater. Res. Bull.* **2001**, *36*, 1721–1727.
- (57) Meerschaut, A.; Roesky, R.; Lafond, A.; Deudon, C.; Rouxel, J. Misfit Layered Compounds: Polytypism, Multilayer Stages, Non-Stoichiometry and Electronic Structure, Self-Misfit Compounds. *J. Alloys Compd.* **1995**, *219*, 157–160.
- (58) Meetsma, A.; Wiegers, G. A.; Haange, R. J.; de Boer, J. L. The Incommensurate Misfit Layer Structure of $(\text{SnS})_{1.17}\text{NbS}_2$, “ SnNbS_3 ”. I. A Study by Means of X-Ray Diffraction. *Acta Crystallogr. A* **1989**, *45*, 285–291.
- (59) Onoda, M.; Kato, K.; Gotoh, Y.; Oosawa, Y. Structure of the Incommensurate Composite Crystal $(\text{PbS})_{1.12}\text{VS}_2$. *Acta Crystallogr. B* **1990**, *46*, 487–492.
- (60) Beekman, M.; Heideman, C. L.; Johnson, D. C. Ferrecrystals: Non-Epitaxial Layered Intergrowths. *Semicond. Sci. Technol.* **2014**, *29*, 064012.
- (61) Falmbigl, M.; Putzky, D.; Ditto, J.; Esters, M.; Bauers, S. R.; Ronning, F.; Johnson, D. C. Influence of Defects on the Charge Density Wave of $([\text{SnSe}]_{1+\delta})_1(\text{VSe}_2)_1$ Ferrecrystals. *ACS Nano* **2015**, *9*, 8440–8448.
- (62) Barrios-Salgado, E.; Rodríguez-Guadarrama, L. A.; Garcia-Angelmo, A. R.; Campos Álvarez, J.; Nair, M. T. S.; Nair, P. K. Large Cubic Tin Sulfide–tin Selenide Thin Film Stacks for Energy Conversion. *Thin Solid Films* **2016**, *615*, 415–422.
- (63) Wrasse, E. O.; Schmidt, T. M. Prediction of Two-Dimensional Topological Crystalline Insulator in PbSe Monolayer. *Nano Lett.* **2014**, *14*, 5717–5720.
- (64) Alemayehu, M. B.; Falmbigl, M.; Ta, K.; Grosse, C.; Westover, R. D.; Bauers, S. R.; Fischer, S. F.; Johnson, D. C. Structural and Electrical Properties of

$([\text{SnSe}]_{1+\delta})_m(\text{NbSe}_2)_1$ Compounds: Single NbSe_2 Layers Separated by Increasing Thickness of SnSe . *Chem. Mater.* **2015**, *27*, 867–875.

- (65) Falmbigl, M.; Hay, Z.; Ditto, J.; Mitchson, G.; Johnson, D. C. Modifying a Charge Density Wave Transition by Modulation Doping: Ferecrystalline Compounds $([\text{Sn}_{1-x}\text{Bi}_x\text{Se}]_{1.15})_1(\text{VSe}_2)_1$ with $0 \leq x \leq 0.66$. *J. Mater. Chem. C* **2015**, *3*, 12308–12315.
- (66) Li, F.; Tu, K.; Chen, Z. Versatile Electronic Properties of VSe_2 Bulk , Few-Layers , Monolayer , Nanoribbons , and Nanotubes : A Computational Exploration. *J. Phys. Chem.* **2014**, *118*, 21264–21274.
- (67) Wasey, A. H. M. A.; Chakrabarty, S.; Das, G. P. Quantum Size Effects in Layered VX_2 (X = S, Se) Materials: Manifestation of Metal to Semimetal or Semiconductor Transition. *J. Appl. Phys.* **2015**, *117*, 064313.
- (68) Chhowalla, M.; Shin, H. S.; Eda, G.; Li, L.-J.; Loh, K. P.; Zhang, H. The Chemistry of Two-Dimensional Layered Transition Metal Dichalcogenide Nanosheets. *Nat. Chem.* **2013**, *5*, 263–275.
- (69) Hite, O. K.; Nellist, M.; Ditto, J.; Falmbigl, M.; Johnson, D. C. Transport Properties of VSe_2 Monolayers Separated by Bilayers of BiSe . *J. Mater. Res.* **2016**, *31*, 886–892.
- (70) Alemayehu, M. B.; Falmbigl, M.; Ta, K.; Ditto, J.; Medlin, D. L.; Johnson, D. C. Designed Synthesis of van Der Waals Heterostructures : The Power of Kinetic Control. *Angew. Chemie Int. Ed.* **2015**, *54*, 15468–15472.

Chapter IV

- (1) Geim, A. K. Graphene : Status and Prospects. *Science.* **2009**, *324*, 1530–1535.
- (2) Wang, Q. H.; Kalantar-Zadeh, K.; Kis, A.; Coleman, J. N.; Strano, M. S. Electronics and Optoelectronics of Two-Dimensional Transition Metal Dichalcogenides. *Nat. Nanotechnol.* **2012**, *7*, 699–712.
- (3) Wang, H.; Yuan, H.; Sae Hong, S.; Li, Y.; Cui, Y. Physical and Chemical Tuning of Two-Dimensional Transition Metal Dichalcogenides. *Chem. Soc. Rev.* **2015**, *44*, 2664–2680.
- (4) El-Bana, M. S.; Wolverson, D.; Russo, S.; Balakrishnan, G.; Paul, D. M.; Bending, S. J. Superconductivity in Two-Dimensional NbSe_2 Field Effect Transistors. *Supercond. Sci. Technol.* **2013**, *26*, 125020.
- (5) Anderson, M. D.; Heideman, C. L.; Lin, Q.; Smeller, M.; Kokenyesi, R.; Herzing, A. a.; Anderson, I. M.; Keszler, D. a.; Zschack, P.; Johnson, D. C. Size-Dependent Structural Distortions in One-Dimensional Nanostructures. *Angew. Chemie - Int. Ed.* **2013**, *52*, 1982–1985.

- (6) Geim, A. K.; Grigorieva, I. V. Van Der Waals Heterostructures. *Nature* **2013**, *499*, 419–425.
- (7) Zeng, Q.; Wang, H.; Fu, W.; Gong, Y.; Zhou, W.; Ajayan, P. M.; Lou, J.; Liu, Z. Band Engineering for Novel Two-Dimensional Atomic Layers. *Small* **2015**, *11*, 1868–1884.
- (8) Qian, X.; Liu, J.; Fu, L.; Li, J. Quantum Spin Hall Effect and Topological Field Effect Transistor in Two-Dimensional Transition Metal Dichalcogenide. *Science* **2014**, *346*, 1344–1347.
- (9) Yang, W.; Chen, G.; Shi, Z.; Liu, C.-C.; Zhang, L.; Xie, G.; Cheng, M.; Wang, D.; Yang, R.; Shi, D.; Watanabe, K.; Taniguchi, T.; Yao, Y.; Zhang, Y.; Zhang, G. Epitaxial Growth of Single-Domain Graphene on Hexagonal Boron Nitride. *Nat. Mater.* **2013**, *12*, 792–797.
- (10) Gong, Y.; Lei, S.; Ye, G.; Li, B.; He, Y.; Keyshar, K.; Zhang, X.; Wang, Q.; Lou, J.; Liu, Z.; Vajtai, R.; Zhou, W.; Ajayan, P. M. Two-Step Growth of Two-Dimensional WSe₂/MoSe₂ Heterostructures. *Nano Lett.* **2015**.
- (11) Heideman, C. L.; Tepfer, S.; Lin, Q.; Rostek, R.; Zschack, P.; Anderson, M. D.; Anderson, I. M.; Johnson, D. C. Designed Synthesis, Structure, and Properties of a Family of Ferrecrystalline Compounds [(PbSe)_{1.00}]_m(MoSe₂)_n. *J. Am. Chem. Soc.* **2013**, *135*, 11055–11062.
- (12) Bayard, M.; Sienko, M. J. Anomalous Electrical and Magnetic Properties of Vanadium Diselenide. *J. Solid State Chem.* **1976**, *19*, 325–329.
- (13) Xu, K.; Chen, P.; Li, X.; Wu, C.; Guo, Y.; Zhao, J.; Wu, X.; Xie, Y. Ultrathin Nanosheets of Vanadium Diselenide: A Metallic Two-Dimensional Material with Ferromagnetic Charge-Density-Wave Behavior. *Angew. Chem. Int. Ed. Engl.* **2013**, *52*, 10477–10481.
- (14) Yang, J.; Wang, W.; Liu, Y.; Du, H.; Ning, W.; Zheng, G.; Jin, C.; Han, Y.; Wang, N.; Yang, Z.; Tian, M.; Zhang, Y. Thickness Dependence of the Charge-Density-Wave Transition Temperature in VSe₂. *Appl. Phys. Lett.* **2014**, *105*, 063109.
- (15) Atkins, R.; Disch, S.; Jones, Z.; Haeusler, I.; Grosse, C.; Fischer, S. F.; Neumann, W.; Zschack, P.; Johnson, D. C. Synthesis, Structure and Electrical Properties of a New Tin Vanadium Selenide. *J. Solid State Chem.* **2013**, *202*, 128–133.
- (16) Falmbigl, M.; Fiedler, A.; Atkins, R. E.; Fischer, S. F.; Johnson, D. C. Suppressing a Charge Density Wave by Changing Dimensionality in the Ferrecrystalline Compounds ([SnSe]_{1.15})₁(VSe₂)_n. *Nano Lett.* **2015**, *15*, 943–948.
- (17) Zhou, W. Y.; Meetsma, A.; de Boer, J. L.; Wiegers, G. A. Characterization and Electrical Transport Properties of the Misfit Layer Compounds (BiSe)_{1.10}NbSe₂ and (BiSe)_{1.09}TaSe₂. *Mater. Res. Bull.* **1992**, *27*, 563–572.

- (18) Wiegers, G. A. Misfit Layer Compounds: Structures and Physical Properties. *Prog. Solid State Chem.* **1996**, *24*, 1–139.
- (19) Petříček, V.; Cisarova, I.; de Boer, J. L.; Zhou, W.; Meetsma, a.; Wiegers, G. a.; van Smaalen, S. The Modulated Structure of the Commensurate Misfit-Layer Compound $(\text{BiSe})_{1.09}\text{TaSe}_2$. *Acta Cryst.* **1993**, *B49*, 258–266.
- (20) Fister, L. Deposition System for the Synthesis of Modulated, Ultrathin-Film Composites. *J. Vac. Sci. Technol. A* **1993**, *11*, 3014.
- (21) Schaffer, M.; Schaffer, B.; Ramasse, Q. Sample Preparation for Atomic-Resolution STEM at Low Voltages by FIB. *Ultramicroscopy* **2012**, *114*, 62–71.
- (22) Van der Pauw, L. J. A Method of Measuring the Resistivity and Hall Coefficient of Lamellae of Arbitrary Shape. *Philips Tech. Rev.* **1958**, *26*, 220–224.
- (23) Heideman, C.; Nyugen, N.; Hanni, J.; Lin, Q.; Duncombe, S.; Johnson, D. C.; Zschack, P. The Synthesis and Characterization of New $[(\text{BiSe})_{1.10}]_m[\text{NbSe}_2]_n$, $[(\text{PbSe})_{1.10}]_m[\text{NbSe}_2]_n$, $[(\text{CeSe})_{1.14}]_m[\text{NbSe}_2]_n$ and $[(\text{PbSe})_{1.12}]_m[\text{TaSe}_2]_n$ Misfit Layered Compounds. *J. Solid State Chem.* **2008**, *181*, 1701–1706.
- (24) Grosse, C.; Atkins, R.; Kirmse, H.; Mogilatenko, A.; Neumann, W.; Johnson, D. C. Local Structure and Defect Chemistry of $[(\text{SnSe})_{1.15}]_m(\text{TaSe}_2)$ Ferecrystals - A New Type of Layered Intergrowth Compound. *J. Alloys Compd.* **2013**, *579*, 507–515.
- (25) Alemayehu, M. B.; Falmbigl, M.; Grosse, C.; Ta, K.; Fischer, S. F.; Johnson, D. C. Structural and Electrical Properties of a New $([\text{SnSe}]_{1.16})_m(\text{NbSe}_2)$ Polytype. *J. Alloys Compd.* **2015**, *619*, 816–868.
- (26) Mitchson, G.; Falmbigl, M.; Ditto, J.; Johnson, D. C. Antiphase Boundaries in the Turbostratically Disordered Misfit Compound $(\text{BiSe})_{1+\delta}\text{NbSe}_2$. *Inorg. Chem.* **2015**, *54*, 10309–10315.

Chapter V

- (1) Novoselov, K. S.; Geim, A. K.; Morozov, S. V; Jiang, D.; Zhang, Y.; Dubonos, S. V; Grigorieva, I. V; Firsov, A. A. Electrical Field Effect in Atomically Thin Carbon Films. *Science*. **2004**, *306*, 666–669.
- (2) Wang, M.-X.; Li, P.; Xu, J.-P.; Liu, Z.-L.; Ge, J.-F.; Wang, G.-Y.; Yang, X.; Xu, Z.-A.; Ji, S.-H.; Gao, C. L.; Qian, D.; Luo, W.; Liu, C.; Jia, J.-F. Interface Structure of a Topological Insulator/superconductor Heterostructure. *New J. Phys.* **2014**, *16*, 123043.
- (3) Fujimoto, Y.; Koretsune, T.; Saito, S. Electronic Structures of Hexagonal Boron-Nitride Monolayer: Strain-Induced Effects. *J. Ceram. Soc. Japan* **2014**, *122*, 346–348.
- (4) Geim, A. K.; Grigorieva, I. V. Van Der Waals Heterostructures. *Nature* **2013**, *499*, 419–425.

- (5) Yang, J.; Wang, W.; Liu, Y.; Du, H.; Ning, W.; Zheng, G.; Jin, C.; Han, Y.; Wang, N.; Yang, Z.; Tian, M.; Zhang, Y. Thickness Dependence of the Charge-Density-Wave Transition Temperature in VSe_2 . *Appl. Phys. Lett.* **2014**, *105*, 63109.
- (6) Xu, K.; Chen, P.; Li, X.; Wu, C.; Guo, Y.; Zhao, J.; Wu, X.; Xie, Y. Ultrathin Nanosheets of Vanadium Diselenide: A Metallic Two-Dimensional Material with Ferromagnetic Charge-Density-Wave Behavior. *Angew. Chemie Int. Ed.* **2013**, *52*, 10477–10481.
- (7) Falmbigl, M.; Fiedler, A.; Atkins, R. E.; Fischer, S. F.; Johnson, D. C. Suppressing a Charge Density Wave by Changing Dimensionality in the Ferrecrystalline Compounds $([SnSe]_{1.15})_1(VSe_2)_n$. *Nano Lett.* **2015**, *15*, 943–948.
- (8) Hite, O. K.; Falmbigl, M.; Alemayehu, M. B.; Esters, M.; Wood, S. R.; Johnson, D. C. Charge Density Wave Transition in $(PbSe)_{1+\delta}(VSe_2)_n$ Compounds with $N = 1, 2$, and 3 . *Chem. Mater.* **2017**, *29*, 5646–5653.
- (9) Fister, L.; Li, X.-M.; McConnell, J.; Novet, T.; Johnson, D. C. Deposition System for the Synthesis of Modulated, Ultrathin-Film Composites. *J. Vac. Sci. Technol. A* **1993**, *11*, 3014–3019.
- (10) Schaffer, M.; Schaffer, B.; Ramasse, Q. Sample Preparation for Atomic-Resolution STEM at Low Voltages by FIB. *Ultramicroscopy* **2012**, *114*, 62–71.
- (11) van der Pauw, L. J. A Method of Measuring the Resistivity and Hall Coefficient of Lamellae of Arbitrary Shape. *Philips Tech. Rev.* **1958**, *26*, 220–224.
- (12) Alemayehu, M. B.; Mitchson, G.; Hanken, B. E.; Asta, M.; Johnson, D. C. Charge Transfer between PbSe and NbSe₂ in $[(PbSe)_{1.14}]_m(NbSe_2)_1$ Ferrecrystalline Compounds. *Chem. Mater.* **2014**, *26*, 1859–1866.
- (13) Bayard, M.; Sienko, M. J. Anomalous Electrical and Magnetic Properties of Vanadium Diselenide. *J. Solid State Chem.* **1976**, *19*, 325–329.
- (14) Garg, A. K. Long-Wavelength Optical Phonons in Semiconducting Mixed Layer Crystals of the Series SnS_xSe_{2-x} ($0 \leq x \leq 2$). *J. Phys. C Solid State Phys.* **1986**, *19*, 3949–3960.
- (15) Wieggers, G. A. Misfit Layer Compounds: Structures and Physical Properties. *Prog. Solid State Chem.* **1996**, *24*, 1–139.
- (16) Wieggers, G. A.; Meetsma, A.; de Boer, J. L.; van Smaalen, S.; Haange, R. J. X-Ray Crystal Structure Determination of the Triclinic Misfit Layer Compound $(SnS)_{1.20}TiS_2$. *J. Phys. Condens. Matter* **1991**, *3*, 2603–2612.
- (17) Wieggers, G. A.; Meetsma, A.; Haange, R. J.; van Smaalen, S.; de Boer, J. L.; Meerschaut, A.; Rabu, P.; Rouxel, J. The Incommensurate Misfit Layer Structure of $(PbS)_{1.14}NbS_2$, “ $PbNbS_3$ ” and $(LaS)_{1.14}NbS_2$, “ $LaNbS_3$ ”: an X-Ray Diffraction Study. *Acta Crystallogr. B* **1990**, *46*, 324–332.
- (18) Ren, Y.; Baas, J.; Meetsma, A.; de Boer, J. L.; Wieggers, G. A. Vacancies and Electron Localization in the Incommensurate Intergrowth Compound

- (La_{0.95}Se)_{1.21}VSe₂. *Acta Crystallogr. B* **1996**, *52*, 398–405.
- (19) Gotoh, Y.; Onoda, M.; Akimoto, J.; Oosawa, Y. Preparation and Characterization of New Sb-Containing Ternary Sulfides with Layered Composite Crystal Structure. *Jpn. J. Appl. Phys.* **1992**, *30*, L1039–L1041.
- (20) Wiegers, G. A.; Haange, R. J. Electrical Transport Properties of the Misfit Layer Compounds (SnS)_{1.20}TiS₂ and (PbS)_{1.18}TiS₂. *Eur. J. Solid State Inorg. Chem.* **1991**, *28*, 1071–1078.
- (21) Wiegers, G. A.; Meetsma, A.; Haange, R. J.; de Boer, J. L. Structure and Physical Properties of (SnS)_{1.18}NbS₂, “SnNbS₃”, a Compound with Misfit Layer Structure. *Mater. Res. Bull.* **1988**, *23*, 1551–1559.
- (22) Wulff, J.; Meetsma, A.; Haange, R. J.; de Boer, J. L.; Wiegers, G. A. Structure and Electrical Transport Properties of the Misfit-Layer Compound (BiS)_{1.08}TaS₂. *Synth. Met.* **1990**, *39*, 1–12.
- (23) Yarmoshenko, Y. M.; Trofimova, V. A.; Shamin, S. N.; Solovyev, N. V; Kurmaev, E. Z.; Ettema, A. R. H. F.; Haas, C. The X-Ray Emission Spectra and Electronic-Structure of the Misfit Layer Compounds (BiS)_{1.08}NbS₂ and (PbS)_{1.14}TaS₂. *J. Phys. Condens. Matter* **1994**, *6*, 3993–3998.
- (24) Meerschaut, A. Misfit Layer Compounds. *Curr. Opin. Solid State Mater. Sci.* **1996**, *1*, 250–259.
- (25) Meerschaut, A.; Deudon, C. Crystal Structure Studies of the 3R-Nb_{1.09}S₂ and the 2H-NbSe₂ Compounds: Correlation between Nonstoichiometry and Stacking Type (= Polytypism). *Mater. Res. Bull.* **2001**, *36*, 1721–1727.
- (26) Meerschaut, A.; Roesky, R.; Lafond, A.; Deudon, C.; Rouxel, J. Misfit Layered Compounds: Polytypism, Multilayer Stages, Non-Stoichiometry and Electronic Structure, Self-Misfit Compounds. *J. Alloys Compd.* **1995**, *219*, 157–160.
- (27) Meetsma, A.; Wiegers, G. A.; Haange, R. J.; de Boer, J. L. The Incommensurate Misfit Layer Structure of (SnS)_{1.17}NbS₂, “SnNbS₃”. I. A Study by Means of X-Ray Diffraction. *Acta Crystallogr. A* **1989**, *45*, 285–291.
- (28) Onoda, M.; Kato, K.; Gotoh, Y.; Oosawa, Y. Structure of the Incommensurate Composite Crystal (PbS)_{1.12}VS₂. *Acta Crystallogr. B* **1990**, *46*, 487–492.
- (29) Hite, O. K.; Nellist, M.; Ditto, J.; Falmbigl, M.; Johnson, D. C. Transport Properties of VSe₂ Monolayers Separated by Bilayers of BiSe. *J. Mater. Res.* **2016**, *31*, 886–892.
- (30) Atkins, R.; Dolgos, M.; Fiedler, A.; Grosse, C.; Fischer, S. F.; Rudin, S. P.; Johnson, D. C. Synthesis and Systematic Trends in Structure and Electrical Properties of [(SnSe)_{1.15}]_m(VSe₂)₁, m = 1, 2, 3, and 4. *Chem. Mater.* **2014**, *26*, 2862–2872.
- (31) Alemayehu, M. B.; Falmbigl, M.; Ta, K.; Ditto, J.; Medlin, D. L.; Johnson, D. C. Designed Synthesis of van Der Waals Heterostructures : The Power of Kinetic

Control. *Angew. Chemie Int. Ed.* **2015**, *54*, 15468–15472.

Appendix

- (1) Kresse, G.; Hafner, J. Ab Initio Molecular Dynamics for Liquid Metals. *Phys. Rev. B* **1993**, *47*, 558–561.
- (2) Kresse, G.; Hafner, J. Ab Initio Molecular-Dynamics Simulation of the Liquid-Metal-Amorphous-Semiconductor Transition in Germanium. *Phys. Rev. B* **1994**, *49*, 14251–14269.
- (3) Kresse, G.; Furthmüller, J. Efficiency of Ab Initio Total Energy Calculations for Metals and Semiconductors Using a Plane Wave Basis Set. *Comput. Mat. Sci.* **1996**, *6*, 15–50.
- (4) Kresse, G.; Furthmüller, J. Efficient Iterative Schemes for Ab Initio Total-Energy Calculations Using a Plane-Wave Basis Set. *Phys. Rev. B* **1996**, *54*, 11169–11186.
- (5) Blöchl, P. E. Projector Augmented-Wave Method. *Phys. Rev. B* **1994**, *50*, 17953–17979.
- (6) Kresse, G.; Joubert, D. From Ultrasoft Pseudopotentials to the Projector Augmented-Wave Method. *Phys. Rev. B* **1999**, *59*, 1758–1775.
- (7) Perdew, J. P.; Burke, K.; Ernzerhof, M. Generalized Gradient Approximation Made Simple. *Phys. Rev. Lett.* **1996**, *77*, 3865–3868.
- (8) Dion, M.; Rydberg, H.; Schröder, E.; Langreth, D. C.; Lundqvist, B. I. Van der Waals Density Functional for General Geometries. *Phys. Rev. Lett.* **2004**, *92*, 246401–1.
- (9) Román-Pérez, G.; Soler, J. M. Efficient Implementation of a van der Waals Density Functional: Application to Double-Wall Carbon Nanotubes. *Phys. Rev. Lett.* **2009**, *103*, 96102.
- (10) Klimeš, J.; Bowler, D. R.; Michaelides, A. Chemical Accuracy for the van der Waals Density Functional. *J. Phys. Condens. Matter* **2010**, *22*, 22201.
- (11) Klimeš, J.; Bowler, D. R.; Michaelides, A. Van der Waals Density Functionals Applied to Solids. *Phys. Rev. B - Condens. Matter Mater. Phys.* **2011**, *83*, 195131.
- (12) Li, F.; Tu, K.; Chen, Z. Versatile Electronic Properties of VSe₂ Bulk, Few-Layers, Monolayer, Nanoribbons, and Nanotubes: A Computational Exploration. *J. Phys. Chem.* **2014**, *118*, 21264–21274.
- (13) Wasey, A. H. M. A.; Chakrabarty, S.; Das, G. P. Quantum Size Effects in Layered VX₂ (X = S, Se) Materials: Manifestation of Metal to Semimetal or Semiconductor Transition. *J. Appl. Phys.* **2015**, *11*, 64313.
- (14) Roisnel, T.; Rodriguez-Carvajal, J. WinPLOTR: A Windows tool for Powder Diffraction Patter Analysis. *Mater. Sci. Forum* **2001**, *118*, 378–381.